ISAS - INTERNATIONAL SCHOOL
FOR ADVANCED STUDIES

A model of surface reconstruction and roughening: a Monte Carlo study

Thesis submitted for the degree of
"Magister Philosophiæ"

CANDIDATE
Giorgio Mazzeo

SUPERVISORS
Prof. Giancarlo Jug
Prof. Andrea C. Levi
Prof. Erio Tosatti

Academic year 1989/90

TRIESTE

SISSA - SCUOLA
INTERNAZIONALE
SUPERIORE
STUDI AVANZATI
TRIESTE
Strada Costiera 11

Scuola Internazionale Superiore di Studi Avanzati

International School for Advanced Studies

A model of surface reconstruction and roughening: a Monte Carlo study

Thesis submitted for the degree of

"Magister Philosophiæ"

CANDIDATE

Giorgio Mazzeo

SUPERVISORS

Prof. Giancarlo Jug

Prof. Andrea C. Levi

Prof. Erio Tosatti

Academic year 1989/90

Quickly, as if she were recalled by something over there, she turned to her canvas. There it was – her picture. Yes, with all its green and blues, its lines running up and across, its attempt at something. It would be hung in the attics, she thought; it would be destroyed. But what did that matter? she asked hersef, taking up her brush again. She looked at the steps; they were empty; she looked at her canvas; it was blurred. With a sudden intensity, as if she saw it clear for a second, she drew a line there, in the centre. It was done; it was finished. Yes, she thought, laying down her brush in extreme fatigue, I have had my vision.

Virginia Woolf
To the lighthouse

Index

Introduction

Clean single-crystal metal surfaces usually possess a well-defined two-dimensional periodicity closely resembling the atomic ordering in the bulk. In some cases, however, the surface lattice reconstructs into a phase with a new symmetry: this can occur spontaneously or it can be induced by small coverages of adsorbed atoms or molecules. In this respect, the (110) surfaces of noble and near-noble metals belong to two different classes. The first class includes the lighter metals (Cu, Ag, Ni, Pd), whose (110) surface remains unreconstructed when clean (although a suitable coverage of alkali adatoms causes their reconstruction[1,2,3,4]), but shows, at least according to X-ray scattering experiments[5], a roughening transition at relatively low temperatures. The second class includes the heavier metals (Au, Pt, Ir), whose ground state is a reconstructed (2×1) phase properly described by the "missing row" model, as experimental evidence clearly indicates[6,7,8,9,10,11,12,13]. By raising temperature, the surface undergoes a deconstruction transition from the (2×1) phase to a disordered phase with no particular long-range structure, the precise nature of which is still controversial. The motivation of the present work arises from the suggestion that two phenomena which thus far have been studied as separate – missing row in-plane reconstruction and off-plane roughening – may instead have a very intimate connection. Theoretical studies by Villain and Vilfan[14], Trayanov *et al.* [15,16], Jug and Tosatti[17,18,19] and Levi and Touzani[20] (which will be reviewed in sections 3.1-3.4) indeed seem to indicate this possibility

quite clearly. A direct confirmation of this suggestion comes from the recent X-ray scattering experiments performed by Robinson, Vlieg and Kern on Pt(110) [21].

The present thesis is organized as follows.

In chapter 1 we will review some recent key experiments carried out on the noble and near-noble (110) metal surfaces, providing evidence for the deconstruction transition (mainly on the noble metals) and for the roughening transition (on the near-noble metals). In the second part, theoretical approaches to reconstruction problems will be discussed, both from a statistical (symmetry-based) and an empirical point of view ("effective medium" and "glue" models for a treatment of many body interactions in these systems).

Chapter 2 is dedicated to the roughening transition in all its various aspects. Particular attention is reserved to the statistical models which have been proposed so far to characterize and describe the transition. The universal features of these models are stressed, and a detailed description of the BCSOS model is given, as the main Hamiltonian studied in the present work starts from the same lattice structure and adopts the same six-vertex constraint on the height variables. We also review the phenomenological studies of the roughening transition which lead to look at the equilibrium shape of crystals in terms of the free energy function, and the experimental evidence confirming the main theoretical predictions (especially for He crystals).

In chapter 3, after a review of the few models which try to account for both transitions, the model of Kohanoff, Jug and Tosatti (KJT) is presented. Particular emphasis is given to the physical motivations underlying the model as well as to a description of the ground state in terms of its energy parameters, which assume values suited to characterize the Au(110) surface. In the second part of this chapter

we discuss a list of quantities which are worth studying for the understanding of the physics embodied by the model. This includes the definition of a possible order parameter which denotes the occurrence of a deconstruction transition and the introduction of the coherent and incoherent scattering intensities, also related to ways of experimentally observing the roughening transition.

Chapter 4 presents a short account of the Monte Carlo algorithm set up in order to investigate the properties of the KJT Hamiltonian, and the results obtained for the BCSOS model (examined for test purposes) are shown. An interesting feature arising in this test is the discovery of finite-size effects in the quasi-Bragg incoherent scattering intensity, implying that these effects require more accurate study than hitherto believed.

Finally, chapter 5 reports the results obtained for the KJT model. It provides evidence for two separate transitions, a deconstruction followed by a roughening transition. The former appears to be a second-order transition while the latter is of a higher, possibly infinite (Kosterlitz-Thouless), order. In the conclusive part of the thesis these results are discussed and compared with the conclusions reached by other authors through model calculations or experiments. Here, a brief outlook of some of the possible developments of the present preliminary study is also given.

Chapter 1

The reconstruction of the (110) surfaces of noble metals

1.1 Experimental aspects

The outermost layer of a (110) surface of an fcc crystal has an anisotropic structure which can be described as made up by atomic rows a distance a apart in the (001) direction (a being the fcc lattice parameter), with the atoms separated by a distance $a/\sqrt{2}$ in the $(1\bar{1}0)$ direction of each row. The (2×1) reconstruction leads to a structure in which half of these rows are missing, the missing ones periodically alternating with the those present. The unit cell is doubled in the (001) direction, and the resulting surface structure is thus made up by a sequence of local (111) facets which form a 35° angle with the surface plane (excluding relaxation effects). For this reason, the occurrence of reconstruction depends on the relative value of the energy densities of the surfaces involved, i.e. on the quantity $\Delta = \sigma_{(110)} - \sqrt{3/2}\sigma_{(111)}$ (the numerical factor arising from geometrical considerations). However, the sign of Δ, though determining the true phase, is not sufficient to give a physical picture of the process. As in the $\Delta > 0$ case the (110) surface would relax towards the more stable (111) structure, some stabilizing interaction has to be considered in order to reproduce the observed low temperature (2×1) phase.

It is worth saying that, although the missing-row nature of the heavy noble metal (2×1) reconstruction has been finally recognised by a considerable num-

ber of experiments, the subject has been a controversial topic for several years. In the case of Au(110) , for instance, the missing row structure has been corroborated by low energy electron diffraction (LEED) analysis[8], low energy atom scattering[9], scanning tunneling microscopy (STM)[22,6], X-ray diffraction[10], electron microscopy[12], high[11] and medium energy[13] ion backscattering. Nonetheless, there have been doubts about the kinetics of the $(1 \times 1) \rightarrow (2 \times 1)$ transition because, as pointed out by Bonzel and Ferrer[23,24], if the (2×1) phase develops from an initially flat surface, it would require mass motion in excess of that consistent with measured diffusion constants. Therefore the above mentioned authors considered a saw-tooth model of the surface, in which every second row is not missing but is simply shifted upwards to form a separate layer. In contrast with this model, perhaps the most direct indication of the true nature of the (2×1) phase has come from the STM experiments performed by Binning, Rohrer and collaborators[22,6] which unambiguously demonstrated the (111) faceted nature of the Au(110) surfaces. Faceting is believed to be the basic mechanism for the reconstruction into the missing row structure, the weak disorder being present on the surface in the form of (3×1) and rare (4×1) corrugations over the ordered (2×1) phase, while wider portions of (111) facets are never observed. Although the mass transport problem, as posed by Bonzel and Ferrer, still stands, it seems very probable that more complex mass transport mechanisms (e.g. anisotropic, across the channels extending parallel to the rows) should be advocated.

In conclusion, in view of the results of this and other quoted studies, the saw-tooth model can be safely ruled out. Furthermore, careful investigations of the detailed structure of the missing row phase show many relaxation effects of the outer atoms, like a (debated) top row contraction, a second layer pairing and a third layer buckling, features some of which have been confirmed by first principle

calculations for the Au(110) surface[25,26], as well as by molecular dynamics studies of gold surfaces [27,28] (see section 1.2).

When the temperature of the system is increased, the completely ordered in-plane structure begins to develop defects due to excited states now thermally available. These thermal effects may be responsible for a phase transition from the ordered structure to some other phase, the nature of which can be investigated by scattering experiments, e.g. through the measurement of some critical exponent. The most experimentally accessible ones are: β, related to the behaviour of a suitably-defined order parameter ψ near the transition temperature T_c ($\psi \sim |T - T_c|^{\beta}$); γ, related to the divergence of the susceptibility χ of that order parameter at T_c ($\chi \sim |T - T_c|^{-\gamma}$); and ν, related to the divergence of the correlation length ξ of the system at T_c ($\xi \sim |T - T_c|^{-\nu}$). For the (2×1) phase transition, the critical exponents can be determined in a LEED experiment, from the temperature dependence of the structure factor

$$S(\mathbf{Q}, T) = I(T)\delta(\mathbf{Q} - \mathbf{Q_0}) + \chi(\mathbf{Q} - \mathbf{Q_0}, T)$$

where $\mathbf{Q_0}$ is a superstructure (or half-order) wave vector (a reciprocal lattice vector with a fractional sum of indices, e.g. $(1/2, 1/2, 1/2)$, $(3/2, 0, 0)$, etc ...in the surface reference frame), thus sensitive to the doubling of the unit cell, and $\mathbf{Q} \equiv \mathbf{Q_0} + \mathbf{q}$ is the usual momentum transfer[29,30].

The first term gives a delta function at $\mathbf{Q} = \mathbf{Q_0}$, with an intensity that depends on the square of the long range order parameter ψ: $I(T) \sim \psi(T)^2 \sim (T - T_c)^{2\beta}$. This term is dominant for $T < T_c$, so that β can be determined after correcting for the Debye-Waller factor temperature dependence and after

assuming a broadening of the delta function into a Gaussian of finite width due to surface imperfections. The second term, while present at $T < T_c$, is the only one present at $T > T_c$, and describes the long-range fluctuations at and near the critical temperature. Very close to T_c ($t \equiv (T - T_c)/T_c < 0.005$), $\xi \rightarrow \infty$, so that $\chi(\mathbf{q}, T) \simeq const \cdot q^{\eta - 2}$ (η being the critical exponent related to the correlation function). For relatively small t and q, so that q is of the same order of magnitude as $1/\xi$, the second term may be approximated by a Lorentzian of the form

$$\chi(\mathbf{q}, T) = \frac{\chi(0, T)}{1 + \xi^2 q^2}$$

with half width $1/\xi$ and height $\chi(0, T)$, $\chi(0, T)$ being the susceptibility associated with the order parameter ψ. In this way, a measure of the diffraction profile leads in principle to the determination of the other two critical exponents γ and ν. In practice, however, surface imperfection and experimental resolution must be carefully taken into account, in order to obtain reliable data.

By fitting the temperature variations of the half-order Au(110) (2×1) LEED diffraction profile with the three parameters of the Gaussian height, Lorentzian height and width, Campuzano *et al.* [31] were able to derive for the critical exponents the values $\beta = 0.13 \pm 0.02$, $\gamma = 1.75 \pm 0.10$ and $\nu = 0.93 \pm 0.09$, which are in fairly good agreement with those of the two-dimensional Ising model, i.e. $\beta = 1/8$, $\gamma = 7/4$ and $\nu = 1$. Therefore, this experiment would indicate that at a temperature of about 660 K the (110) surface of Au undergoes a phase transition from an ordered (2×1) phase to a disordered phase (deconstruction), which falls into the same universality class of the Ising model.

Possible theoretical explanations for this apparently well-defined behaviour will be given in section 1.2. Nonetheless, the question about the nature of the

transition has re-opened again after very recent X-ray diffraction experiments performed by Robinson, Vlieg and Kern on the (2×1) reconstructed (110) face of Pt[21]. They, in fact, provide data in favour of a deconstruction transition which seems to coincide, however, with the roughening one at a temperature $T_C \simeq 1080K$. Although the critical exponents yielded by the usual procedure are in accordance with a two dimensional Ising transition, a new feature (not present in the experiment on Au by Campuzano *et al.*) is represented by a shift in the half-order peak position above T_C, which is also temperature dependent, strongly indicating, in their view, a spontaneous proliferation of steps above T_C and hence that the phase transition is also a roughening transition (see chapter 2).

For the lighter metals, the experimental situation seems clearer. In the case of Ag(110) , Held *et al.* [5] show that an X-ray scattering study performed at glancing angle can provide direct information about thermal variations of the surface height-height correlation function, the behaviour of which is closely connected to the the existence of a roughening transition. These authors look at the surface in anti-Bragg conditions (i.e. for values of the momentum transfer which should give exact cancellation of intensity for a smooth surface but not for a disordered one, thus probing the occurrence of steps on it), and show clearly that the peaks evolve from a delta function to a power law line-shape with an exponent η. This experiment is a direct measure of the logarithmic divergence of the correlation function, and hence of the surface roughness: their results give evidence for a roughening transition on the Ag(110) surface at temperature $T_R = 450 \pm 25°C$, well below the bulk melting point.

For Cu(110) two experiments have been performed, an X-ray diffraction study by Mochrie[32], and a helium atom scattering experiment by Zeppenfeld *et al.* [33].

Mochrie scans in temperature between $200°C$ and $700°C$, finding a very fast decay with temperature of the integrated intensity of the (110) Bragg peak. The peak intensity, approximately constant between $T = 200°C$ and $350°C$, decreases with increasing temperature till, by $T = 600°C$, it has fallen essentially to zero. It diminishes more rapidly than it can be accounted for by a simple Debye-Waller factor, thus suggesting the presence on the surface of thermally generated steps. The behaviour of the intensity in this experiment, as well as in the previous one by Held *et al.*, is completely reversible, thus cannot be ascribed to an irreversible faceting transition, providing instead evidence for a roughening phase transition for which the value of $T \simeq 600°C$ can be considered a lower bound.

The scattering experiments by Zeppenfeld *et al.* show a dramatic change in the slope of the specular diffracted peak intensity at $T \simeq 550K$ ($\simeq 280°C$), inconsistent with a Debye-Waller behaviour. After this, they perform a momentum resolved experiment which shows a decrease of the specular peak height, while no appreciable broadening of the peak is observed up to $900K$ ($\simeq 630°C$). Finally they analyze the diffuse elastic scattering intensity finding a decrease with increasing temperature (this quantity is a measure of the density of scatterers in the surface, and should increase in the case of truly rough surfaces). They interpret their result in terms of an anomalous Debye-Waller effect due to increased anharmonicity of the surface vibrations, concluding that no phase transition occurs for $T < 900K$.

These two experiments actually point in two different directions: it is thus worth saying that the first evidence has been somehow reconsidered by its author, due to a miscut of the sample used, so that the more reliable information on the Cu (110) roughening transition is to be found rather in Zeppenfeld *et al.* experiment.

1.2 Theoretical models

This wealth of experimental evidence presented above has found its theoretical counterpart in a number of studies carried out to elucidate from different points of view the nature of the (2×1) structure of heavy noble metals and of its phase transition.

1.2.1 Statistical approaches

A statistical mechanics approach is the way through which Bak[34] recognizes in the (2×1) deconstruction transition a simple physical realization of the two-dimensional Ising model. He begins with the observation of the gradual vanishing of the half-order diffraction peaks as the temperature is raised, and sees in this phenomenon a clear indication of a second order transition to the non reconstructed (1×1) "ideal" surface. The wave vector characterizing the ordered phase is $\mathbf{k} = \frac{2\pi}{a}(\frac{1}{2}, 0)$, and the corresponding distortion pattern is given by

$$\mathbf{u}(\mathbf{r}) = \psi \hat{\mathbf{e}} \cos(\mathbf{k} \cdot \mathbf{r}) \tag{1.1}$$

where $\hat{\mathbf{e}}$ is a unit vector which may be parallel or perpendicular to $\mathbf{k}$. Now the symmetry operations of the (110) surface are applied to (1.1), $\psi \rightarrow \pm\psi$, and ψ therefore results in a one-component Ising order parameter, leading one to expect two-dimensional Ising critical behaviour for the transition.

This first attempt to describe the intermediate temperature behaviour of reconstructed surfaces was generalized to all types of two dimensional crystal lattices by Schick[35]. A general approach will be given below, successively particularized to rectangular lattices with the symmetry of the space group $p2mm$, as is the

case of the (110) surface of fcc crystals. The framework of Schick's classification is the possibility to model the systems under consideration as well as those including adsorbed atoms by a two dimensional lattice gas, where the statistical variables are the site occupation numbers n_i which have the value 0 or 1 according to whether the site i on the lattice is empty or occupied. One can now employ the well-known isomorphism between lattice gas models and spin 1/2 models, given by the mapping

$$n_i = \frac{1+\sigma_i}{2}$$

to reduce all the different situations to corresponding spin Hamiltonians. On the other hand, for classification purposes it is perhaps more convenient to remain in a lattice gas language, introducing the density ρ_i which is the ensemble average of n_i, and writing the Hamiltonian, consisting only of pairwise interactions, as

$$H = \frac{1}{2}{\sum_{ij}}' v_{ij} n_i n_j$$

where the prime on the sum ensures that terms with $i = j$ are excluded from the summation. Introduce now the Fourier transforms of ρ_i and of v_{ij}

$$\rho_i = \rho + \sum_{\mathbf{q}} \rho(\mathbf{q}) e^{i\mathbf{q}\cdot\mathbf{r}_i}$$
$$v_{ij} = \sum_{\mathbf{q}} v(\mathbf{q}) e^{i\mathbf{q}\cdot\mathbf{r}_{ij}}$$

where the sums are over the first Brillouin zone of the reciprocal lattice, $\mathbf{r}_{ij} = \mathbf{r}_i - \mathbf{r}_j$ and ρ is the average density $\rho = \frac{1}{N}\sum_i \rho_i$, N being the number of sites. With this

definition, $\rho(\mathbf{q}=0)$ vanishes, so that henceforth terms with $\mathbf{q}=0$ will be ignored. The inverse of the above relations are

$$\rho(\mathbf{q}) = \frac{1}{N}\sum_i \rho_i e^{-i\mathbf{q}\cdot\mathbf{r}_i} \tag{1.2}$$

$$v(\mathbf{q}) = \frac{1}{N}\sum_{\mathbf{r}_{ij}} v_{ij} e^{-i\mathbf{q}\cdot\mathbf{r}_{ij}} \tag{1.3}$$

In a disordered phase, ρ_i will be uniform, so that $\rho(\mathbf{q})$ will vanish for all $\mathbf{q}$'s. However, in the ordered phase, the density will vary with some wave vector $\mathbf{Q}$ for which $\rho(\mathbf{Q}) \neq 0$. Therefore, $\rho(\mathbf{Q})$ is a quantity which goes to zero at the phase transition from an ordered to a disordered phase and hence can be identified with the order parameter field. The value of $\mathbf{Q}$ in the ordered phase is that one which minimizes $v(\mathbf{Q})$. Then

$$\left.\frac{\partial v(\mathbf{q})}{\partial \mathbf{q}}\right|_{\mathbf{Q}} = 0 \tag{1.4}$$

defines $\mathbf{Q}$, and conditions on the second derivatives of $v(\mathbf{q})$ will ensure $\mathbf{Q}$ is indeed a minimum. Now, if eq. (1.4) is satisfied for a particular value $\mathbf{Q}$, then it will be so also for all other wave vectors obtained by operations belonging to the symmetry group of the lattice, i.e. those leaving the lattice invariant. In general, there will be l such vectors, labeled $\mathbf{Q}_1$, $\mathbf{Q}_2$, ..., $\mathbf{Q}_l$ (including $\mathbf{Q}$ itself), which are not related to one another by a reciprocal lattice vector: this set of vectors form what is called the "star" of $\mathbf{Q}$. All the density components $\rho(\mathbf{Q}_1)$,$\rho(\mathbf{Q}_2)$,..., $\rho(\mathbf{Q}_l)$ will be nonzero below the critical temperature, so that the density will have the expression

$$\rho_i = \rho + \sum_{s=1}^{l} \rho(\mathbf{Q}_s) e^{i\mathbf{Q}_s \cdot \mathbf{r}_i} \tag{1.5}$$

which can be written

$$\rho_i = \rho + \sum_{s=1}^{l} \rho(\mathbf{Q}_s) \cos(\mathbf{Q}_s \cdot \mathbf{r}_i), \qquad \rho(\mathbf{Q}_s) \text{ real}$$

It may be noted that in this case the l functions $\cos(\mathbf{Q}_s \cdot \mathbf{r}_i)$ constitute a basis of a real l-dimensional irreducible representation of the space group of the lattice. The general expansion (1.2) is simply an expansion of the density in terms of the complete set of irreducible representations of the space group, that is, the expansion contains all q's. The fact that (1.4) is satisfied for only one $\mathbf{Q}$ (and the other vectors in its star) indicates that below T_c the phase is ordered, then the density has the more restricted form of (1.5), i.e. it can be written in terms of a single irreducible representation of the space group.

For the fcc rectangular lattice, given a vector $\mathbf{Q}$ satisfying (1.4), its star is generated by applying to $\mathbf{Q}$ the point group operations of the rectangle, but all vectors so generated are related to the original one by reciprocal lattice vectors, hence the star of $\mathbf{Q}$ consists of the single vector $\mathbf{Q}$. In the case of nearest-neighbour interactions only, (1.3) is rewritten in the form

$$v(\mathbf{Q}) = 2v_x \cos(q_x a) + 2v_y \cos(q_y a/\sqrt{2})$$

the minima of which provide the possible values of $\mathbf{Q}$. The 3 possible stars obtained with this procedure are $\frac{2\pi}{a}(\frac{1}{2}, 0)$, $\frac{2\pi}{\sqrt{2}a}(0, \frac{1}{2})$, and $\frac{2\pi}{\sqrt{2}a}(\frac{\sqrt{2}}{2}, \frac{1}{2})$. Each one of them is related to a particular reconstruction of the ordered phase, the first to the

(2×1) , the second to the (1×2) and the third to the $c(2 \times 2)$. These symmetry considerations are now to be confronted with real physical systems which, as shown in the preceeding section, recognize in the (110) surface of fcc noble metals the first type of reconstruction. The Landau expansion for the free energy in terms of the one-component order parameter $\rho(\mathbf{Q})$ is of the form

$$f = a\rho^2(\mathbf{Q}) + b\rho^4(\mathbf{Q}) + \cdots$$

which, although it cannot be extended up to the transition, permits to predict that the universality class is the Ising one.

A different approach due to Guillopé and Legrand[36] reduces the problem to an Ising model with effective pair, triplet and quadruplet interactions fitted from tight-binding calculations, which is then solved by a molecular dynamics calculation. Reducing the number of interactions to two new effective ones only, the model becomes solvable and the result is the existence of an Ising-like phase transition for Au, but also for the Cu, Ag and Pd unrecostructed (1×1) (110) surfaces, which is not consistent with currently available experimental data.

To conclude this section, it seems important to mention the point recently made by Kohanoff, Jug and Tosatti[19], which seems to invalidate the details of much of the symmetry-based analysis outlined above. They have pointed out essentially the following:

1) There is an Ising-like parameter even in the $T = 0$ (1×1) (110) surface, which corresponds to specifying to what sublattice the outermost layer belongs. The two sublattices are equivalent but not identical (i.e., not related by a space group symmetry operation), and are therefore completely distinct.

2) In the presence of the BCSOS constraint (see section 2.1.2), the Ising-like

symmetry of the problem does not necessarily imply a phase transition of the Ising universality class. The BCSOS case (where there is only a Kosterlitz-Thouless type of transition) is an explicit example of this, once the existence of a $T = 0$ order parameter, defined as above, is pointed out.

3) The (1×2) missing row reconstructed (110) surface does not have *two* degenerate states, but *four*, corresponding to two possible phases of the missing row, and two possible outermost sublattices. Hence, implications that this problem should belong to the Ising universality class[31,14] are, at least in principle, incorrect.

The detailed consequences of these points need clarification. Although the results presented here are not properly pertinent to this question, the answer is contained in principle in our Hamiltonian (section 3.5) which does embody the symmetry requirements specified by Kohanoff, Jug and Tosatti.

1.2.2 First principles and empirical approaches

A completely different theoretical approach in order to understand the nature of (110) surfaces is a computational one, either via first principle calculations or many body effective interaction models.

Although the missing-row structure has now gathered general consensus, the detailed geometry of the reconstruction as well as the basic mechanism stabilizing such geometry has not been clear at all up to the first principle calculations performed by Ho and Bohnen[25,26]. Their pseudopotential approach within the local density functional formalism was successful in providing accurate information on the atomic positions at the surface and in elucidating the driving mechanism of reconstruction. The fact that missing row roughening is stable on the (110) face of

the fcc $5d$ metals Au, Pt and Ir, but unstable for the corresponding $4d$ metals Rh, Pd and Ag, suggests the importance of the d-electrons in such process. The $5d$ electronic wave functions are more delocalized than the $4d$ ones, leading to larger hybridization for the $5d$ band. This results in a stronger contribution of the d electrons to the bonding of the crystal, which shows up also in the bulk properties: the $5d$ metals have substantially bigger cohesive energies. By carefully examining the different contributions to the surface energies of the (1×1) and (2×1) structures (kinetic, exchange correlation and electrostatic potential energy) it is apparent that the missing row surface is stabilized over the bulk-truncated surface by having a smaller electronic kinetic energy. In this regard, two opposite factors are mainly contributing: one is the breaking of the surface d-bonds, which leads to an increase in the surface kinetic energy, the second (and most important) is the lowering of that energy by the s- and p-electrons near the Fermi level, whose wave functions become more spread out at the surface. The total surface energy is kept positive by the breaking of the d-bonds; however, if the system can increase its area without breaking extra d- bonds it would do so, with a lowering of the total surface energy. The missing row geometry provides a solution to the problem of minimizing the kinetic energy of the s-electrons while retaining as much of the bulk cohesion as possible; the (2×1) surface has the same number of broken bonds as the (1×1) surface but provides more room for the electrons to spread out and lower their kinetic energy. The difference in behaviour between the $5d$ and the $4d$ metals comes from the stronger d-bonding in the $5d$ metals (as mentioned above), leading to a bigger contraction of the lattice and causing a stronger compression of the sp-electrons in the bulk. Therefore it is possible to stabilize the missing-row reconstruction by increasing the surface s-electron concentration, for example by deposition of submonolayers of alkali metals, as experimentalists have done[1,2,3,4].

From the structural point of view, results from glancing incidence X-ray diffraction[10] and high resolution microscopy[12] indicate an outward relaxation of the top half filled surface layer of atoms by $\sim 40\%$ of the interlayer spacing, in direct contradiction with the conclusions of low-energy electron diffraction[8], ion scattering[13] and helium diffraction[9] experiments, which indicate a contraction of the top interlayer spacing. Distortions of the inner layers were also reported, including lateral displacements of second layer atoms[10,8] and a buckling of the third atomic layer[8,13]. For the relaxed (110) missing row surface, Ho and Bohnen find a contraction of the top interlayer spacing, a lateral displacement for the atoms in the second and fourth layer, and a buckling of the third layer atoms in the direction of the surface normal, in accordance with the majority of the experiments reported above.

Parallel to a first principle approach, which copes with the full complexity of electronic effects, there can also be more empirical approaches, reviewed by Nieminen[37], where the atoms are treated as points interacting through some potential energy function $V(\mathbf{r}_1, \ldots, \mathbf{r}_n)$: this attitude has generated, among the others, the so-called "glue" model[27,28] and the "embedded atom method"[38,39,40,41].

All the past empirical schemes based on pair-wise potentials, which work reasonably well to describe rare gas solids, badly fail when attempting to model other kinds of materials, owing to many-body effects of electronic origin. As seen previously, electronic cohesion in noble and near noble metals is largely caused by the *d*-electrons, which form very broad filled *d*- bands. Thus the main problem of an empirical approach is the way to express the forces acting on an ion in terms of the positions of the other ions: the non-directional nature of the filled *d*-bands, which have no possibility to re-hybridize to form directional bonds, strongly suggests that

the key ingredient is the concept of coordination, i.e. roughly speaking, the number of neighbours of a given ion, which should represent in some way the amount of local electronic density: the energy should lower once an atom is surrounded by many other identical atoms.

These concepts can be expressed in mathematical form by writing the potential energy of a system of N atoms as

$$V = \frac{1}{2} \sum_{i,j=1(i\neq j)}^{N} \Phi(r_{ij}) + \sum_{i=1}^{N} U(n_i) \tag{1.6}$$

where a standard two-body part is still present, together with the new many body term, U. Here, n_i is the coordination of the atom i, and the function $U(n)$ associates an energy value to this coordination: for this reason, $U(n)$ has been nicknamed the "glue" and eq. (1.6) the "glue Hamiltonian". The simplest choice for n_i consists in building it as a superposition of contributions from the neighbouring atoms

$$n_i = \sum_{j=1(j\neq i)}^{N} \rho(r_{ij}) \tag{1.7}$$

where $\rho(r)$ is a short-ranged monotonically decreasing function of distance. Eq. (1.7) can be seen as a generalization of the usual idea of coordination. The glue Hamiltonian (1.6) has been introduced from a purely empirical point of view, and the three functions $\Phi(r)$, $U(n)$ and $\rho(r)$ are built empirically and clearly depend on the metal chosen for the study. In the case of Au, for example, they have been determined by fitting exactly the $T = 0$ lattice parameter, the cohesive energy, the bulk modulus and the transverse phonon frequency at the X point. This procedure however, does not definitely fix Φ, U and ρ, but just provides some fitting points,

so that a large arbitrariness remains in the shape of these functions, and it is in this freedom that lie both the strength and the weakness of the glue Hamiltonian, because the more careful will be the fitting of Φ, U and ρ with other properties of the systems under consideration (e.g. thermal properties like thermal expansion coefficients, melting temperature, etc ...), the more appropriate and conclusive will be the results thus obtained.

When applied to a molecular dynamics procedure to study the Au(110) $T = 0$ structure, the model has given interesting results, also providing useful insights in the physical mechanism underlying reconstruction. First of all, the (2×1) missing row structure turns out correctly to be the optimal structure (i.e. that of the lowest energy). Other (2×1) models, such as the saw-tooth model, are found to be unstable. The resulting structure furthermore presents a large inward relaxation of the top row, a somewhat unexpected slight inward pairing of the second layer rows, and a third layer buckling. All in accordance (with the exception of the second layer relaxation) with Ho and Bohnen and experimental results[10,12,8,13,9]. Since there is some arbitrariness in the choice of the triplet Φ, U and ρ, the glue term $U(n)$ can be chosen so as to be minimal at some optimal coordination number n_0 (for example $n_0 = 12$, the bulk coordination number), so that it will increase for both insufficient and excessive coordination. In this way, for the missing row reconstruction, the close packing which is locally achieved by this geometry keeps the glue energy small, so that the surface energy decreases in spite of the larger exposed microscopic area. So, while (2×1) is the preferred cell, the (3×1), (4×1), ... missing-row structures are found to be very close in surface energy: these structures have been also observed in STM experiments[22,6], as reviewed in section 1.1, and confirm the (111) faceting tendency of the (110) surface.

As a conclusion, the driving force for surface reconstruction in noble metals,

as it arises from the glue model, is the tendency of surface atoms to increase their coordination, induced in turn by electronic effects. While in most metals this tendency is weak, so that the first layer contraction suffices, in noble metals it is so strong so as to favour extensive first layer rearrangements. Complicated geometries arising from these rearrangements are simply a consequence of the packing tendency, and angular forces (not included in the glue) play no important role.

Another effective-medium theory involving many-body potentials is the "embedded atom method", introduced within the framework of density functional theory by Daw and Baskes[38,39,40,41]. It is well known that the total electronic energy for an arbitrary arrangement of nuclei can be written as a unique functional of the total electron density. The starting point of the "embedded atom method" is the observation that such density in a metal is reasonably approximated by the linear superposition of contributions from the individual atoms. The energy of each atom is so written as the energy associated with the electron density of the atom plus a contribution from all the surrounding atoms, which can be approximated as constant, being a slowly-varying function of position. This procedure defines an embedding energy as a function of the background electron density and of the atomic species considered; in addition, there is an electrostatic energy contribution due to core-core overlap. These ideas lead to an approximation for the total energy of the form

$$E = \sum_i F_i(\rho_{h,i}) + \frac{1}{2} \sum_{i,j(i \neq j)} \Phi_{ij}(R_{ij}) \qquad (1.8)$$

where $\rho_{h,i}$ is the host electron density at atom i due to the remaining atoms of the system, $F(\rho)$ is the energy to embed atom i in this background electron density

ρ, and $\Phi_{ij}(R_{ij})$ is the core-core pair repulsion between atoms i and j separated by the distance R_{ij}. The electron density is approximated by the superposition of atomic densities

$$\rho_{h,i} = \sum_{j(\neq i)} \rho_j^a(R_{ij}) \tag{1.9}$$

where $\rho_j^a(R)$ is the electron density contributed by atom j, which is taken from Hartree-Fock calculations. Hamiltonian (1.8) together with (1.9) leads to a scheme similar to that of the glue model, even in the fitting required to obtain the shape of the "universal" (i.e. just depending on the atomic species considered) function $F(\rho)$ ($F_i = F$, in that all atoms are equivalent).

Applied to surfaces, the "embedded atom method" predicts, for example, the (2×1) reconstruction of Pt (110). Very recent studies[40,41] using an extension of the original method in order to prove the accuracy of treatment in regions of large density gradients, provide new informations on both the energetics and the kinetics of the Au (2×1) missing row reconstruction. It has been found that steps whose edges lie parallel to the close-packed rows on the (110) surface have extraordinarily low energies, so low indeed that it should be difficult to prepare a surface not having a substantial number of steps by ordinary means. If the surface starts in disordered form, (2×1) order can thus develop without long range movements of individual atoms, and the mass motion problem pointed out by Bonzel and Ferrer[23,24] is no more present. Even so, diffusion clearly remains of interest, and in this regard complex processes like concerted (multi-atom) moves have been found relevant on that as well as on other metal surfaces.

Chapter 2

The roughening transition

2.1 Statistical models

2.1.1 From Burton, Cabrera and Frank to the Discrete Gaussian model

In 1949 Burton and Cabrera[42] first put forward the idea (further developed in a now classical article by Burton, Cabrera and Frank[43]) that a phase transition may occur in the equilibrium structure of crystal surfaces. They conjectured that low index crystal faces in equilibrium with vapor, melt or solution, would become rough above a certain transition temperature T_R: this can have important consequences for the speed of growth and the equilibrium shape of the crystal. The idea was to divide the three-dimensional (3D) space into building blocks containing one atom each (lattice cells), and to map the resulting 3D lattice-gas model onto the 3D Ising model, where solid regions are described by occupied cells (e.g. up spins) and vapor ones by empty cells (down spins). The transition is characterized by the interface becoming infinitely "rough" in the sense of a divergent interfacial width. The argument used by Burton, Cabrera and Frank for the existence of such transition was partly based on a mapping of the interface problem onto the 2D Ising model, which had just recently been solved by Onsager[44] and which could lead to large fluctuations in the surface structure at the critical temperature

T_c^{2D}. The idea is undoubtedly valid at low temperatures, but breaks down near the transition temperature, when the interface tends to delocalize before becoming infinite in width and any mapping onto a model which takes into account one layer of atoms only is no longer valid. This failure ends up in a wrong prediction about the universality class to which a correct roughening model should belong, which is not of the 2D Ising type.

Since 1949, a wealth of theoretical work (reviewed in refs. [45,46]) was produced, especially after a certain class of models was introduced, imposing the Solid-on-Solid (SOS) restriction on the Hamiltonian. This is the further requirement that every occupied site is directly above another occupied site (thus excluding "overhangs" in the surface shape, as well as voids in the solid phase or "bubbles" in the vapor phase). A SOS model can thus be thought of as an array of interacting columns of variable integer heights. The surface configuration is represented by the 2D array of integers specifying the number of atoms in each column perpendicular to the chosen low index face or, equivalently, by the heights of the columns relative to a flat reference surface. Growth or evaporation of the crystal involves just the "surface atoms" on the top of their columns. In this way, the SOS Hamiltonian is expressed in terms of a set of height variables $\{h_{ij}\}$ defined at each site ij of a two dimensional lattice, and the surface energy is a function of the number of broken bonds due to the existence of surface fluctuations. A wide variety of SOS models can be considered, in which the interaction energy between neighbouring columns is some increasing function V of their height difference, which is proportional to the number of broken bonds, so that the Hamiltonian can be written as follows:

$$H_{SOS} = \sum_{ij<i'j'} V(h_{ij} - h_{i'j'}) \tag{2.1}$$

It is worth noting that the number of vertical broken bonds is conserved in the excitations permitted by the SOS model, hence one can arrive at (2.1) formally by considering the interface in an anisotropic lattice gas with a vertical bond strength $J_\perp$, and then letting $J_\perp \to \infty$. If in (2.1) the interaction energy is taken of quadratic form, one arrives at the so-called Discrete Gaussian model (DG), first studied by Chui and Weeks[47]:

$$H_{DG} = \sum_{ij<i'j'} J(h_{ij} - h_{i'j'})^2 \tag{2.2}$$

The partition function of Hamiltonian (2.2) was rewritten, via a duality transformation, into the partition function of a neutral 2D Coulomb gas, but with the ratio J/T inverted. In this way the existence of a transition was established between a smooth, low-temperature phase, and a rough, high- temperature one and, what is more, it was placed in the Kosterlitz-Thouless universality class[48,49] (believed to be the correct one). Different forms of the interaction energy V will not change the universality class because the roughening transition involves long-wavelength fluctuations in the position of different parts of the interface, thus changes in the interaction energy between columns that affect only short-wavelength properties should be irrelevant at the roughening point[45].

It is now useful to present some of the results of the Renormalization Group calculations on the SOS model[46].

The singular part of the free energy is not analytic at T_R, its form being

$$F_S \approx B\exp\left(-\frac{C}{\sqrt{|T-T_R|}}\right) \tag{2.3}$$

for T in the neighbouring of T_R (B and C are non-universal constants), but the singularity is a very weak one as all the derivatives of F_S with respect to T are smooth functions of T vanishing at T_R. In particular, there is no specific heat anomaly at T_R, in contrast with the Ising model: the transition is said to be of infinite order.

The correlation length, which is the characteristic length for correlations between thermal excitations of the crystal surface, is finite well below T_R, while it diverges at T_R like

$$\xi \approx \begin{cases} \xi^0 \exp\left(\frac{A}{\sqrt{T_R-T}}\right), & T < T_R \\ \infty, & T \geq T_R \end{cases} \tag{2.4}$$

with ξ^0 and A again non-universal constants.

But the most striking result concerns the behaviour of the height-height correlation function,

$$G(R) \equiv \langle [h(R_{ij}) - h(R_{00})]^2 \rangle \tag{2.5}$$

where $R \equiv |R_{ij} - R_{00}|$, and the angular brackets denote an ensemble average in the SOS system; this function gives a measure of the diffusiveness of the interface due to fluctuations in height between different regions of the surface. Its full expression is

$$G(R) = K(T) a_\perp^2 \ln\left[a_\parallel^2 \left(\frac{1}{R^2} + \frac{1}{\xi^2}\right)\right]^{-1} \tag{2.6}$$

where $a_\perp$ and $a_\parallel$, respectively, are the lattice constants in the direction orthogonal and parallel to the plane of the surface under consideration (where it is implicitely assumed that $a_\parallel$ is the same for different principal directions in this plane). ξ is the correlation length introduced in (2.4), hence for $T > T_R$ one has $\xi^{-1} = 0$ and a logarithmic divergence of $G(R)$. The coefficient $K(T)$ is an increasing function of temperature, whose behaviour is specifically predicted by Renormalization Group calculations. At the roughening temperature, $K(T)$ assumes the universal value

$$K(T_R) = \frac{1}{\pi^2} \tag{2.7}$$

approached from above in the following way:

$$K(T) = \frac{1}{\pi^2} + C\sqrt{(T - T_R)} \tag{2.8}$$

where the power $\frac{1}{2}$ is universal, but the constant C is not. The correlation function is clearly related to the fluctuations in height of a point of the interface about its average value $\langle h(R_{00})\rangle$, being

$$\langle \delta h^2 \rangle \equiv \langle h^2(R_{00})\rangle - \langle h(R_{00})\rangle^2 = \lim_{R_{ij}\to\infty} \frac{1}{2}\langle [h(R_{ij}) - h(R_{00})]^2 \rangle \tag{2.9}$$

so that

$$\langle \delta h^2 \rangle \approx \begin{cases} K(T)\ln\left(\xi/a_\parallel\right), & T < T_R \\ K(T)\ln\left(L/a_\parallel\right), & T \geq T_R \end{cases} \tag{2.10}$$

thus saturating at a constant value for temperatures below T_R (smooth phase), instead logarithmically diverging with the size L of the system for $T > T_R$: this

delocalization of the interface is the concept more closely related to the statistical mechanics idea of roughening. It should also be remarked that (2.6) and subsequent formulae should hold for anisotropic surfaces as well, at least in the limit of large R.

2.1.2 The BCSOS model (and the six vertex model)

Another type of SOS model presenting a roughening transition and, what is more, exactly solvable, is the BCSOS (Body Centered Solid-on-Solid) model introduced by van Beijeren[50] in 1977. The system under consideration is the (100) face of a bcc crystal, in which both the atoms at the corner of the cube and those at the center are taken into account. At $T = 0$, nearest neighbour columns differ by one atom since half the columns terminate in the layer directly below the outermost surface layer. Now the system is constrained such that at all temperatures these nearest neighbour columns can differ by at most ± 1 atom. Thus the higher-energy multiple jumps between neighbouring columns are completely suppressed but, as argued before, this should have no effect on the critical behaviour: the BCSOS model is expected to be (and actually is) in the same universality class as the other SOS models.

In practice, the system is composed of two standard SOS models defined on two interpenetrating square sublattices, where on one of the sublattices the height variables may assume only odd values ($\pm 1, \pm 3, \ldots$) and on the other sublattice only even values ($0, \pm 2, \pm 4, \ldots$). Also, the additional (and very relevant, as it will be seen later) restriction is imposed that the height jumps between neighbouring sites (belonging to different sublattices) may be just ± 1. Van Beijeren showed with a simple argument that the allowed configurations in the BCSOS model can be placed in exact correspondence with the vertex configurations of Lieb's six vertex

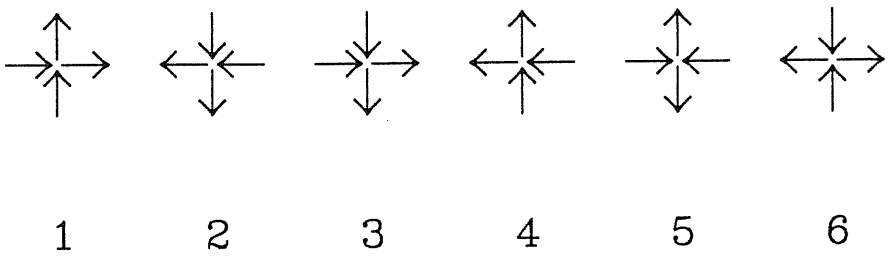

Fig. 2.1: The six vertices.

model[51,52,53], which is the 2D version of the ice model, introduced by Pauling[54] and Slater[55] in order to study the residual entropy of ice at $T = 0$, as well as the ferroelectric phase transition. Hence the two models are isomorphic.

Van Beijeren's construction proceeds by assigning arrows to the bonds of the dual lattice, fixing their direction in such a way that the higher of the two neighbouring height variables always lies to the right of an up-pointing arrow. It is easy to see that at the sites of the dual lattice, where four arrows meet, just six of the sixteen possible combinations of four arrows are realised. They are precisely the vertices allowed by the six vertex model (shown in fig. 2.1), satisfying the so called "ice rule" (at each node of the dual lattice two arrows point inwards and two outwards) which is an immediate consequence of the uniqueness of the height variables of the surface system. This also makes one-to-one the correspondence between vertex configurations and BCSOS height configurations (up to an overall vertical shift of the height variables, a symmetry which can be removed by fixing the value of a simple height variable).

The six vertex model, which was exactly solved by Lieb and Wu[52], can be divided

into different classes according to the values of the energies ε_i assigned to each vertex. If the system is invariant under arrow reversal, the energies satisfy $\varepsilon_1 = \varepsilon_2$, $\varepsilon_3 = \varepsilon_4$ and $\varepsilon_5 = \varepsilon_6$. The exact solution is available for general ε_1, ε_3 and ε_5, and is given in terms of the quantity

$$\Delta = \frac{a^2 + b^2 - c^2}{2ab} \tag{2.11}$$

where a, b and c are the Boltzmann factors associated with ε_1, ε_3 and ε_5 respectively. This quantity has a great relevance in the analytic solution, because most properties of the six vertex model do not depend on a, b and c separately, but on their combination Δ. Three cases are of special interest:

1) The Ice model: $\varepsilon_1 = \varepsilon_3 = \varepsilon_5 = 0$

   The ice rule, according to which the arrows are arranged around the sites, is nothing but a topological constraint imposed to model the effective structure of the solid phase of water (hence its name). In all ice phases, in fact, each oxygen atom is tetrahedrically surrounded by four other identical atoms, and the hydrogen can randomly choose the oxygen to which to bound with, the only limitation being the fact that each oxygen can be bound only to two hydrogens (the water molecule is H_2O). Since all the six vertices are equivalent, only entropy, not energy, is involved in this particular realization of the six vertex model, so that it allows to calculate, for example, the residual entropy of ice at $T = 0$, which is not zero because of the amount of disorder resulting from the structure described above.

2) The KDP model: $\varepsilon_1 = 0$, $\varepsilon_3 = \varepsilon_5 \equiv \varepsilon > 0$

   KH_2PO_4 (potassium dihydrogenphosphate, in jargon KDP), a hydrogen-bonded crystal whose structure contains easily recognizable electric dipoles,

undergoes a ferroelectric phase transition at $T = 122K$. KH_2PO_4 is tetragonal with every phosphate group tetrahedrically surrounded by four other phosphate groups, where the hydrogens (that is, the protons) are located between each pair of phosphate groups, near one or the other, so that all the resulting structure is very similar to ice. But not all the vertices are equivalent now, since the lower temperature phase is ferroelectric, so that an easy suggestion by Slater[55] was to energetically encourage the 'ferroelectric' vertices 1 and 2, and to discourage all the others by raising their energies with respect to the first ones. In this case, the six vertex model presents a low temperature phase with complete ferroelectric order and correlation length $\xi = 0$, and a high temperature one with $\xi = \infty$. The transition from one phase to the other turns out to be first order, and occurs at $\Delta = 1$, that is when $a = b + c \ \rightarrow k_B T_C = \varepsilon / \ln 2$.

3) The F model: $\varepsilon_1 = \varepsilon_3 \equiv \varepsilon > 0$, $\varepsilon_5 = 0$

Rys[56] suggested to discourage vertices 1 to 4 in favour of 5 and 6, if one wanted to get an antiferroelectric order for the low-temperature phase. The high-temperature phase is the same as in the KDP model, however the transition becomes of infinite order, occurring for $\Delta = -1$, that is when $a + b = c \ \rightarrow k_B T_C = \varepsilon / \ln 2$.

The BCSOS model corresponds to the six vertex model in its F version, where ε equals the interaction energy J between atoms in each sublattice (isotropic in the x and y directions), while, as said before, interaction between the two sublattices are taken of infinite strength, thus allowing just for a height difference of ± 1. As shown by van Beijeren[50], this model can be thought of as the limit of a lattice

gas model on a bcc crystal lattice with strong nearest-neighbour interactions and much weaker next-nearest- neighbour interactions.

From the physical point of view, the complete low T antiferroelectric order of the F model corresponds here to the presence of vertices 5 and 6 only, thus, according to van Beijeren's construction, to a flat surface (one sublattice, for example, with all sites at height 1, the other all at 0). The rise in temperature is accompanied by the comparison as excitations of all the other vertices, that is of steps and adatoms on the surface, leading to the rough phase.

Being exactly solvable, all the properties of this Kosterlitz-Thouless phase transition are known. All the Renormalization Group predictions discussed in the preceeding section for the Discrete Gaussian model (which is in the same universality class as the BCSOS model), are confirmed, in particular the non-analytic behaviour of the free energy at the transition temperature, and the resulting absence of a heat capacity peak at T_R. However, a rounded anomaly is predicted to occur below T_R, due to a rapid continuous change in the surface disorder. In fact, roughening corresponds to an inverted XY model transition (i.e. with an inverted ratio J/T), where the appearance of defects which break short range order occurs above the critical point; the specific heat thus shows a maximum not at T_R but for $T \simeq 0.81 T_R$.

Further developments of van Beijeren's idea are due to Jayaprakash and Saam[57,58,59], and by Trayanov *et al.* [16], who specialize to an anisotropic version of the BCSOS model in order to account for the roughening of the (110) face of fcc crystals. This model is again exactly solvable when mapped onto the six vertex model. The details are left to chapter 3, when the Kohanoff-Jug-Tosatti model is introduced and studied, since the initial underlying physical considerations are the same for all these models.

2.2 Phenomenological studies and experimental evidence

2.2.1 Wulff's construction and the equilibrium shape of crystals

If from the statistical point of view one can characterize the roughening transition by the divergence of the height-height correlation function, from the phenomenological point of view one can associate it with the disappearance of a cusp in the so-called γ-plot, microscopically corresponding to the vanishing of the step free energy of the roughening surface.

The γ-plot is nothing but the polar plot of $\gamma(\hat{\mathbf{n}})$, i.e. the surface free energy γ as a function of the surface orientation $\hat{\mathbf{n}}$. Since the crystal, at a fixed volume, tends to achieve minimum total energy by suitably distorting its shape, there is a clear relation between $\gamma(\hat{\mathbf{n}})$ and the equilibrium crystal shape, first mathematically expressed by Wulff[60] in 1901 and completed by Herring[61] 50 years later. Wulff's construction permits to draw the equilibrium shape of the crystal starting from the knowledge of its free energy, or to reconstruct the latter from measurements of the former[62]. In particular, cusps at certain orientations of the γ-plot correspond to facets in the crystal shape, i.e. regions with zero curvature.

In general, the surface of a crystal in equilibrium consists of these facets, which are macroscopically flat and, at $T \neq 0$, of rounded parts between them. The facets are crystal faces in a smooth phase, i.e. below their roughening temperature and the rounded parts may be considered as constructed from infinitesimal pieces of rough faces. So, if the temperature is raised through $T_R(\hat{\mathbf{n}})$ (the roughening temperature of a face of orientation $\mathbf{n}$), the facet size shrinks to zero and the orientation $\mathbf{n}$ becomes part of a rounded area. Therefore, for the relation between the γ-plot and crystal shape, the roughening transition can be characterized by

the disappearance of a cusp from the γ-plot.

If now one wants to obtain an expression for the surface free energy γ (or f) as a function of orientation from a simple model, one is lead to study a vicinal surface, which is a surface under a tiny angle from a low index one. Adopting an SOS model on a square lattice to describe the situation, one can build at $T = 0$ the vicinal surface of orientation $(p, 0, 1)$, with $|p| \ll 1$, by creating p straight steps per unit length in the x direction on the (001) flat facet[46]. At non zero temperature the straight steps will develop kinks, and the terraces between them will develop thermal excitations in form of small bumps (adatoms) and pits (vacancies). The surface free energy of the surface per unit area is expressed as

$$f(p, 0, 1) = f(0, 0, 1) + f^S(0)|p| + \ldots \tag{2.12}$$

where $f^S(\varphi)$ is the free energy associated to a step forming an angle φ with the y direction per unit length and unit step height, and the dots stand for entropic contributions (ignored because of no interest in what follows), and interaction terms between steps (neglected in the limit $|p| \to 0$ because of order p^2 or greater).

If $f^S(0) > 0$, one sees from (2.12) that $f(p, 0, 1)$ exhibits a cusp as a function of p at $p = 0$. According to the preceeding discussion, this implies that the equilibrium crystal shape exhibits a facet in the (001) direction; furthermore it can be proved that the diameter of this facet in the y direction is proportional to $f^S(0)$. More generally, $f(\lambda \cos\varphi, \lambda \sin\varphi, 1)$ as a function of λ exhibits a cusp at $\lambda = 0$ under a slope given by

$$\left.\frac{\partial f}{\partial \lambda}\right|_{\lambda=0} = f^S(\varphi) \tag{2.13}$$

But, since the roughening transition macroscopically corresponds to a facet in the

equilibrium crystal shape shrinking to zero at T_R, that is to the disappearance of a cusp in the Wulff's plot, one can conclude from (2.13) that the roughening transition can be characterized microscopically by the vanishing of the step free energy for steps on the facet that roughens up. Once this happens, steps of arbitrary length will form spontaneously on this face, so that the height $h(r_{00})$ of a chosen point on the interface will fluctuate more and more about its average value, thus causing the divergence of the height-height correlation function, as results from the statistical mechanics definition of roughening of formulæ (2.5)–(2.10).

Experimental observations of roughening are generally difficult, since the transition is an infinite order one, with no specific heat peak at T_R, for example, and no characteristic line in the diffusion spectrum, just a characteristic shape which can be observed only if inelastic scattering is carefully subtracted. Certain groups of researchers have thus directed their attention to the measure of the equilibrium shape of crystals, bun even in this case difficulties arise since, as pointed out by Lipson[63], none of the well known symmetric shapes of natural minerals represents what the crystal would look like were it in thermodynamic equilibrium with its surroundings. They are all growth shapes, "frozen" because their relaxation rates increased so much with size that only in geological times they could achieve their final form. For these reasons, the roughening transition was experimentally observed only in the early 1980s, more or less 30 years after the first theoretical developments, on the surface of helium crystals[64,65,66].

Solid ^4He is the only material known whose macroscopic crystals can achieve a thermodynamic equilibrium shape within an experimentally convenient scale of time, due to two main features: the large effective thermal conductivity together

with the near absence of latent heat at the solid-liquid cohexistence line.

Various roughening transitions where so observed on the different faces of hcp helium crystals just by looking at the sample (either via light filtering or interferographic techniques[63,67,68]) and detecting the disappearance of a facet as T_R is reached. The three transitions so far observed are at $1.28K$ on a c-facet (0001), $0.95K$ on a $(1\bar{1}00)$ and $0.35K$ on s $(1\bar{1}01)$.

A property of the crystal which is strongly affected by the state (smooth or rough) of the interface, is the growth rate. It can be shown, for a model of a surface square lattice of spacing a, that this quantity is proportional to $\exp\{-4a^2[f^S(T)]^2/k_BT\delta\mu\}$, where $f^S(T)$ is the step free energy and $\delta\mu$ is the chemical potential difference per atom between the solid and the fluid phase. By measuring the growth rate of the c-facet as a function of $\delta\mu$ in a small temperature region just below T_R, Wolf *et al.* [69] and Gallet *et al.* [70] were able to investigate the critical behaviour of $f^S(T)$ near T_R. The result of these experiments was the definite confirmation of the prediction of the SOS models, i.e. of eq. (2.3), as well as the most accurate determination of the value of T_R for this orientation, $1.28K$.

Other experimental evidence on the equilibrium shape of crystals is provided by Heyraud et Métois[62] on small lead crystallites. For the above-mentioned equilibration difficulties, their sizes are 3 orders of magnitude smaller than those of helium crystals ($\sim \mu$m instead of $\sim$ mm), and the equilibration times are about 2 orders of magnitude greater ($\sim$ 10 hours instead of few minutes). Nonetheless, the crystallites were visualized by scanning electron microscopy, 3 facets at least were recognized, the (100) , (110) and the (111) , and employing the Wulff theorem, the surface free energy as function of the orientation was obtained from the clear photographs of crystal shapes for four temperatures confirming, for example, the decrease of this quantity with temperature.

2.2.2 Universal behaviour of crystal shapes

As pointed out by Rottmann *et al.* [71], the equilibrium crystal shape is nothing but a geometrical expression of interfacial thermodynamics. From the knowledge of the free energy per unit area $f(T, \hat{\mathbf{n}})$ on the interfacial orientation $\hat{\mathbf{n}}$, Wulff's construction permits to determine the equilibrium shape $r(T, \hat{\mathbf{m}})$, where r is the radius to the interface from the center of the crystal in the direction $\hat{\mathbf{m}}$. Andreev[72] made explicit the sense in which Wulff's construction is simply a Legendre transform, so that f, $\hat{\mathbf{n}}$ and r, $\hat{\mathbf{m}}$ are thermodynamically conjugate pairs and the relation $\hat{\mathbf{n}}(T, \hat{\mathbf{m}})$ defined by the Wulff's construction is an equation of state. From this perspective, $r(T, \hat{\mathbf{m}})$ is a free energy as well as f, and its singularities define an interfacial phase diagram. But at fixed T, the singularities in r are simply the crystal edges. In the intermediate temperature regime, where both facets and curved interfacial regions are present, the two meet at edges which may be either sharp (with a slope discontinuity) or smooth (no slope discontinuity). Near a smooth edge the shape of the curved interface varies as

$$z = A(x - x_C)^{\theta} \quad + \quad \text{higher order terms} \tag{2.14}$$

where $z = 0$ for x extending up to x_C, the edge position, represents the flat facet, and the rounded regions start at x_C. For what was just observed, the behaviour near a smooth edge is critical behaviour, and θ is a critical exponent. While mean field calculations[72] provide the value $\theta = 2$, Renormalization Group calculations including fluctuations[73] and exact solutions [59] lead to the universal prediction

$$\theta = \frac{3}{2} \tag{2.15}$$

universal in the sense that it is independent of temperature and facet orientation.

Careful analysis of crystal shape data near a smooth edge for Pb crystallites performed by Heyraud and Métois[71] lead to the value $\theta = 1.60 \pm 0.15$, while other experiments by Carmi *et al.* [74] on helium crystals provided a best fit value of $\theta = 1.55$, both in accordance with the Renormalization Group prediction (2.15), and inconsistent with the mean field result.

It is worth noting that the value $\theta = \frac{3}{2}$ is reached also from another way: a simple model of step-step interaction leads to a $|p|^3$ term in addition to those already present in (2.12), so that the expression of the free energy per unit area, for small p, becomes

$$f(p,0,1) = f(0,0,1) + f^S(0)|p| + C|p|^3 + \dots \tag{2.16}$$

Performing a Wulff's construction from (2.16), one obtains the behaviour

$$(z - z_C) = -\frac{2}{3}C'|x - x_C|^{\frac{3}{2}}$$

where again the result shows $\theta = \frac{3}{2}$.

Another striking property of the Renormalization Group theory[58,59], also connected with the interface shape, is that the radius of curvature for the surface element with the orientation of the roughening facet jumps from ∞ (the flat facet for $T < T_R$) to the universal value

$$R_C = \frac{\pi}{2}\frac{z_0(k_B T_R)}{\gamma_0 a_\perp^2} \tag{2.17}$$

where z_0 is the distance of the crystal center from the tangent plane at the surface, and γ_0 is the surface tension per unit area (for an anisotropic surface R_C has to

be replaced by $(R_C^1 R_C^2)^{1/2}$, R_C^1 and R_C^2 being the principal radii of curvature[75]). A well-known analog of the result (2.17) is the universal jump in superfluid areal density at superfluid onset in ^4He films, but it is not at all an unexpected connection between two systems which apparently have nothing in common. In fact the XY model describing the transition in ^4He films is dual, as seen, to SOS models exhibiting roughening. Experimental confirmation of (2.17) has been obtained, for example, by Wolf *et al.* [69].

2.2.3 Other experiments

Other experimental evidence on the roughening transition is provided by atom beam diffraction experiments, mainly performed on metal surfaces by the Saclay group[76,77,78] and by the Seattle group[79,80,81]. Both groups chose to investigate the roughening of stepped metal surfaces. The first focused on Cu(113), (115) and (117), all vicinals of (100), and found that while for close packed faces like (111) and (100) the data were consistent with a Debye-Waller factor for the decrease of the anti-phase peak intensity with temperature, it was not so for the vicinal surfaces where, from a certain threshold temperature up, a sudden decrease from the expected behaviour in the direction of a greater decrease of intensity was observed. This was interpreted as an occurrence of roughening on the surface, and the threshold temperature was considered a lower bound for T_R. Such data have clarified, as a general feature, that $T_R(117) < T_R(115) < T_R(113)$. The less close packed the surface is, the lower its roughening temperature will be, because roughening on stepped surfaces is mainly due to formation of defects (kinks, adatoms and vacancies) on the preexisting steps, and their creation is easier on more open surfaces than on more compact ones. Successive refinements of the method[78], together with an empirical model of a stepped surface, provided

a definite value for the roughening temperature of the (115) face of Cu, for example ($T_R = 380K$), and for the step-step interaction energy.

Similar considerations were made by the other group, who measured the roughening temperature on Ni stepped surfaces, obtaining $T_R(113) = 750 \pm 50K$, $T_R(115) = 450 \pm 50K$, $T_R(117) = 400 \pm 50K$ (and a lower bound for the roughening temperature of the (100) face, $1400K$, but no real evidence of its actual occurrence). The decrease in T_R with the increase of the Miller indices of the vicinal is interpreted also in terms of the step-step interaction energy, so that the small reduction in T_R in correspondence with a further increase in the terrace widths (i.e. from (115) to (117)) is an indication of the short range of the step-step repulsive interaction, which falls off rapidly with distance and does not change considerably any more between 6 and 9 Å (the mean terrace width of (115) and (117) respectively).

Chapter 3

Models for surface reconstruction and roughening

A number of models have been proposed so far in order to describe the roughening of reconstructed noble heavy metal (110) surfaces, that is, to study the link between two phenomena which have a priori no reason to be thought of as separate. One of these models is the object of our study, and will be described in detail in section 3.5, while the others will be briefly reviewed here.

3.1 The model of Levi and Touzani

The starting point of Levi and Touzani[20] is the six vertex model in its anisotropic version, as already proposed by Jayaprakash and Saam[57,58,59] for the study of the (110) face of fcc crystals. The antiferroelectric phase (i.e. the unreconstructed surface) corresponds to the inequality $\varepsilon_5 < \varepsilon_1 < \varepsilon_3$ for the vertex energies, whereas the missing-row structure appearing in the heavier metals, translated into a vertex language, is made of an ordered array of rows of vertices 1, 5, 2 and 6, where vertices 1 form the ascending slopes, 5 the ridges, 2 the descending slopes and 6 the valleys, so that no two adjacent vertices belong to the same type. Thus, it would look natural at first to increase the density of vertices 1 and 2 by changing the order of the inequality to $\varepsilon_1 < \varepsilon_5 < \varepsilon_3$. Unfortunately, this change brings the

six vertex model to the ferroelectric phase, the structure of which is disappointingly simple: up to the transition all vertices are type 2 (or 1, which is the same). This situation does not correspond to reconstruction but to a constant descent in the surface with a slope $\alpha = \arccos\sqrt{2/3} = 35°16'$, i.e. to an effective replacement of the (110) surface by a (111) surface. In order to really obtain a missing row ground state, the six vertex model has to be modified, and it can be done mainly in three ways: 1) by introducing, along with the energy inequality $\varepsilon_1 < \varepsilon_5 < \varepsilon_3$, a repulsive interaction ε_{11} between adjacent vertices of the same type, to discourage the creation of a (111) facet; 2) by still considering $\varepsilon_5 < \varepsilon_1 < \varepsilon_3$, which favours the unreconstructed (110) surface, but encouraging reconstruction by introducing a repulsive energy ε_{56} between adjacent vertices of type 5 and 6; 3) by introducing both ε_{11} and ε_{56} (e.g. of the same strength).

However, in order to perform a transfer matrix finite-size scaling, a drastic simplification must be employed, that is to consider the interactions between vertices in a direction only, and to put them to zero in the other. All the three models give qualitatively the same results, in terms of the parameter $\gamma = (\varepsilon_1 - \varepsilon_5)/\varepsilon_{\text{int}}$ (where $\varepsilon_{\text{int}} = \varepsilon_{11}$ in model 1, $\varepsilon_{\text{int}} = \varepsilon_{56}$ in models 2 and 3). They find that for very low values of γ the ground state forms a faceted (111)-like phase (a "macroscopic sawtooth"), then for increasing γ a (2×1) reconstructed phase, and finally a (1×1) unreconstructed phase. They are able to locate the roughening transition temperature of their models by looking at the vanishing of a quantity strictly connected to the step free energy, drawing in the end a phase diagram where a smooth phase (of one of the three forms listed above, according to the value of γ) occurs at low temperature a rough one at higher temperature.

The results obtained contrast the existence of other phase transitions, as suggested by some authors, like a possible order-disorder transition (for example

of Ising character) occurring at intermediate temperatures from the (2×1) phase to a floating one with presence of higher order reconstructions or directly to a rough phase. In the model of Levi and Touzani, the roughening transition remains in the Kosterlitz-Thouless universality class.

3.2 The model of Villain and Vilfan

Villain and Vilfan[14,82], subsequent to the LEED experiments of Campuzano *et al.* [31] suggesting an Ising behaviour of the Au(110) deconstruction transition, proposed a model to investigate this system.

The (110) surface is anisotropic, the "hard" direction being the missing-row direction (hereafter denoted by y), the "weak" one being that perpendicular to it (x). If defects are introduced on the (2×1) reconstructed surface at $T > 0$, they will show up as line defects in the y direction (that is, breaking weak bonds rather than strong ones) resulting in chains of nearest neighbour atoms. The structure is thus simply characterized by a cross section of the sample perpendicular to the y direction, as in figure 3.1.

The reconstructed ground state has a two-fold degeneracy, since the missing rows can be chosen in two possible ways, odd rows or even rows, therefore Villain and Vilfan expect the transition to be in the Ising universality class, just as in Bak[34]. On the (2×1) surface, the Ising variable may be thought of as the parity of the missing row, and a domain wall may be defined as a defect dividing two regions of the surface with opposite Ising order parameter. That is, if even rows are missing on the left hand side of the wall, odd rows are missing on the right hand side, and conversely.

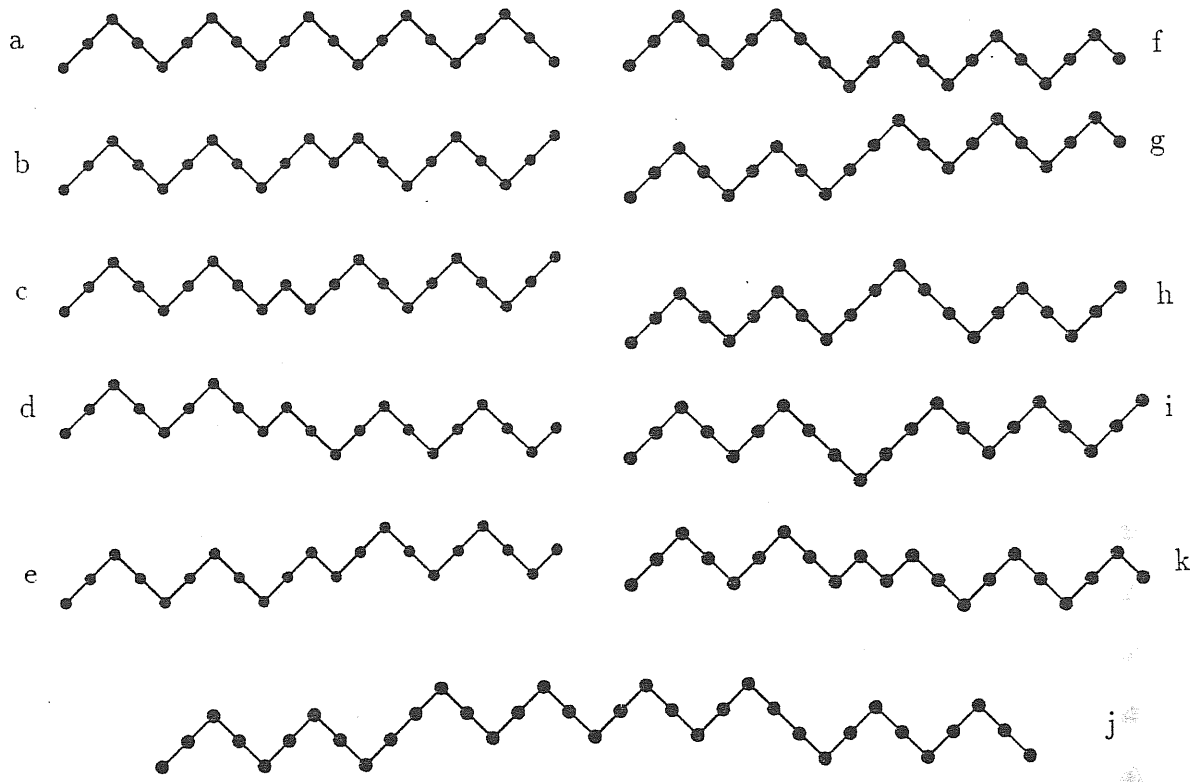

Fig. 3.1: Side view of the (2×1) reconstructed (110) surface. a) Ideal surface without defects; f,g) elementary excitations characteristic of a roughening transition; h,i) Ising excitations; d,e,k) higher energy roughening excitations; b,c,j) higher energy Ising excitations.

In an ordinary Ising model, order is destroyed by these domain walls, while in the SOS models roughness is created by steps. Villain and Vilfan noticed that in the case of Au(110), both domain walls (fig. 3.1–b,c) and steps (fig. 3.1–d,j) might be expected to be relevant, and assigned different energies, η to domain walls and ε to steps, with the simplifying assumption that all domains of the same type (all kind of walls as well as all kind of steps) have the same energy. Moreover, since a domain wall is made of two steps, they considered $\eta = 2\varepsilon$.

When the temperature is raised, the only change in this picture is that these line defects are no more straight, but develop kinks which break the hard bonds, so that a very high contribution W_0 in energy is required, with $W_0 \gg \varepsilon$. All other structures of fig. 3.1 were considered to be higher in energy, thus neglected.

Within this approach, they calculated the partial partition function Z_I of states with one domain wall, and located the Ising transition temperature T_C at the point when Z_I equals Z_0, the partition function of the ground state. The same procedure was used to locate the roughening transition temperature T_R, taking into account only step-like defects. Only the lowest between T_C and T_R makes sense, and determines the nature of the (2×1) deconstruction transition. They established that $T_C < T_R$, so that the deconstruction transition belongs to the Ising universality class, in full agreement with Campuzano's results. Then the roughening transition should occur at a reasonably higher temperature, so that Ising exponents are not blurred with roughening effects, but it might belong to the Ising universality class as well.

In a very recent version of their study, however, Villain *et al.* [82,83] reconsidered the energetics of their model, recognizing in type 3.1–f,g the lowest energy steps, and in 3.1–h,i the lowest-energy domain walls, in accordance with Ercolessi *et al.* [27,28] whose calculations showed that the (3×1) phase was only slightly

shifted upwards in energy with respect to the (2×1). With this change, the answer to the question of the nature of the transition is not so clear as before, especially in the absence of reliable estimates for the energy parameters associated with each defect.

Nonetheless, they presented a new model for a roughening transition which lies outside the Kosterlitz-Thouless universality class, just by considering Ising order on the surface and the behaviour of domain walls, i.e. of steps. Up (fig. 3.1–e,g) and down (fig. 3.1–d,f) steps can be represented by lines and distinguished by arrows, but for topological reasons two steps of identical sign cannot cross, while two steps of different sign can cross and a free energy U may be assigned to each crossing (i.e. to each lattice site common to two steps). The surface is so traversed by lines which oscillate around the y direction due to the presence of kinks on them, but which present no overhangs, for topological reasons too: it is thus natural to replace the y coordinate with time, and to think of them as the trajectories of spin $\frac{1}{2}$ fermions, subject to a two dimensional Hubbard Hamiltonian. The Hubbard model was exacty solved by Lieb[84] in 1968, but only some special cases are taken into account ($U = 0$, $U = \infty$) by Villain *et al.*: in the latter case, they get very unusual exponents for the transition driven by steps, $\alpha = \nu = \chi = \frac{1}{2}$, which places it outside the Kosterlitz-Thouless (but also outside the Ising) universality class.

With their model, they do not expect to account directly for the Au(110) phase transition, but simply to show that roughening can occur with an upper critical dimension (4 instead of 3) and critical exponents which are not those of the SOS model.

3.3 The model of den Nijs

Den Nijs[85,86] has recently introduced in the field a new concept, that of a preroughening transition between an ordered flat (OF) phase and a disordered flat (DOF) phase. The difference between the DOF phase and the rough one is that the former contains an array of steps with positional disorder but long range up-down order (i.e. up and down steps strictly alternate), so that the surface remains flat on average, while the latter shows the usual height fluctuations. The preroughening transition is so identified by the vanishing of the free energy for the creation of steps, although the energy associated with the tilting of the surface does not vanish. Its vanishing will instead locate the true roughening transition which lies in the Kosterlitz-Thouless universality class as usual.

A fairly complex phase diagram is then proposed, with four different possibilities for the transitions of the (110) surface of noble metals, the discriminating parameter being the energy difference ΔE between the ordered flat and reconstructed surfaces. For $\Delta E \gg J$, as it is supposed to be the case for Cu and Ni, there is a direct transition (of the Kosterlitz-Thouless type) from the OF phase to the rough one. For ΔE still positive, but small, den Nijs proposes a preroughening transition from OF to DOF, and successively for higher temperatures the usual roughening one, choosing Ag and Pd as candidates for this type of path. The third possibility is similar to that conceived by Villain and Vilfan[14], and should hold for Ag and Pt: an Ising deconstruction transition, followed by a roughening transition (still in the Kosterlitz-Thouless universality class). The fourth possibility is an interchange in the order of these two transitions, which ends first in roughening simultaneously inducing deconstruction. Further analysis led den Nijs to propose a "four state chiral clock-step model" in order to account for the behaviour of the

system near the multicritical point in which the Ising and the roughening transition lines meet. The missing row structure is in fact characterized by four possible locations of the top rows, while arrows can be assigned to domain walls of the resulting four state clock model, in a way similar to that of Villain and Vilfan. The intersections of these arrows suggest to define on them a six vertex model, so that the resulting partition function is weighted by a six vertex one, and additional chirality Δ is imposed in order to account for differences in energies between "clockwise" walls (like those of fig. 3.1–d) and "anti-clockwise" ones (like those of fig. 3.1–f).

The model is quite complex, and up to now just the $\Delta = 0$ case has been examined via a finite-size transfer-matrix method: the result seems to be a simultaneous coexistence of Ising and roughening critical behaviour, not only at the multicritical point but all along the roughening driven deconstruction line too. Further work is needed also to clarify the role that supersymmetry and conformal invariance considerations may play in the game.

3.4 The model of Jug and Tosatti

The model proposed by Jug and Tosatti[17,87,18,19] is described in terms of an anisotropic SOS Hamiltonian of discrete column height variables $\{h_i\}$ and $\{l_i\}$, each set of heights being defined on one of two interpenetrating sublattices corresponding to the first two inequivalent surface layers, like in van Beijeren's construction. The Hamiltonian is, then

$$
\begin{aligned}
H/J =& \alpha \sum_i [(h_i - l_i)(l_i - h_{i+\hat{\mathbf{x}}}) + (l_i - h_{i+\hat{\mathbf{x}}})(h_{i+\hat{\mathbf{x}}} - l_{i+\hat{\mathbf{x}}})] + \\
&+ \sum_i [(h_i - l_i)(l_i - h_{i+\hat{\mathbf{y}}}) + (l_i - h_{i+\hat{\mathbf{y}}})(h_{i+\hat{\mathbf{y}}} - l_{i+\hat{\mathbf{y}}})] + \\
&- \beta \sum_i (h_i - h_{i+\hat{\mathbf{x}}})^2 + \Delta H(\alpha)/J
\end{aligned}
\tag{3.1}
$$

where

$$
\Delta H(\alpha)/J = (1+\alpha) \sum_i [(h_i - l_i)^2 + (l_i - h_{i+\hat{\mathbf{x}}})^2]
$$

is an ordinary nearest neighbours SOS contribution needed in order to fix J as the effective step energy cost in the y direction. Here, as usual, x and y are respectively the soft and hard (missing-row) directions and $\hat{\mathbf{x}}$ and $\hat{\mathbf{y}}$ their unit vectors. The first two terms in eq. (3.1) induce at sufficiently low temperatures (so that the height jumps between two nearest neighbour sites $h_i - l_i \equiv s_i$ are constrained to be ± 1), a ferromagnetic ordering in the "spins" s_i, corresponding to the ordered (1×1) structure. The parameter α $(0 < \alpha < 1)$ measures the local anisotropy in the x vs y directions. The next term corresponds to next-nearest-neighbour interactions, inducing a more stable missing row profile in the x direction for $\beta > 0$.

Ground state energy considerations show that in this model $E^{\circ}_{(1\times1)} \leq E^{\circ}_{(2\times1)}$ for $\beta \leq \frac{1}{2}\alpha$. Hence, at zero temperature it behaves like an Anisotropic Next Nearest Neighbour Ising (ANNNI) model in terms of the spins s_i, in that there is a switch from the ferromagnetic (1×1) phase to the $\langle + + - - \rangle$ (2×1) phase as a function of the parameter $\kappa = 4\beta - 2\alpha$. On the other hand, the true symmetry of the model is that of an SOS model, so it is likely to exhibit a roughening transition. The model so has all the needed properties to properly describe the

noble metal (110) surfaces, together with the presence of higher energy, higher order reconstructions.

Two possible solutions can be attempted: the first is an analytic low-temperature investigation[17] of the properties of the model near the multiphase point at $\kappa = T = 0$, where both (2×1) and (1×1) phases cohexist, together with all the reconstructed $(n \times 1)$ phases, with $n = 3, 4, \ldots$, which are all degenerate ground states provided only the first-layer $n-1$ rows are missing (these structures are called "shallow reconstructions"). The different (actually ∞) domain walls between all these structures are then considered within a free-fermion approximation, as done by Villain and Bak[88] for the 2D ANNNI model.

The second possibility is a transfer-matrix finite-size scaling[87,18,19] performed on Hamiltonian (3.1) with the additional (six vertex) constraint of ± 1 height jumps only between nearest neighbours heights (restricted Jug-Tosatti model), which should not affect the main conclusions of the investigation, at low and intermediate temperatures at least.

Both the approaches agree in predicting $T_C < T_R$, T_C being the deconstruction temperature, T_R the roughening one. However, T_C now strictly denotes a pseudo-transition, characterised by a non-divergent peak in the heat capacity, while T_R denotes a transition with, possibly, variable critical exponents, so that its universality class is not necessarily Kosterlitz-Thouless any more. Between the two transitions a sequence of disordered incommensurate phases, arising from the presence of the shallow reconstruction states degenerate at $T = 0$, is present as a precursor to roughening. Physically, the lower transition at T_C should correspond to a proliferation of defects in the missing-row structure, while it is only at T_R that these defects become unbound. The model also predicts two transitions, one of order-disorder character and a roughening transition at a higher temperature

for fcc (110) surfaces which do not reconstruct. Then, precisely at the point where reconstruction sets in ($\kappa = 0$) the disordering temperature appears to vanish, unlike the roughening one, so that not only the physics of, say, Au(110) , but also that of Cu(110) may be accounted for by the Jug-Tosatti model, by employing for the latter a small negative value of κ, which ensures a (1×1) phase at low temperature.

3.5 The model of Kohanoff, Jug and Tosatti

3.5.1 A description of the model

The Jug-Tosatti model, unlike real pure (110) surfaces, contains an inevitable intrinsic asymmetry between the h and l sites, so that its physical realization would be obtained, e.g., in an ordered alloy (e.g. CuAg) or in a pure metal surface with an adsorbed overlayer, rather then in pure metal surfaces. However, the authors expect the main physics to carry over also to pure surfaces, as the $h - l$ asymmetry can be thought of as a weak external field added to a fully symmetric Hamiltonian, the main effect of which should be a mere rounding of any otherwise sharp transition. Nonetheless, this asymmetry is an additional and unwanted feature of the model, and its elimination leads us to write the following Hamiltonian

$$\begin{aligned} H/J = & \sum_i (h_i - h_{i+\hat{\mathbf{y}}})^2 - K_2 \sum_i (h_i - h_{i+\hat{\mathbf{x}}})^2 + \\ & + \frac{K_3}{2} \left[\sum_i (h_i - h_{i+\frac{3}{2}\hat{\mathbf{x}}+\frac{1}{2}\hat{\mathbf{y}}})^2 + \sum_i (h_i - h_{i+\frac{3}{2}\hat{\mathbf{x}}-\frac{1}{2}\hat{\mathbf{y}}})^2 \right] \end{aligned} \tag{3.2}$$

where the two sublattices are treated exactly in the same way, i.e. with the same

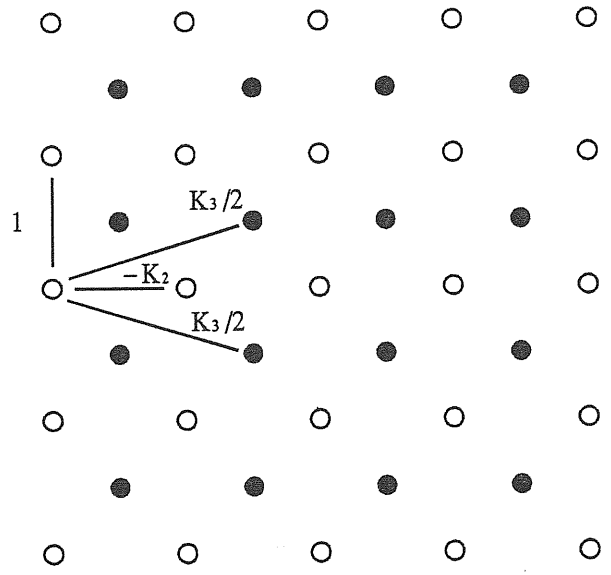

Fig. 3.2: The scheme of the couplings between sites in the KJT model. The parameters are expressed in units of J.

couplings between sites belonging to one or the other of them: h_i is the height variable, and the index i runs on both the two sublattices. The y direction in, as usual, the hard one (that of the missing rows), $\hat{\mathrm{x}}$ and $\hat{\mathrm{y}}$ are the unit vectors.

The interaction J_0 between nearest neighbours sites is taken to be infinitely strong, which means that the additional six vertex constraint is imposed on Hamiltonian (3.2), while the interactions in the rectangular unit mesh of each sublattice, J and $JK_2 \equiv J_2$ are anisotropic, with the relation $J > J_2$. This description is meaningful only because of inward relaxation of the top layer: without that relaxation, the assumption $J_0 = \infty$ would be inappropriate, because for an fcc crystal, in the absence of relaxation and for pairwise potentials, $J_0 = J_2$ (or even $J_0 < J_2$ if outward relaxation takes place !).

An additional third-neighbour interaction $JK_3 \equiv J_3$, the relevance of which will be described below, is included in the model. The geometry of the coupling is described in figure 3.2, where for the sake of simplicity the lattices are taken to be squared instead of rectangular, the anisotropy being introduced through the coupling strengths in one and in the other direction. If on one sublattice (say, the white one) the heights can assume only odd values, on the other (the black one) they can assume only even values, due to the presence of the constraint. The height jumps between nearest neighbour sites are so restricted to be ± 1, which permits to associate to each bond connecting the two sublattices a spin variable s_i. This is done as follows: the spin is always defined as the height difference between white and black sublattices, i.e. if the site on the white sublattice is above the black one, the spin takes the value $+1$, and viceversa. The spin analogy makes Hamiltonian (3.2) similar to an ANNNI model[34], but the equivalence is only apparent, because excitations in KJT model involve the flipping of spins in groups of four, while in the ANNNI model any single spin can be reversed. The height conservation constraint is actually stronger than it seems at a first glance, causing the universality class of the model to shift from an Ising one to a Kosterlitz-Thouless one, at least for some values of the energy parameters.

3.5.2 Ground state considerations

It is easy to understand the main features which have led to Hamiltonian (3.2) by examining it at $T = 0$ and determining which different ground state configurations show up by varying the value of the energy parameters. At $T = 0$, the first term $\sum_i (h_i - h_{i+\hat{y}})^2$ assigns an energy penalty to neighbouring sites willing to be at different heights on each sublattice in the hard y direction, encouraging in this way the formation of uninterrupted rows in this direction. The second

term $-K_2 \sum_i (h_i - h_{i+\hat{x}})^2$ has either a similar or opposite effect on the surface configurations in the x direction, according to whether $K_2 < 0$ or $K_2 > 0$. A negative value for K_2 induces the formation of rows also in this direction, thus of an overall flat (1×1) surface. A positive value would encourage the surface to perform a constant descent (or rise) in the x direction instead, so that the (110) starting surface is effectively replaced by a (111) system, which can also be described in terms of a $(\infty \times 1)$ reconstruction.

But since the model has been concocted to fit (110) noble metal surfaces and their reconstructions, a (2×1) stabilizing term is needed: this is represented by $\frac{K_3}{2}\left[\sum_i (h_i - h_{i+\frac{3}{2}\hat{x}+\frac{1}{2}\hat{y}})^2 + \sum_i (h_i - h_{i+\frac{3}{2}\hat{x}-\frac{1}{2}\hat{y}})^2\right]$, which, with $K_3 > 0$, acts to interrupt the descent of the surface induced by a negative K_2 by raising third neighbour sites in the x direction to height values as near as possible (hereafter, unless otherwise stated, it will always be considered $K_3 \geq 0$).

A ground state phase diagram is easy to draw, provided the energies of all the possible $(n \times 1)$ reconstructions are calculated and compared. The $(n \times 1)$ reconstruction is intended to be a structure showing a periodicity of n sublattice sites in the x direction, but no broken bonds in the y direction, so that the y rows are preserved in their lengths. Its side view along the y direction is of a sawtooth configuration.

If $\mathcal{N} = 2N_xN_y$ is the total number of sites (the factor two arising due to the presence of the two sublattices), the result is, apart from a constant contribution E_0 which can be neglected by suitably fixing the zero of energies,

$$
\begin{aligned}
E_{1\times1}/J\mathcal{N} &= K_3 \\
E_{2\times1}/J\mathcal{N} &= -2K_2 + K_3 \\
&\vdots \\
E_{n\times1}/J\mathcal{N} &= -4\frac{n-1}{n}K_2 + \frac{9n+16}{n}K_3 \\
E_{\infty\times1}/J\mathcal{N} &= -4K_2 + 9K_3
\end{aligned}
\tag{3.3}
$$

It is easy to show that three distinct cases are possible for the ground state, just depending on the value of a new parameter $K = \frac{K_2}{K_3}$:

1) $K < 0$: the ground state is (1×1)

2) $0 < K < 4$: the ground state is (2×1)

3) $K > 4$: the ground state is $(\infty \times 1)$

and the points $K = 0$ and $K = 4$ are points of coexistence of two difference phases. As noted before, the sign of K_2 has a primary influence in deciding if the surface will remain flat (1×1) or will be replaced by a sloping $(\infty \times 1)$. A value of K_3 greater than $\frac{1}{4}K_2$ is sufficient to stabilize the (2×1) missing row reconstructed phase at the expenses of the $(\infty \times 1)$ phase.

It is worth noting that, at fixed K, the model assigns higher energies to all possible "shallow reconstructions", which instead play a significant role in the Jug-Tosatti model (see section 3.4). This rules out the possibility of these phases to be degenerate with the actual ground state, which has instead a simpler structure.

It is also possible to enrich Hamiltonian (3.2) by enlarging the number of interactions, in order to include the fourth, fifth,..., neighbours too. For example, by adding a term of the form

$$
H_4 = K_4 \sum_i (h_i - h_{i+2\hat{\mathbf{x}}})^2
$$

which represents a fourth neighbours interaction, one gets for the ground state a bidimensional phase diagram in terms of the variables $\frac{K_2}{K_3}$ and $\frac{K_4}{K_3}$ which, in addition to (1×1) , (2×1) and $(\infty \times 1)$ phases, also contains a (3×1) region. It is probable, moreover, that by adding a fifth neighbours interaction, a (4×1) region in a three dimensional phase diagram would appear, and so on (sixth neighbours interaction $\rightarrow$ (5×1) phase, etc ...). The additional terms have not been considered in what follows, but may turn out to be relevant if the object of study goes beyond the (2×1) deconstruction transition. A more detailed description of the reconstructed phase would result, as some (3×1) facets have been experimentally observed[22,6], and the energy of the (3×1) phase obtained in the "glue" model appears to be only slightly higher than that of the (2×1) phase.

3.5.3 Energy parameters

If one wishes to describe a real physical situation, e.g. Au(110), it is of course necessary to assign specific values to the energy parameters of the KJT model. The best way to do so is to consider numerical data for the energies of the various phases at $T = 0$ and to compare them with expressions like the (3.3), extracting in this way values for J, K_2 and K_3.

At first sight, one may think of obtaining the needed energies from experiments. However, the experimental data, even if available and free from accuracy problems, are generally taken at relatively high temperature. They are, in fact, surface free energies including entropic contributions not present in expressions like (3.3). For the purpose of the present study, $T = 0$ values are needed, and it is necessary to obtain the relevant surface energies from theory. The solution is provided by the calculations of Ercolessi *et al.* [27] for Au, which are based on the "glue" model reviewed in section 1.2.2.

The values represent energies per unit surface area, and are as follows:

$$\begin{aligned}
\mathcal{E}_{100} &= 128.5 \text{ meV/Å}^2 \\
\mathcal{E}_{110} &= 122.5 \text{ meV/Å}^2 \\
\mathcal{E}_{111} &= 96.6 \text{ meV/Å}^2 \\
\mathcal{E}_{2\times1} &= 107.4 \text{ meV/Å}^2
\end{aligned} \tag{3.4}$$

All these energies refer to relaxed $T = 0$ configurations, so that the resulting energy parameters will be "effective" values. Thus relaxation effects are taken into account in this way, the only possible for a two dimensional rigid lattice model.

The corresponding expressions obtained from Hamiltonian (3.2), under the form of energies per site, are

$$\begin{aligned}
E_{100}/\mathcal{N} &= 4J + J_3 + E_0 \\
E_{110}/\mathcal{N} &= J_3 + E_0 \\
E_{111}/\mathcal{N} &= -4J_2 + 9J_3 + E_0 \\
E_{2\times1}/\mathcal{N} &= -2J_2 + J_3 + E_0
\end{aligned} \tag{3.5}$$

where the additional energy constant E_0 is added, becoming another unknown variable to be fitted together with the others. A direct comparison between (3.4) and (3.5) is not yet possible, owing to the tilting of the (111) and (100) surfaces with respect to the reference (110) plane. The tilting angle is $\theta_{111} = \arccos\sqrt{2/3} \simeq 35°$ in the first case and $\theta_{100} = 45°$ in the second. Since, as observed, the energies provided by "glue" calculations are measured per unit area, a geometric factor $\mathcal{A}/\cos\theta$ must be inserted to multiply each value of (3.4). Here $\mathcal{A} = \frac{1}{2}\frac{\sqrt{2}}{2}a \cdot a$ is the area per atom of the (110) surface (for Au, the lattice parameter a equals

$a = 4.07$ Å $\rightarrow$ $\mathcal{A} = 5.85$ Å^2) and $\cos\theta$ arises from the projection of the (111) and (100) surfaces onto the (110) face. In this way, the values (3.4) transform into

$$\begin{aligned} E_{100}/\mathcal{N} &= 1064.3 \text{ meV} \\ E_{110}/\mathcal{N} &= 717.4 \text{ meV} \\ E_{111}/\mathcal{N} &= 692.9 \text{ meV} \\ E_{2\times1}/\mathcal{N} &= 629.0 \text{ meV} \end{aligned} \tag{3.6}$$

The comparison of (3.5) with (3.6) finally gives

$$\begin{aligned} E_0 &= 698.4 \text{ meV} \\ J &= 86.7 \text{ meV} \\ J_2 &= 44.2 \text{ meV} \\ J_3 &= 19.0 \text{ meV} \end{aligned} \tag{3.7}$$

and the values

$$\begin{aligned} K_2 &= \frac{J_2}{J} = 0.51 \\ K_3 &= \frac{J_3}{J} = 0.22 \end{aligned} \tag{3.8}$$

for the relevant parameters of Hamiltonian (3.2) (J in fact just fixes the temperature scale and E_0 is a constant).

Two aspects are worth noticing here. The first is the fact that the coupling in the hard direction is twice that in the soft one, so that the anisotropy expected from preliminary considerations is actually confirmed by the numerical values (3.8) and, moreover, the next-nearest-neighbour interaction strength K_3 is approximately half the nearest neighbour one K_2. In this way, $K = K_2/K_3 = 2.3$, which places

the ground state of the system in the (2×1) phase, as it was predicted for the Au(110) surface.

A self-consistency test for the parameters (3.7) is the calculation of the energy of the $T = 0$ (3×1) reconstructed phase, and its comparison with the "glue" values. The first procedure gives 111.0 meV/Å^2, the second 109.8 meV/Å^2, very similar values and, what is more, showing that the model reproduces the correct behaviour of the energies of the reconstructed phase, yielding a value for $E_{3\times1}$ which is slightly greater than $E_{2\times1}$, as previously observed with the "glue" data.

From now on, temperatures will be expressed in reduced adimensional units, each unit corresponding to

$$\frac{J}{k_B} = \frac{86.7 \text{ meV} \quad 1.6 \cdot 10^{-22} \ \mathcal{J}/\text{meV}}{1.38 \cdot 10^{-33} \ \mathcal{J}/K} = 1005.2 \ K \tag{3.9}$$

For future convenience, we provide values for the parameters K_2 and K_3 which make Hamiltonian (3.2) equivalent to the BCSOS Hamiltonian. It is easy to see that the requirements are

$$\begin{aligned} K_2 &= -1 \\ K_3 &= 0 \end{aligned} \tag{3.10}$$

Moreover, one can express the parameter J in terms of the energy ε of vertices 1, 2, 3 and 4 of the F model (the six vertex realization of the BCSOS model) in the following way. The energy per site corresponding to a (111) surface is, from (3.5) and (3.10)

$$E_{111}/\mathcal{N} = E_{\infty\times1}/\mathcal{N} = 4J$$

but a (111) surface is represented by an ordered array of vertices of type 1, so that the total energy of the surface per vertex is ε. One obtains the relation

$$\varepsilon = 4J \tag{3.11}$$

As seen in section 2.1.2, the roughening transition of the BCSOS model occurs at $k_B T_R = \varepsilon / \ln 2$, so that in terms of J it will result

$$k_B T_R = \frac{4J}{\ln 2} = 5.77J \tag{3.12}$$

while the peak of the specific heat will be located at

$$k_B T_P = 0.81 k_B T_R = 4.67J. \tag{3.13}$$

3.5.4 Order parameters

Since one of the objectives of this thesis is the study of the (2×1) reconstruction transition, it would seem useful to define some appropriate order parameter and to look at its behaviour with temperature. One of the possible ways to do so is to make use of the mapping of the surface into a spin configuration, as mentioned in section 3.5.1, and then construct an order parameter for the spins, following Landau and Binder[89,90,91,92,93]. While the spin configuration corresponding to the (1×1) phase is a simple ferromagnetic arrangement (fig. 3.3–a), that corresponding to the (2×1) phase is similar to the ANNNI model[88] ground state, and has a four-fold degeneracy, being equally described by the repeated sequences $\langle ++--\rangle$, $\langle +--+\rangle$, $\langle --++\rangle$ and $\langle -++-\rangle$ (fig. 3.3–b).

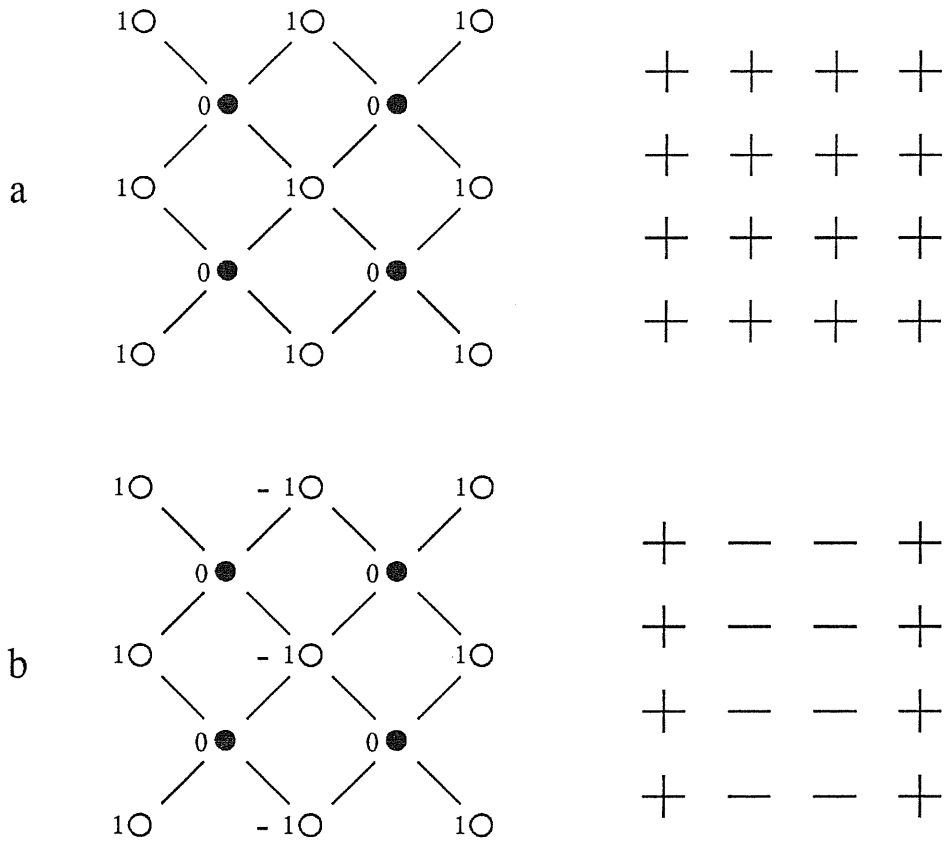

Fig. 3.3–a,b: The surface configurations (left) and the corresponding spin configurations (right) for the (1×1) (a) and (2×1) (b) phases. The numbers indicate the heights of the sites.

The idea is to divide the lattice into rows along the y direction, and then to group together rows whose distance is four lattice units, obtaining in this way four different groups of rows. It is possible now to define four "row magnetizations" by summing over all spins in each group of rows, as follows:

$$M_\Lambda = \frac{4}{\mathcal{N}'} \sum_{i \in \Lambda} s_i \ , \qquad \Lambda = 1,2,3,4$$

where Λ represents the index for the group of rows and $\mathcal{N}'$ is the total number of spins , that is $\mathcal{N}' = 4N_xN_y$. The four components corresponding to the structures listed above are

$$\begin{aligned}
\mathcal{M}_{\langle ++--\rangle} &= \frac{1}{4}\left[M_1 + M_2 - M_3 - M_4\right] \\
\mathcal{M}_{\langle +--+\rangle} &= \frac{1}{4}\left[M_4 + M_1 - M_2 - M_3\right] \\
\mathcal{M}_{\langle --++\rangle} &= \frac{1}{4}\left[M_3 + M_4 - M_1 - M_2\right] \\
\mathcal{M}_{\langle -++-\rangle} &= \frac{1}{4}\left[M_2 + M_3 - M_4 - M_1\right]
\end{aligned} \tag{3.14}$$

and the overall (2×1) order parameter may be obtained by introducing a root-mean-square magnetization from (3.14),

$$P_{(2\times 1)} = \sqrt{\frac{1}{2}\left[\mathcal{M}^2_{\langle ++--\rangle} + \mathcal{M}^2_{\langle +--+\rangle} + \mathcal{M}^2_{\langle --++\rangle} + \mathcal{M}^2_{\langle -++-\rangle}\right]} \tag{3.15}$$

This parameter is well defined in the sense that, as it may be verified, its value is 1 in the (2×1) ordered phase, and 0 in the (1×1) ordered phase.

3.5.3 Scattering intensities

Scattering problems have already been discussed in chapter 1 in connection with the analysis and interpretation of experimental data. In this section more details will be given, especially about the consequences of the roughening transition on scattering intensities and in conjunction with a treatment suited to the particular situation of the (110) surface. The discussion follows closely the presentation in ref. [15].

What follows applies to scattering from non-penetrative probes (e.g. helium atoms), but many of the results are suited also to other probes, e.g. grazing X-rays.

In the corrugated hard wall model for He-surface interaction and in the eikonal (or Kirchhoff, or kinematic) approximation[94], the elastic scattering probability per unit solid angle may be written as follows[95]

$$\frac{\mathrm{d}P}{\mathrm{d}\Omega} = \frac{k(\mathbf{k}_i \cdot \mathbf{q})^2}{8\pi^2 A|k_{iz}|q_z^2} \int \mathrm{e}^{i[\mathbf{Q}\cdot(\mathbf{R}_2-\mathbf{R}_1)]} \langle \mathrm{e}^{iq_z[\zeta(\mathbf{R}_2)-\zeta(\mathbf{R}_1)]} \rangle \mathrm{d}^2R_1 \ \mathrm{d}^2R_2 \tag{3.16}$$

Here $\hbar\mathbf{k}_i$ and $\hbar\mathbf{k}_f$ are the initial and final wavevectors, $\mathbf{q} = \mathbf{k}_i - \mathbf{k}_f$, and $|\mathbf{k}_i| = |\mathbf{k}_f| = k$. The components of $\mathbf{q}$ parallel and perpendicular to the surface are denoted by $\mathbf{Q}$ and q_z, and those of $\mathbf{k}_i$ as $\mathbf{K}_i$ and k_{iz}.

The surface area is A and $\zeta(\mathbf{R})$ is the surface corrugation at $\mathbf{R}$, which may approximately be taken as the envelope of corrugations due to simple ions, which in turn may be written as

$$\zeta(\mathbf{R}) = \mathrm{max}_j[h_j a_\perp + Z(\mathbf{R} - \mathbf{R_j})] \tag{3.17}$$

where $Z(\mathbf{R})$ is an ionic shape function, and j labels surface ions of height $h_j a_\perp$, h_j being an integer, and $a_\perp (= a/2\sqrt{2}$ for the (110) surface) is the perpendicular lattice spacing.

Using approximation (3.17), the scattering integral (3.16) (apart from the trivial prefactors) factorizes[96], as in the Born approximation, into an ionic form factor $|F(\mathbf{Q})|^2$ and a structure factor $S(\mathbf{Q})$, defined respectively by

$$F(\mathbf{Q}) = \int_\Omega \mathrm{e}^{[i\mathbf{Q}\cdot\hat{\mathbf{R}}+iq_z Z(\hat{\mathbf{R}})]} \mathrm{d}^2\hat{R} \tag{3.18}$$

$$S(\mathbf{Q}) = \sum_{\mathbf{R}} E_{\mathbf{R}}(p) \mathrm{e}^{i\mathbf{Q}\cdot\mathbf{R}} \tag{3.19}$$

In (3.18-19), Ω is the volume of the surface unit cell, $p = -a_\perp q_z$, $\mathbf{R}$ runs over the 2D-lattice, and $E_{\mathbf{R}}(p)$ is the correlation function given by

$$E_{\mathbf{R}}(p) = \langle e^{-ip[h(\mathbf{R})-h(0)]}\alpha^*(p,0)\alpha(p,\mathbf{R})\rangle \tag{3.20}$$

where the surface level at $\mathbf{R}$ is $h(\mathbf{R})h$, and $\alpha(p,\mathbf{R})$ is a shadowing factor given by

$$\alpha(p,\mathbf{R}) = \frac{\int_{S(\mathbf{L})} e^{[i\mathbf{Q}\cdot\hat{\mathbf{R}}+iq_z Z(\hat{\mathbf{R}})]}d^2\hat{R}}{\int_\Omega e^{[i\mathbf{Q}\cdot\hat{\mathbf{R}}+iq_z Z(\hat{\mathbf{R}})]}d^2\hat{R}} \tag{3.21}$$

$S(\mathbf{R})$ being the surface region, where $h(\mathbf{R})h + Z(\hat{\mathbf{R}} - \mathbf{R})$ is the largest term in (3.17), displaced back towards the origin by $\mathbf{R}$. The shadowing factor α is larger or smaller than 1 for a very exposed or poorly exposed surface ion respectively. The exact expression (3.21) depends on the heights of the ion at $\mathbf{R}$ and of its neighbors. A reasonable approximation is[97]

$$\alpha(\mathbf{R}) = 2 - \frac{1}{2}n(\mathbf{R}), \tag{3.22}$$

where $n(\mathbf{R})$ is the number of surface neighbors to site $\mathbf{R}$ that are higher than the ion at $\mathbf{R}$. Second-layer atoms are completely shadowed at $T = 0$, but become gradually visible as T increases.

The structure factor (3.19) splits into a coherent part (arising from the limit of $E_{\mathbf{R}}(p)$ for $|\mathbf{R}| \to \infty$) and an incoherent part. Above the transition, however, the coherent part vanishes and only incoherent scattering is left.

Coherent scattering

Below the transition both coherent and incoherent scattering occur, which makes the treatment somewhat involved. Coherent, i.e. Bragg scattering, however, is simple enough. The coherent contribution is obtained from eq. (3.20) by letting $|\mathbf{R}|$ go to infinity. In this way the heights at the points $\mathbf{R}$ and $\mathbf{0}$ loose any correlation, so that (3.20) becomes

$$E_{\mathbf{R}}(p) = \langle \mathrm{e}^{-iph(\mathbf{R})}\alpha(\mathbf{R})\rangle\langle \mathrm{e}^{iph(\mathbf{0})}\alpha(\mathbf{0})\rangle \tag{3.23}$$

Since the averages in (3.23) do not depend on the lattice point in which they are evaluated, due to the translational invariance, a substitution of (3.23) into (3.19) leads to the following formula for the coherent scattering intensity:

$$S^{\mathrm{coh}}(\mathbf{Q}) = \delta(\mathbf{Q}-\mathbf{G})|\langle \mathrm{e}^{-iph}\alpha\rangle|^2 \tag{3.24}$$

where $\mathbf{G}$ is a Bragg peak, and the δ function originates from the $\sum_{\mathbf{R}} \mathrm{e}^{i\mathbf{Q}\cdot\mathbf{R}}$. The calculation is straightforward and the resulting behaviour of coherent scattering is a steady decrease from its zero-temperature value to zero at the transition.

Incoherent scattering

Incoherent scattering below T_R is much more difficult to evaluate, while the scattering from a rough surface is simpler and experimentally more straightforward. Since the (110) surface is formed of two sublattices, the reciprocal lattice vectors $\mathbf{G} \equiv \frac{2\pi}{a}(n_x, \sqrt{2}n_y)$ split into two classes, according to whether the sum $n_x + n_y$ is

even (the class will be referred to as even or principal peaks) or odd (odd or superlattice peaks). At low temperatures where the shadowing factors are completely effective (the second layer atoms are invisible) both types of peaks are similar, but when the surface roughens the even and the odd peaks behave very differently.

The shadowing factor, given by eq. (3.22) can also be written as

$$\alpha(\mathbf{R}) = \frac{1}{4}\sum_{\mathbf{D}}[1 - h(\mathbf{R}+\mathbf{D}) + h(\mathbf{R})]$$

where $\mathbf{D}$ runs over the nearest neighbors. Substituting this expression into (3.20) and rearranging the sums one gets different results for the principal and the superlattice peaks. In formula (3.19) the correlation function $E_{\mathbf{R}}(p)$ may be replaced by an effective correlation function $E^{\text{eff}}_{\mathbf{R}}(p)$, which for the principal peaks is given by

$$E^{\text{eff}}_{\mathbf{R}}(p) = \frac{1}{16}\sum_{\mathbf{D},\mathbf{D}'}\langle e^{-ip[\mu(\mathbf{R},\mathbf{D})-\mu(\mathbf{0},\mathbf{D}')]}\rangle \tag{3.25}$$

and for the superlattice peaks by

$$E^{\text{eff}}_{\mathbf{R}}(p) = \frac{1}{16}\sum_{\mathbf{D},\mathbf{D}'}\langle e^{-ip[\mu(\mathbf{R},\mathbf{D})-\mu(\mathbf{0},\mathbf{D}')]}[h(\mathbf{R}+\mathbf{D}) - h(\mathbf{R})][h(\mathbf{D}') - h(\mathbf{0})]\rangle$$

In the above formulæ $\mu(\mathbf{R},\mathbf{D})$ indicates the higher level between the atom at $\mathbf{R}$ and its neighbor at $\mathbf{R}+\mathbf{D}$:

$$\mu(\mathbf{R},\mathbf{D}) = \max[h(\mathbf{R}), h(\mathbf{R}+\mathbf{D})]$$

It is important to notice that for any distance $\mathbf{R}$, the heights μ, in contrast to h, span both even and odd integers.

For the particular relevance it has in connection with the roughening transition, the structure factor S, given by (3.19), will be analytically evaluated for the principal peaks and for small $|\tilde{\mathbf{Q}}| = |\mathbf{Q} - \mathbf{G}|$ values (where $\mathbf{G}$ is a two dimensional reciprocal lattice vector). Although a rigorous derivation is provided in ref. [15], here a greatly simplified version will be given, starting from the consideration that for small $|\tilde{\mathbf{Q}}|$ the main contributions to the scattering functions come from the long distance correlations, and therefore only these will be considered.

For long distances, short range features of the surface may be neglected, so it is not relevant if μ is replaced by $h(\mathbf{R})$ or by $h(\mathbf{R}+\mathbf{D})$ in formula (3.25), for example, since they just differ by ± 1. It is thus possible to rewrite (3.25) in the simple form

$$E_{\mathbf{R}}^{\mathrm{eff}}(p) = \langle \mathrm{e}^{-ip[h(\mathbf{R})-h(\mathbf{0})]} \rangle \tag{3.26}$$

Moreover, at long distances, it is natural to assume that the probability $P(h|\mathbf{R})$ of finding a height difference $ha_{\perp}$ between two surface sites a distance $\mathbf{R}$ apart will tend towards a discrete Gaussian distribution. As a consequence, average in (3.26) may be substituted with

$$E_{\mathbf{R}}^{\mathrm{eff}}(p) = \mathrm{e}^{-\frac{p^2}{2}\langle [h(\mathbf{R})-h(\mathbf{0})]^2 \rangle} \tag{3.27}$$

There is a periodicity in the variable p simply arising from eq. (3.26), since $[h(\mathbf{R}) - h(\mathbf{0})]$ is an integer: two values of p differing of $2\pi k$, with k integer, are thus completely equivalent. It is so possible to restrict the range of variation of p, that

is to define a variable $\hat{p} = p - 2\pi k$, k integer and $|\hat{p}| \leq \pi$: with this substitution the right formula reads

$$E_{\mathbf{R}}^{\text{eff}}(p) = \mathrm{e}^{-\frac{\hat{p}^2}{2}\langle[h(\mathbf{R}) - h(\mathbf{0})]^2\rangle} \tag{3.28}$$

But, as already seen in section 2.1.1, the quantity $\langle[h(\mathbf{R}) - h(\mathbf{0})]^2\rangle$ is nothing but the $G(r)$ defined in eq. (2.5); its divergence as the logarithm of the size of the system for $T \geq T_R$ must be studied in more detail here, and it can be done, since the analytic solution of the BCSOS model for roughening is known. Above the roughening transition $G(\mathbf{R})$ increases to infinity[98,99] as

$$G(\mathbf{R}) \approx 2K \ln \rho(\mathbf{R}) \tag{3.29}$$

where K is a universal function of Δ, independent of distance and of anisotropy

$$K = \frac{1}{\pi \arccos \Delta} \tag{3.30}$$

where Δ, the six vertex parameter, is given by expression (2.11). The function K increases with temperature: three important values assumed by K are

$$\begin{aligned} K(T = T_R) &= 1/\pi^2 \\ K(T = 2T_R) &= 2/\pi^2 \\ K(T = \infty) &= 3/\pi^2 \end{aligned} \tag{3.31}$$

(note that the first of (3.31) is actually (2.7)). The distance parameter ρ in eq. (3.29) can be expressed in terms of $\mathbf{R} \equiv \frac{1}{2}\left[m_x a_x \hat{\mathbf{x}} + m_y a_y \hat{\mathbf{y}}\right]$ (where a_x and a_y are the lengths of the unit cell sides), with $(m_x + m_y)$ even, by

$$\rho = \left(\frac{m_x^2}{\Lambda} + \Lambda m_y^2 \right)^{\frac{1}{2}}$$

where the anisotropy parameter Λ is given by

$$\Lambda = \frac{1 + \sin z}{\cos z}$$

and $z = \pi\phi_0/(2\mu)$, with μ and ϕ_0 respectively given by

$$\mu = \arccos(-\Delta)$$
$$\phi_0 = \arccos\left[\left(2ab - \Delta a^2 - \Delta b^2\right)/c^2\right], \quad 0 \leq \phi_0 \leq \mu$$

where the above formulæ hold for $-1 < \Delta < \frac{1}{2}$, and a, b and c are the Boltzmann weigths of the vertex energies ε_1, ε_3 and ε_5 respectively. A direct substitution of (3.29) into (3.28) leads to a fairly simple expression for $E_{\mathbf{R}}^{\text{eff}}(p)$,

$$E_{\mathbf{R}}^{\text{eff}}(p) = \rho(\mathbf{R})^{-\tau} \tag{3.32}$$

where

$$\tau(T, \hat{p}) = K(T)\ \hat{p}^2 \tag{3.33}$$

For small $\tilde{\mathbf{Q}} = |\mathbf{Q} - \mathbf{G}|$, if $\mathbf{G}$ corresponds to a principal peak, only the long distance correlations are important, and therefore eq. (3.32) can be used to calculate the scattering structure factor. The sum (3.19) may be replaced by integrals, so

$$
\begin{aligned}
S^{\mathrm{inc}} &\sim \sum_{\mathbf{R}} \mathrm{e}^{i\tilde{\mathbf{Q}}\cdot\mathbf{R}} \rho(\mathbf{R})^{-\tau} \approx \\
&\approx \sum_{m_x m_y} \mathrm{e}^{i[m_x a_x \tilde{Q}_x + m_y a_y \tilde{Q}_y]} \left(\frac{m_x^2}{\Lambda} + \Lambda m_y^2 \right)^{-\frac{\tau}{2}} \approx \\
&\approx \int\int \mathrm{e}^{i[m_x a_x \tilde{Q}_x + m_y a_y \tilde{Q}_y]} \left(\frac{m_x^2}{\Lambda} + \Lambda m_y^2 \right)^{-\frac{\tau}{2}} \mathrm{d}m_x \mathrm{d}m_y = \\
&= 2\pi \left(\Lambda a_x^2 \tilde{Q}_x^2 + \frac{a_y^2 \tilde{Q}_x^2}{\Lambda} \right)^{-1+\frac{\tau}{2}} \int_0^\infty J_0(t)\, t^{1-\tau} \mathrm{d}t
\end{aligned}
\tag{3.34}
$$

The integral occurring in (3.34) equals

$$
2^{1-\tau} \frac{\Gamma(1-\frac{\tau}{2})}{\Gamma(\frac{\tau}{2})}
$$

but is well behaved only for $\frac{1}{2} \leq \tau \leq 2$. However, it was shown by Villain *et al.* [77] how the range can be extended down to $\tau = 0$. For $0 \leq \tau \leq 2$, eq. (3.34) shows that there is a power-law divergence in the scattering factor S as $|\tilde{\mathbf{Q}}| \to 0$; if $\tilde{Q}_y$ is set to 0, (3.34) simplifies into

$$
S^{\mathrm{inc}} \sim \tilde{Q}_x^{-2+\tau} \tag{3.35}
$$

where the power-law divergence is clearly visible.

Although defined for every temperature, τ is meaningful only for $T \geq T_R$, and has a characteristic behaviour. From (3.33), τ results an increasing function of temperature, and assumes the peculiar value 1 exactly at the roughening temperature and for $\hat{p} = \pi$, that is

$$
\tau(T_R, \pi) = 1 \tag{3.36}
$$

For this reason, many experimentalists, after measuring the behaviour of $S(\tilde{\mathbf{Q}})$ as a function of $\tilde{\mathbf{Q}}$, locate the roughening temperature precisely where the value of τ obtained by fitting their data with eq. (3.34) equals 1, for $\hat{p} = \pi$ or, more generally, when

$$\tau(T_R, \hat{p}) = \hat{p}^2/\pi^2 \tag{3.37}$$

This procedure will be discussed in section 4.3.2, and a comparison of Monte Carlo simulation and experimental data will be attempted.

Chapter 4

The Monte Carlo simulation and the results

In order to elucidate the phase structure of the interface system described by the Hamiltonian introduced in the preceeding chapter, a Monte Carlo simulation has been carried out.

4.1 The Monte Carlo method

The Monte Carlo method[100] is a well-established technique of computer simulation of a system with many degrees of freedom. It allows to simulate statistical fluctuations in order to numerically generate the equilibrium probability distribution of complex systems. It provides an efficient method of calculating, in a conceptually simple way, the statistical averages of relevant quantities.

If the system is described by a Hamiltonian $H(\mathrm{x})$ (omitting kinetic energy terms), where the set of variables $\mathrm{x} \equiv \{x_1, \ldots x_N\}$ specifies one of its possible configurations (N = number of degrees of freedom), we are concerned with the statistical average of a generic physical quantity $Q(\mathrm{x})$, defined as

$$\langle Q \rangle = \frac{\int_\Omega Q(\mathrm{x}) \mathrm{e}^{-\beta H(\mathrm{x})} \mathrm{dx}}{\int_\Omega \mathrm{e}^{-\beta H(\mathrm{x})} \mathrm{dx}} \tag{4.1}$$

in the canonical ensemble, where Ω is the volume of the phase space and

$\beta = 1/k_B T$.

A simple random sampling method for the numerical calculation of the integrals in eq. (4.1) is not useful, since the integrand $e^{-\beta H(\mathbf{x})}$ is sharply peaked in a small region of the phase space centered around the equilibrium distribution. To overcome this difficulty, Metropolis *et al.* [101] introduced a sampling algorithm based on the idea of "importance sampling". Starting from a given initial configuration, $\{\mathbf{x}\}$, successive configurations are generated by random changes of the variables $\{\mathbf{x}\} \rightarrow \{\mathbf{x}'\}$, but each change is not accepted a priori. The decision of acceptance of a new configuration is taken so as to ensure, for a large enough number of configurations, that the phase space is sampled in accordance with the probability distribution suited for the particular statistical ensemble chosen. In the case of the canonical ensemble the Metropolis criterion prescribes to accept the new configuration if, being $\Delta E = H(\mathbf{x}') - H(\mathbf{x})$, it results $\Delta E < 0$ or (even if $\Delta E > 0$), $e^{-\beta \Delta E} < R$, R being a random number in the interval $0 < R < 1$. After a (large) number of such Monte Carlo steps, a sampling of the equilibrium configurations will be obtained. In this way, averages like (4.1) simplify in the form

$$\langle Q \rangle = \frac{1}{N} \sum_{i=1}^{N} Q_i \tag{4.2}$$

where Q_i is the quantity $Q(\mathbf{x})$ evaluated in the i-th configuration, and N is the number of configurations taken into account. Every configuration contributing to (4.2) in fact results already weighted by the Boltzmann factor $e^{-\beta H(\mathbf{x})}$ due to the very acceptance criterion described above.

One of the main problems in this procedure is that the Q_i appearing in eq. (4.2) are supposed to be all independent "measures" of the quantity Q, while in

reality they are strongly correlated with each other if they are considered at every Monte Carlo step. To avoid this excessive correlation between a value and the successive one, the Q_i are not calculated at each step, but every $2\mathcal{N}$ steps, where $\mathcal{N} = 2N_xN_y$ is the total number of sites, so as to leave the system enough "time" to change its configurations and to acquire less correlated values.

Nevertheless, some correlation remains in the procedure: this will not affect the averages, but will contribute to their statistical error, which can be calculated as follows. It is well known that the variance $Var(Q)$ of a set of N measures of a quantity Q, supposed to be distributed according to a Gaussian probability, is defined as

$$\begin{aligned} Var(Q) \equiv \frac{1}{N-1}\sum_{i=1}^{N}\left[Q_i - \langle Q\rangle\right]^2 \simeq \\ \simeq \langle Q^2\rangle - \langle Q\rangle^2 \end{aligned} \tag{4.3}$$

where the last equality holds if $N \gg 1$. The statistical error associated with the measure of Q is

$$\sigma_Q = \sqrt{\frac{Var(Q)\tau_Q}{N}} \tag{4.4}$$

where τ_Q is the so called "correlation length", and may be estimated by the method outlined by Jacucci and Rahman[102]. For a set of independent quantities, $\tau_Q = 1$, but in general $\tau_Q > 1$. As it is clear in eq. (4.4), the correlation length has the effect of enlarging the statistical error relative to the quantity Q. This effect is very important near the critical points of a statistical system ($\tau \gg 1$), where some other problems arise too, like a critical slowing down in the convergence of the Monte Carlo procedure. No special prescription has been adopted to cure such

problems near the critical point: a greater number of configurations has simply been taken into account in these regions.

4.2 The algorithm

The Monte Carlo algorithm for the KJT Hamiltonian has been constructed as follows. A configuration is represented by the ordered array of height variables divided in two sublattices of $N_x \times N_y$ sites each, and with the overall six vertex constraint. Periodic boundary conditions are imposed in order to simulate with a finite size the behaviour of an infinite system. At fixed temperature, starting from a given initial configuration, a site is chosen randomly and its height is changed of either $+2$ or -2 (another random choice is needed to decide the sign), preserving the parity of its value which is fixed by the symmetry of the system and, moreover, making sure that the six vertex constraint is verified in the new configuration. If it cannot be verified due to the height values assumed by its neighbouring sites, another site is randomly chosen. Once the new configuration is generated, the usual Monte Carlo acceptance criterion is adopted, and the whole procedure is iterated for a sufficient number of steps. Meanwhile, summations of relevant quantities are accumulated for their final averages, according to expression (4.2).

Several values of the temperature have been examined, and the initial configuration is chosen to be equal to the known ground state of the system for the first temperature, while it coincides with the configuration appropriate to the preceeding temperature for the other cases.

The quantities Q_i calculated in the program have been normalized per site in

order to permit an easier finite-size scaling analysis, and are the following (N is the number of Monte Carlo configurations, $\mathcal{N}$ is the number of sites):

1) the energy $\langle E \rangle$, defined as

$$\langle E \rangle = \frac{1}{\mathcal{N}} \frac{1}{N} \sum_{i=1}^{N} E_i \tag{4.5}$$

2) the specific heat C_v, defined as

$$C_v = \frac{1}{k_B T^2} \left[\langle E^2 \rangle - \mathcal{N} \langle E \rangle^2 \right] \tag{4.6}$$

3) the order parameter $\langle P_{2\times 1} \rangle$, defined as in formulæ (3.13)–(3.15):

$$P_{2\times 1} = \frac{1}{\mathcal{N}} \frac{1}{N} \sum_{i=1}^{N} \sqrt{\mathcal{M}_i^{\mathrm{RMS}}} \tag{4.7}$$

where $\mathcal{M}_i^{\mathrm{RMS}}$ is the quantity in the square root in eq. (3.15)

4) the susceptibility of the order parameter, which is

$$\chi_{2\times 1} = \frac{1}{k_B T} \left[\langle P_{2\times 1}^2 \rangle - \mathcal{N} \langle P_{2\times 1} \rangle \right] \tag{4.8}$$

5) the height fluctuations $\langle \delta h^2 \rangle$, relevant for the roughening transition, defined as[103,104]

$$\langle \delta h^2 \rangle = \frac{1}{\mathcal{N}} \sum_{s=1}^{\mathcal{N}} \frac{1}{N} \sum_{i=1}^{N} \langle [h_{s,i} - \langle h \rangle_i]^2 \rangle \tag{4.9}$$

where $h_{s,i}$ represents the height of site s of the lattice in the i-th configuration, and

$$\langle h \rangle_i = \frac{1}{\mathcal{N}} \sum_{s=1}^{\mathcal{N}} h_{s,i} \tag{4.10}$$

is the average height of the whole surface in the i-th configuration. At first sight, one may think that the substitution in eq. (4.9) of $\langle h \rangle_i$ by $\langle h \rangle$, that is by the surface height in the global Monte Carlo run (averaged both over all sites and over the ensamble) would be more appropriate. However, the Hamiltonian (3.2) is invariant for global vertical translations of the interface and a Goldstone mode arises (capillary waves). As a consequence of this mode, there are global fluctuations in height (contained in $\langle h \rangle$) that do not strictly contribute to roughening; by employing $\langle h \rangle_i$ (averaged over all sites in one Monte Carlo configurations) as reference interfacial height we keep only those fluctuations that give rise to the roughening transition.

6) the coherent scattering intensity I^{coh}; this is just the proportionality factor of the δ function of equation (3.24), which depends only on q_z, the perpendicular momentum component of the transfer, and is calculated as follows

$$I^{\mathrm{coh}}(q_z) = \frac{1}{\mathcal{N}} \sum_{s=1}^{\mathcal{N}} \frac{1}{N} \sum_{i=1}^{N} \left| \langle \mathrm{e}^{-ip[h_{s,i} - \langle h \rangle_i]} \alpha_{s,i} \rangle \right|^2 \tag{4.11}$$

where $p = -\frac{a}{2\sqrt{2}} q_z$ and $\alpha_{s,i}$ is the shadowing factor of site s in the i-th configuration. Moreover, from the height variable $h_{s,i}$ the term $\langle h \rangle_i$ has been subtracted, for the reasons explained above for the height fluctuations (all quantities containing $h_{s,i}$ are meaningless if they are not referred to the instantaneous average reference level represented by $\langle h \rangle_i$).

7) the incoherent scattering intensity S^{inc}. A very simple form of the scattering intensity can be obtained from formulæ (3.16)–(3.22), and reads

$$S^{\mathrm{inc}}(\mathbf{Q}) = \left\langle \left| \sum_{\mathbf{R}} \mathrm{e}^{i\mathbf{Q}\cdot\mathbf{R}} \mathrm{e}^{-ip h(\mathbf{R})} \alpha(\mathbf{R}) \right|^2 \right\rangle \tag{4.12}$$

which, with the usual $1/\mathcal{N}$ normalization and with the conventions of the preceeding formulæ, transforms into

$$S^{\mathrm{inc}}(\mathbf{Q}) = \frac{1}{\mathcal{N}} \sum_{s=1}^{\mathcal{N}} \frac{1}{N} \sum_{i=1}^{N} \left| \mathrm{e}^{i\mathbf{Q}\cdot\mathbf{R}_{s,i}} \mathrm{e}^{-ip[h_{s,i} - \langle h \rangle_i]} \alpha_{s,i} \right|^2 \tag{4.13}$$

where $\mathbf{R}_{s,i}$ is the position of site s in the configuration i.

Another observation is in order here: while there is no constraint on the possible values of q_z, due to the discrete structure of the lattice and to the presence of the periodic boundary conditions, not all the values of Q_x and Q_y are allowed. Any physical quantity dependent on the position $\mathbf{R}$ on the lattice must be invariant under the transformation $\mathbf{R} \rightarrow \mathbf{R} + N_x a_x \hat{\mathbf{x}} + N_y a_y \hat{\mathbf{y}}$. Thus the exponential factor appearing in formula (4.13) must be invariant under the same transformation, so that

$$\mathbf{Q} \cdot [N_x a_x \hat{\mathbf{x}} + N_y a_y \hat{\mathbf{y}}] = 2\pi n$$

with n integer. The above equation may be rewritten as

$$\mathbf{Q} = \left(\frac{2\pi n_x}{N_x a_x}, \frac{2\pi n_y}{N_y a_y} \right) \tag{4.14}$$

and provides the allowed values which can be assumed by the parallel momentum transfer in a simulation adopting periodic boundary conditions.

4.3 Results obtained

4.3.1 The BCSOS model

In order to test the algorithm to be applied to the KJT model, a study of the BCSOS model has been carried out to compare the results of the simulation with the known properties of the model which is exactly solved. The energy parameters for this case are those presented at the end of section 3.5.3.

A finite-size scaling procedure has also been adopted to characterize the behaviour of the quantities under examination. For this purpose, square ($N_x = N_y$) systems have been considered, for sizes $N_x = 10,\ 16$ and 24.

In order to ensure that equilibration is achieved, the number of Monte Carlo steps has been taken, after some tests, to be of the order of $N = 2 \cdot 10^4 \mathcal{N}$, except in the critical region where up to $4 \cdot 10^4 \mathcal{N}$ Monte Carlo steps are considered. In general, it is well known that these effects have greater relevance for larger systems, and this is observed in the present study too.

The results of the test are presented in figures 4.1 to 4.10. No error bar is reported if smaller than the size of a measured point. Fig. 4.1 shows the mean energy per site of the surface which, as expected, increases with temperature. More information can be extracted from the specific heat (fig. 4.2), with its peculiar behaviour: no singularity of any kind is present at the transition temperature $T_R = 5.77$, while a rounded peak appears around $T_P \simeq 4.67$, as theoretically predicted. Thus, the main feature of the specific heat is the absence of any divergence as seen in the small dependence on the system size.

The height fluctuation $\langle \delta h^2 \rangle$, defined in eq. (4.8), is shown in fig. 4.3 as a function of temperature for the three different sizes, and in fig. 4.4 as a function of

the logarithm of the size for various temperatures. The first graph shows a marked size effect in the intermediate and high temperature regions, which is reflected in the second graph where it is clear that for low temperatures the quantity is independent of the size, while the slope of $\langle \delta h^2 \rangle$ vs. $\ln N$ increases for higher temperatures. This behaviour is not only consistent with what expected for the BCSOS model, but provides a method of establishing if a roughening transition takes place in the system, allowing for the estimate of T_R. In fact, from equations (2.7) to (2.10) it is known that the height fluctuations of an infinite system remain finite for $T < T_R$, diverging instead logarithmically with the size for $T \geq T_R$. In a finite system, the divergence of the correlation length ξ (which causes this behaviour) saturates to the value of the linear size of the system. Nonetheless relevant information may be extracted from the universal properties of the quantity $K(T)$ of formula (2.6), which for $T \to T_R^+$ behaves like (see formula (2.8))

$$K(T) = \frac{1}{\pi^2} + C\sqrt{T - T_R} \tag{4.15}$$

The quantity $K(T)$ is the slope of $\langle \delta h^2 \rangle$ vs. $\ln N$, and is shown in fig. 4.5.

At first sight, $K(T)$ behaves as expected, since it increases with temperature and assumes the critical value $1/\pi^2$ at the transition temperature $T_R = 5.77$. A more quantitative analysis is performed by plotting the quantity $\left[K(T) - \frac{1}{\pi^2}\right]^2$ vs. T, since, from eq. (4.15)

$$\left[K(T) - \frac{1}{\pi^2}\right]^2 \simeq C'\,(T - T_R) \tag{4.16}$$

This behaviour is confirmed (fig. 4.6) and may even lead to an estimate of the roughening transition temperature. The data of fig. 4.6 provide the value $T_R \simeq 5.68 \pm 0.42$, which is consistent with the exact value of $T_R = 5.77$.

Figures 4.7 and 4.8 show the behaviour of the coherent scattering intensity as a function of temperature, for two values of the momentum transfer, $q_z = 3\pi/4$ and π respectively. The behaviour coincides with theoretical calculations, since a drop in $I^{\rm coh}$ with temperature is observed. This drop should end at $T = T_R$, where $I^{\rm coh}$ should vanish, but here finite-size effects clearly give rounding of an otherwise sharp behaviour. This is confirmed by the fact that an increase in the size of the system leads to a more pronounced drop and a faster approach to zero for $T \geq T_R$.

By comparing figs. 4.7 and 4.8, one may observe that the above features are more transparent for $q_z = \pi$, as this value corresponds to the antiphase scattering condition (the most sensitive to the surface structure).

4.3.2 Size effects on the apparent power law behaviour of the quasi-Bragg peak above roughening

A rather common method used by experimentalists in order to detect the roughening temperature T_R of a given surface, is to fit $S^{\rm inc}(\mathbf{Q}-\mathbf{G})$ with the quasi-Bragg power-law decay $(\mathbf{Q}-\mathbf{G})^{-2+\tau}$, and extract T_R by the request expressed in formula (3.37).

We have therefore calculated the incoherent scattering intensities in order to extract the exponent τ in our Monte Carlo simulation. The values of momentum transfer adopted are $Q_y = 0$, $q_z = 3\pi/4$ and π, with Q_x as small as possible (according to formula (4.14), we have employed the values $n_x = 1, 2, 3$ and 4).

In principle, $S^{\rm inc}$ should contribute a term $\sim (\mathbf{Q}-\mathbf{G})^{-2+\tau}$ to the total structure factor $S = S^{\rm inc} + S^{\rm coh}$. The coherent part $S^{\rm coh}$ is expected to decay like a Gaussian away from $\mathbf{Q} = \mathbf{G}$, and its amplitude should vanish above T_R. Owing to the finite size of the system, a small non-zero value of $S^{\rm coh}$ remains, but here,

somewhat unrigorously, we neglect S^{coh} and identify for practical purposes S^{inc} with S^{tot}.

The values of S^{inc} thus calculated can be fitted by a straight line only for $T \geq T_R$, since the procedure acquires sense only in this temperature range. Nonetheless a least-squares fit may be applied to the whole set of data, and leads to the curves shown in figs. 4.9 and 4.10, for the different system sizes.

This method is analogous to that followed by experimentalists, for example by Held *et al.* [5] in an X-ray scattering experiment on Ag(110) , carried out near the bulk-forbidden $(1\bar{1}0)$ peak, or by Zeppenfeld *et al.* [33], who provide evidence for the absence of thermal roughening of Cu(110) up to $900K$ also by examining the slope of $\ln S^{\mathrm{inc}}$ vs. $\ln \mathbf{Q}$. They in fact note that above T_R the power-law line shape is the theoretically expected form for the scattering intensity (and thus τ is a measure of the decay of spatial order), whereas below T_R, τ represents only an effective parametrization of the peak-to-tail ratio of the line shape.

A fit of $S^{\mathrm{inc}}(\mathbf{Q})$ according to a power law at all temperatures gives a peculiar behaviour for τ, represented by a monotonically increasing curve climbing up quite rapidly near the transition temperature, which is located approximately in the region where τ coincides with the value of formula (3.37). This monotonic increase is not reproduced by the simulation data reported in figs. 4.9 and 4.10, and the reason is probably the fact that no subtraction of the coherent scattering intensity is done, so that the graphs actually show a fit of the total scattering intensity, and not only of its incoherent part. Nonetheless, a very interesting feature is represented by the strong size effects, clearly visible in the graphs. In fact, although it has been recognized that the problem of the finite size of the coherent surface domains may affect the fitting procedure and should somehow be taken into account, it is still not clear how to do that and, more generally, how

the procedure is sensitive to size.

The results of figs. 4.9 and 4.10 seem to reveal another effect, that is a non trivial dependence of the behaviour of τ as a function of the perpendicular momentum transfer q_z. Formula (3.33) applied to the antiphase condition $q_z = 1$ leads to the value of eq. (3.36), $\tau = 1$, assumed at the roughening temperature, and the corresponding behaviour shows that the curves of graph 4.9 are distinctly below this value for $T = T_R = 5.77$. This has the important consequence that if one attempts to extract T_R from these data, the procedure will systematically lead to an overestimate of the roughening temperature. This can happen also in the interpretation of experimental data, if the finite domain size problem is neglected or not precisely accounted for.

Size effects can be found in graph 4.10 too, relating to $q_z = 3\pi/4$, for which formula (3.37) predicts a value of $\tau = 9/16 = 0.5625$. Here a roughly correct estimate of T_R can be obtained from data referring to the largest ($N = 24$) size available, as if some compensating effect has arisen in order to suppress or diminish the overestimation error of the $q_z = 1$ data.

Naturally, these are only preliminary results; before coming to any conclusion more work is needed, particularly in two directions. First, an increase in the system size, together with the prediction of some systematic trend in the results (like a possible scaling of τ extracted from formulæ (3.25) to (3.35)). Second, an investigation of rectangular system shapes in order to simulate non isotropic domains, and to extract information on the dependance of τ not only on the global size, but also on possible anisotropy of the scaling lengths in the two directions on the surface. Last, but not least, the coherent part has to be subtracted from the total scattering intensity, in order to perform a closer comparison with experiments and to attempt to say something conclusive about these size effects.

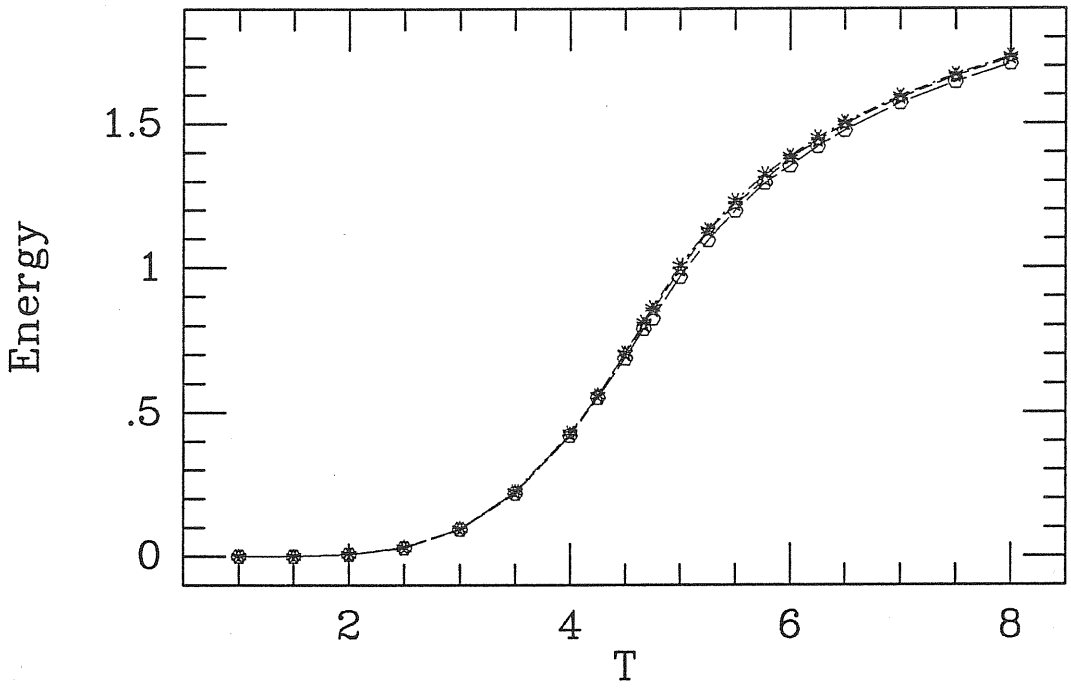

Fig. 4.1: Energy vs. temperature in the BCSOS model. Here as in the successive graphs, the asterisks refer to the size N=24, the stars to N=16 and the hexagons to N=10. No error bar is reported if smaller than the size of a measured point. The lines plotted are only a guide for the eye.

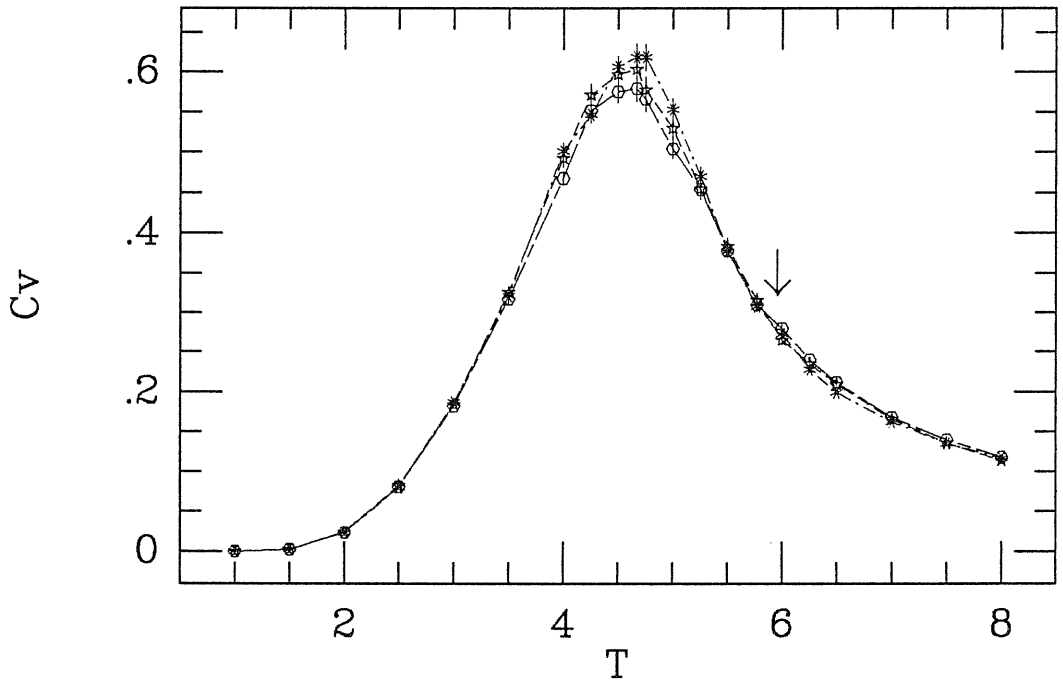

Fig. 4.2: Specific heat vs. temperature in the BCSOS model. The arrow indicates the position of the roughening temperature T_R=5.77.

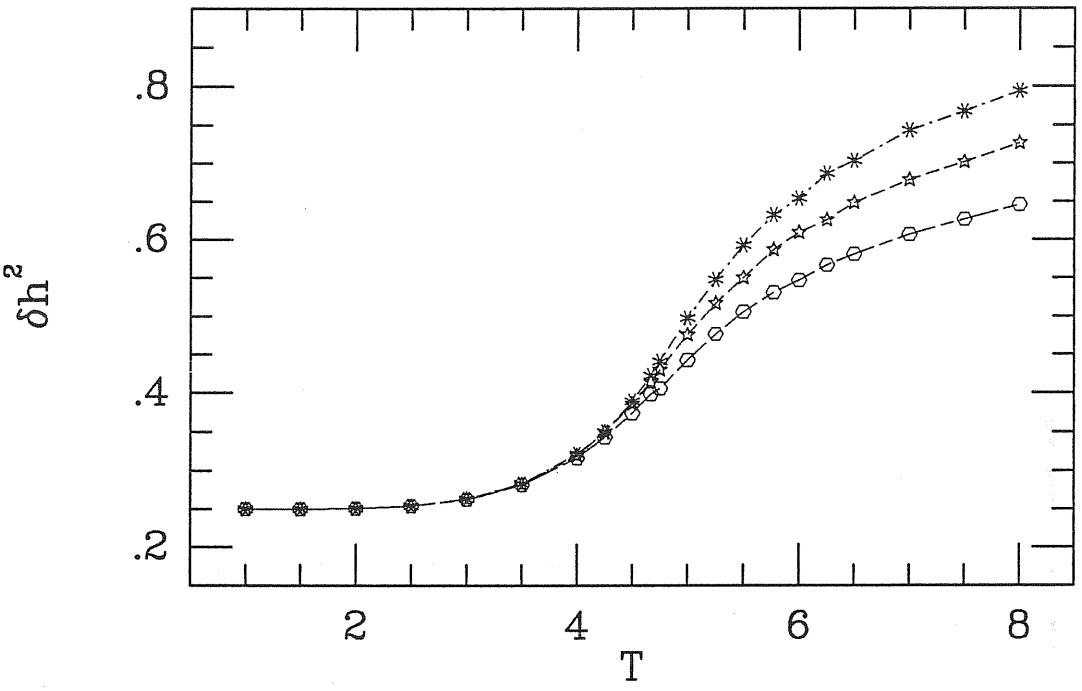

Fig. 4.3: Height fluctuations vs. temperature in the BCSOS model.

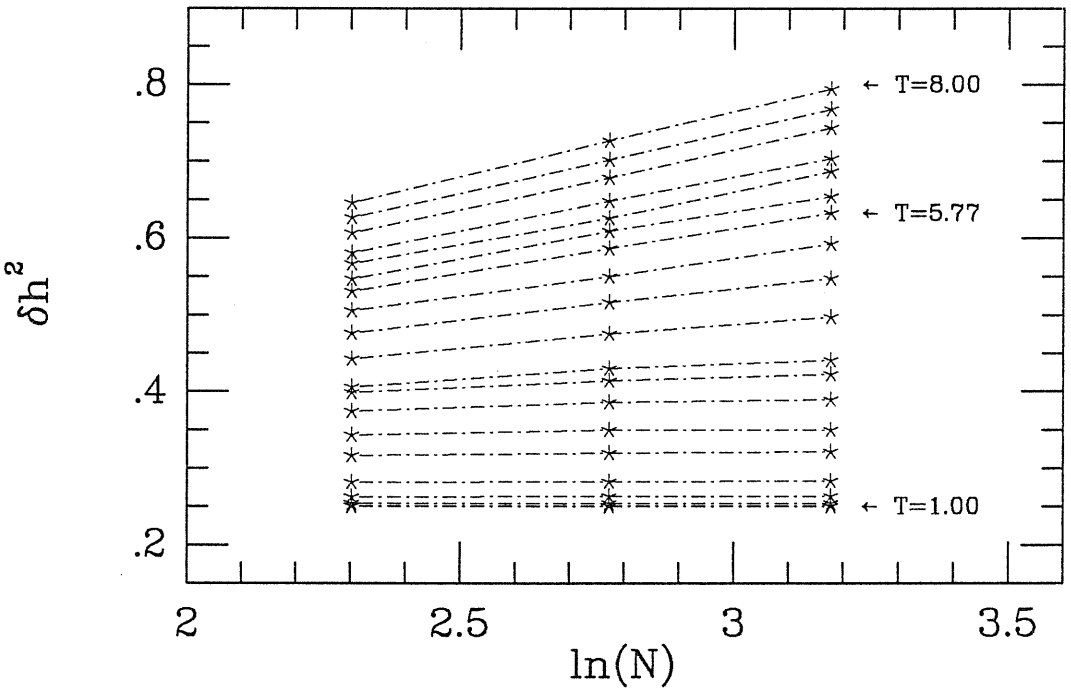

Fig. 4.4: Height fluctuations vs. logarithm of the size in the BCSOS model for the 21 temperature values investigated. The lines plotted should be straight only for $T \geq T_R = 5.77$.

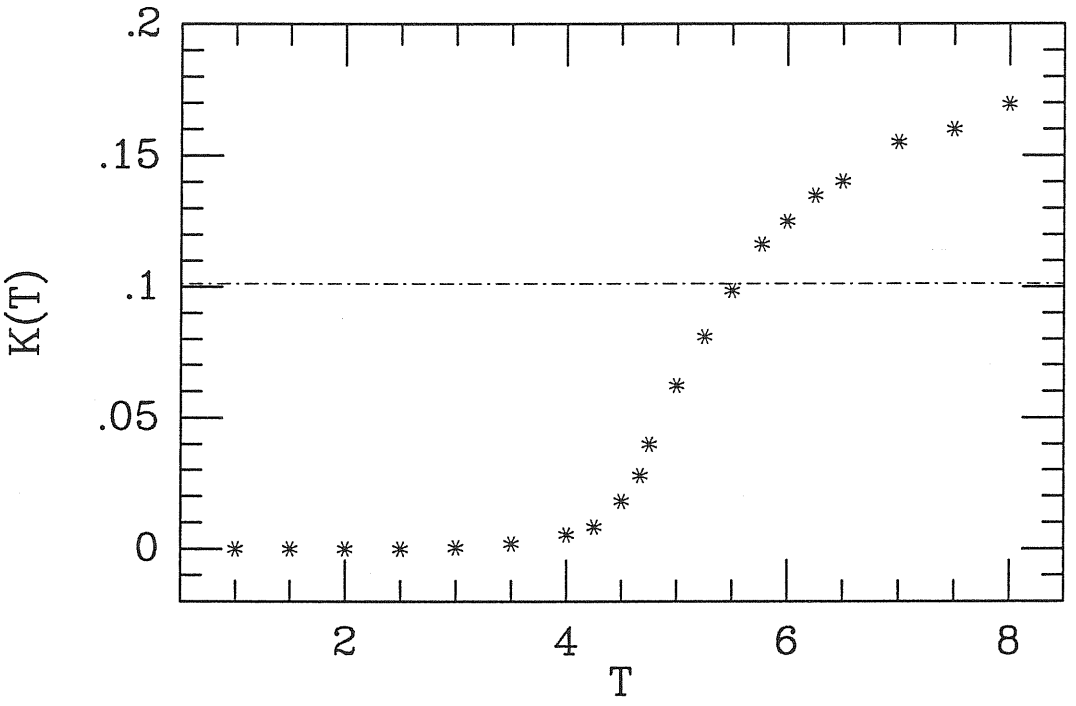

Fig. 4.5: $K(T)$ vs. temperature in the BCSOS model. The line indicates the position of the universal value $1/\pi^2$.

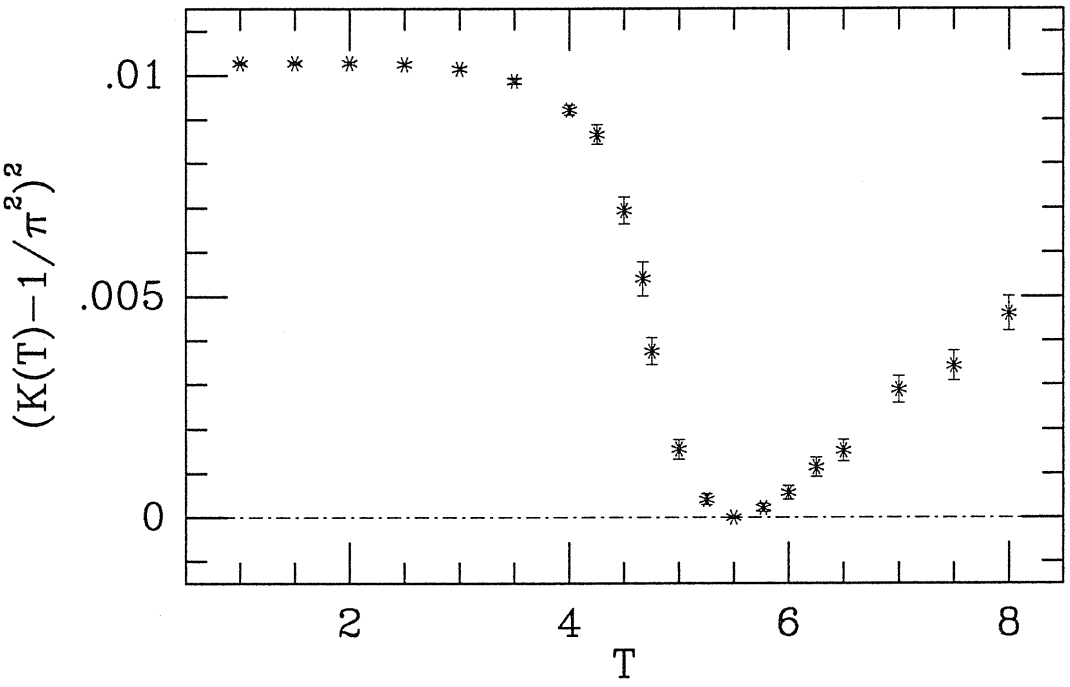

Fig. 4.6: $[K(T)-1/\pi^2]^2$ vs. temperature in the BCSOS model. The line indicates the position of the zero.

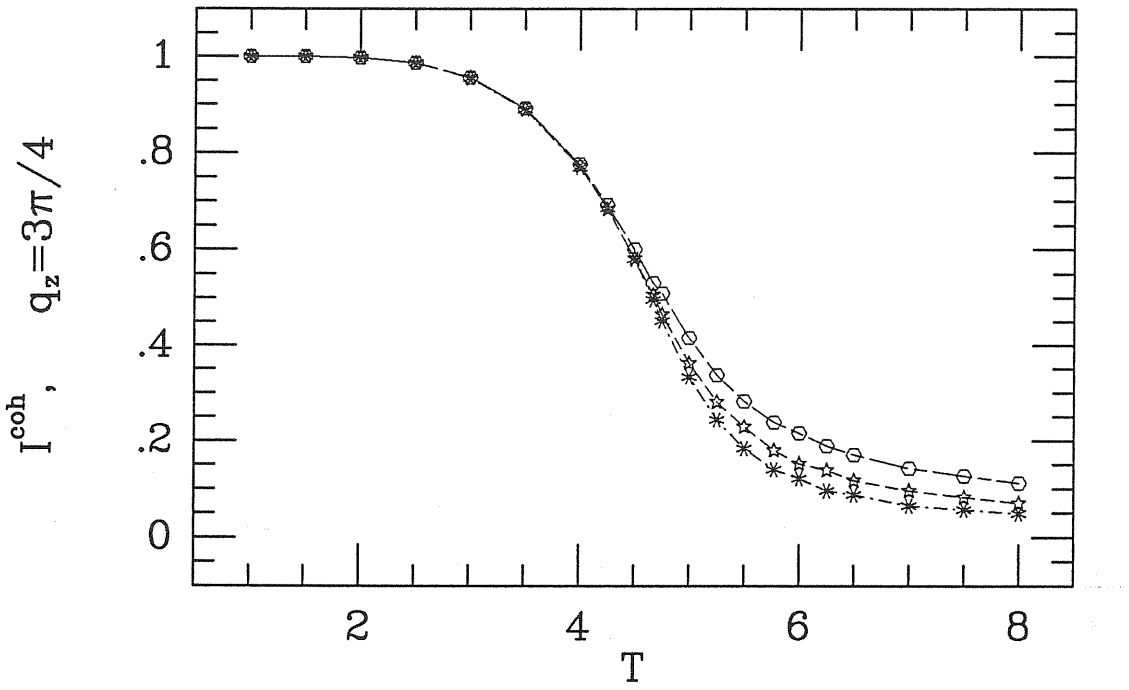

Fig. 4.7: Coherent scattering intensity vs. temperature of the BCSOS surface, for perpendicular momentum transfer $q_z=3\pi/4$.

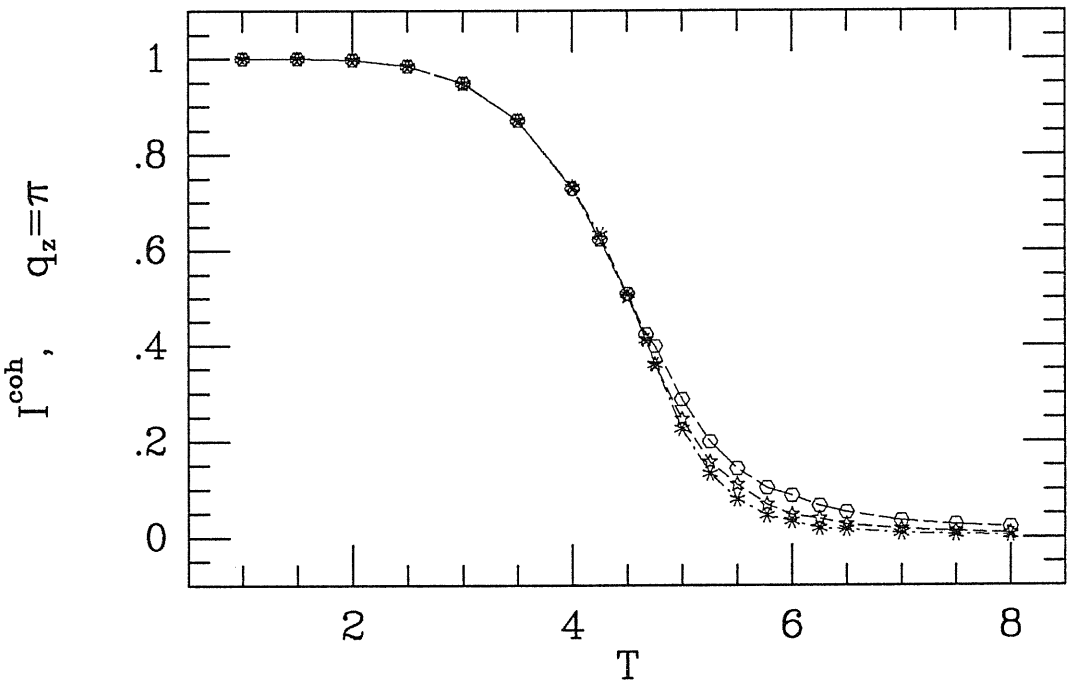

Fig. 4.8: Coherent scattering intensity vs. temperature of the BCSOS surface, for perpendicular momentum transfer $q_z=\pi$.

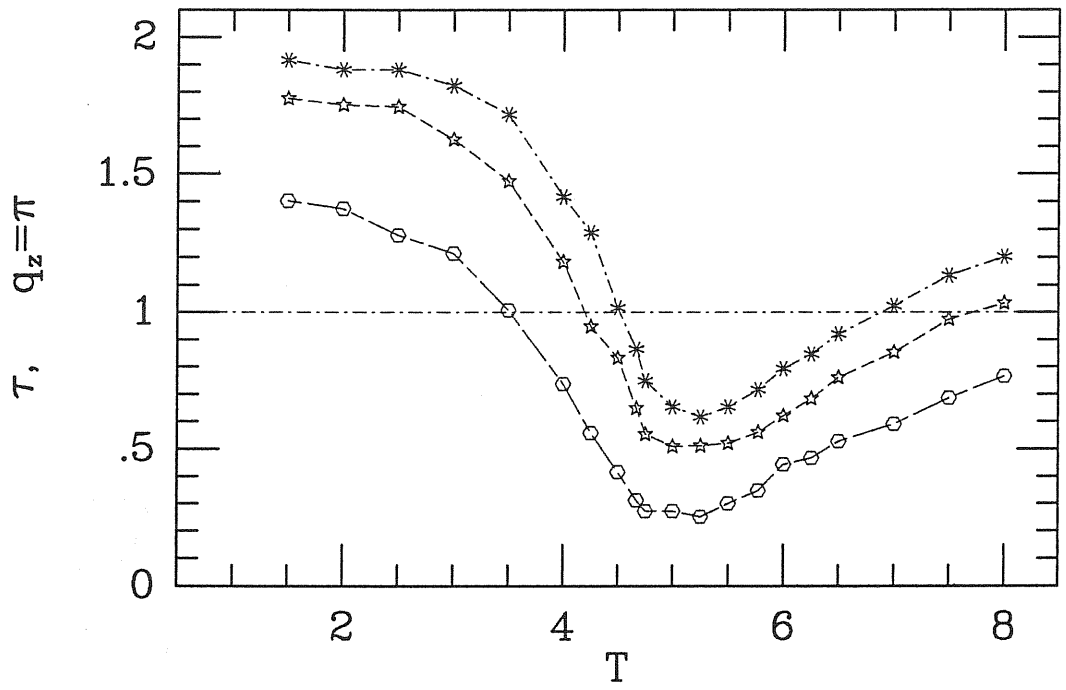

Fig. 4.9: Exponent τ of the power law behaviour of the quasi-Bragg peak vs. temperature, for perpendicular momentum transfer $q_z=\pi$. The line indicates the value τ should assume at the roughening temperature.

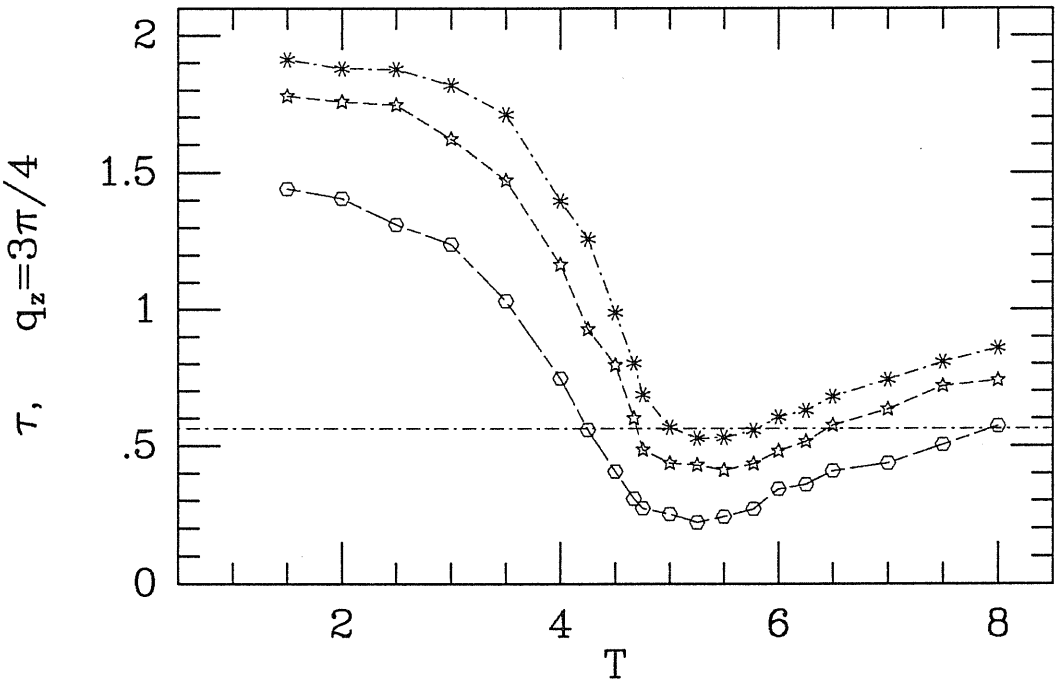

Fig. 4.10: Exponent τ of the power law behaviour of the quasi-Bragg peak vs. temperature, for perpendicular momentum transfer $q_z=3\pi/4$. The line indicates the value τ should assume at the roughening temperature.

Chapter 5

The KJT model of surface reconstruction and roughening

In this section, the results obtained for the KJT model through the Monte Carlo simulation will be presented.

The procedure adopted in section 4.3.1 is followed here too, the only change being the greater number of configurations which need be considered to overcome equilibration problems. The presence of third-neighbour interactions enhances the spatial correlation between successive configurations, and Monte Carlo runs of up to $8 \cdot 10^4 \mathcal{N}$ configurations are adopted in order to obtain meaningful data (with no widely fluctuating averages) and to overcome the large correlation times. The three system sizes are $N_x = 12, 16$ and 24.

Fig. 5.1 shows the energy of the system as a function of T for the three system sizes. A comparison with fig. 4.1 (referring to the BCSOS model) reveals the steeper slope of the curves in the temperature region near $T \sim 3.0$, which reflects the anomalous specific heat behaviour (fig. 5.2). The specific heat data are very different from those obtained for the BCSOS model and strongly suggest the occurrence of a phase transition with some kind of critical point around $T_P \simeq 2.87$. Three main features indicate such a possibility: the presence of a well-defined peak at T_P, the rapid rise in the peak height as the system size increases (suggesting

a divergent behaviour for $N_x \to \infty$), and the concomitant narrowing of the peak half-height width.

The presence of a transition at T_P, which is apparently critical, is corroborated by the behaviour of the (2×1) order parameter and of its related susceptibility, shown in figs. 5.3 and 5.4. The order parameter $P_{2\times1}$ has a value of 1 at low temperatures (where the surface is actually in the missing row phase, except for the appearance of rare defects in the ordered structure), then shows a sudden decrease around T_P and a drop to zero for higher temperatures may be observed in fig. 5.3. Finite size effects, as usual, tend to smooth down an otherwise sharp behaviour. Nonetheless they indicate that the above picture is correct since for larger system sizes the order parameter drops more sharply at T_P and approaches zero more rapidly for $T > T_P$.

The susceptibility $\chi_{(2\times1)}$ (fig. 5.4) shows similar features as the specific heat at the same temperature T_P, that is a peak diverging rapidly with size. The evidence presented here is therefore suggestive of a second order transition occurring at $T_P \simeq 2.87$.

The indication for a second phase transition of infinite order at a slightly higher temperature comes from the analysis of the height fluctuations. The procedure is the same adopted to determine the occurrence of a roughening transition and to localize T_R in the BCSOS model. This begins by considering the plot of $\langle \delta h^2 \rangle$ vs. T for different sizes (fig. 5.5) and vs. $\ln N$ for different temperatures (fig 5.6). The data for $\langle \delta h^2 \rangle$ vs. T show a clear size effect, not only for T sufficiently high ($T \geq 3$), but also for lower temperatures, where the size effect appears to be reversed.

This implies a peculiar behaviour of the slope $K(T)$ of the straight lines $\langle \delta h^2 \rangle$ vs. $\ln N$, as shown in fig. 5.7. Starting from zero slope (no size effect), negative

values are first seen ("reversed" size effect), followed by positive ones, which seem to saturate for higher temperatures. Assuming the transition to be infinite-order (Kosterlitz-Thouless) it is then be possible to estimate the roughening transition temperature at the value where the quantity $K(T)$ takes the universal KT value $1/\pi^2$. From our data, this seems to occur at a temperature value slightly greater than $T = 3.0$.

By plotting $\left[K(T) - \frac{1}{\pi^2}\right]^2$ vs. T, the assumption of a KT roughening transition for $T > 3.0$ is corroborated by two main features: the linear behaviour of the data shown in fig. 5.8 for $T \rightarrow 3.0^+$ and the estimate of the roughening transition temperature obtained by extrapolating the linear behaviour. This analysis provides a value of $T_R = 3.1 \pm 0.4$. Although the error bar (possibly overestimated) is large enough so as to permit the temperatures T_P and T_R to coincide, we believe this is not the case as for $T = 2.87$ (T_P for the first transition) $K(T)$ is significatively different from the universal KT roughening value $1/\pi^2$, assuming a value very close to zero.

From the evidence provided its seems thus quite possible that two successive transitions take place in the system described by the KJT Hamiltonian, first a possibly second-order deconstruction transition followed by a second transition of the infinite-order roughening type.

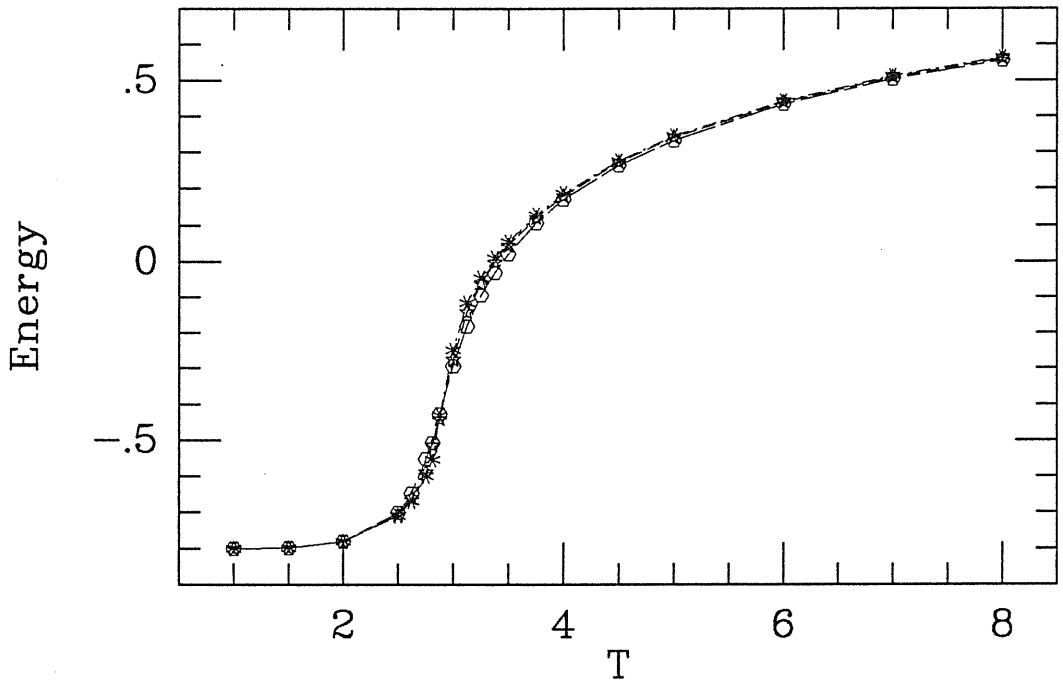

Fig. 5.1: Energy vs. temperature in the KJT model. Here as in the successive graphs, the asterisks refer to the size N=24, the stars to N=16 and the hexagons to N=12. No error bar is reported if smaller than the size of a measured point. The lines plotted are only a guide for the eye.

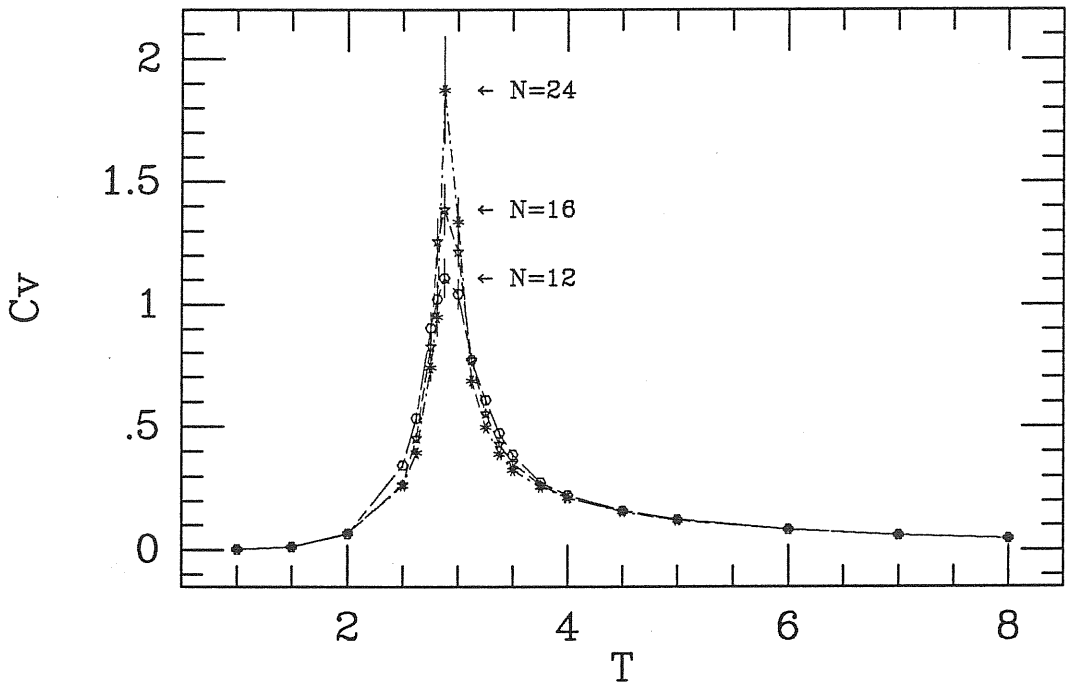

Fig. 5.2: Specific heat vs. temperature in the KJT model. The arrows indicate the position of the peaks for the three different sizes of the system.

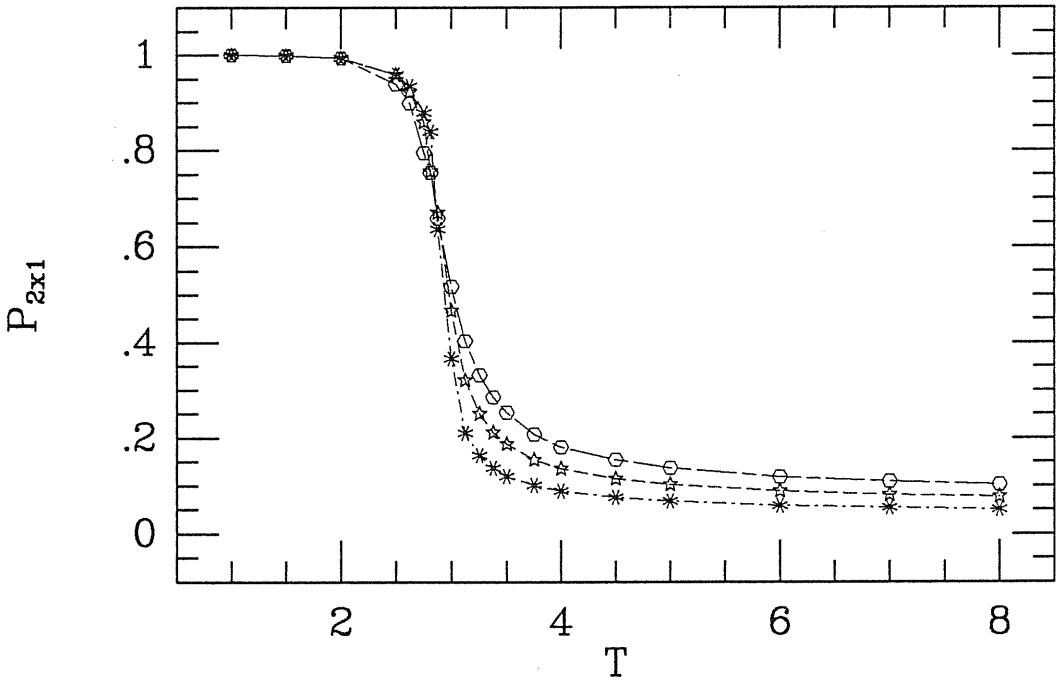

Fig. 5.3: Order parameter relative to the (2×1) phase vs. temperature in the KJT model.

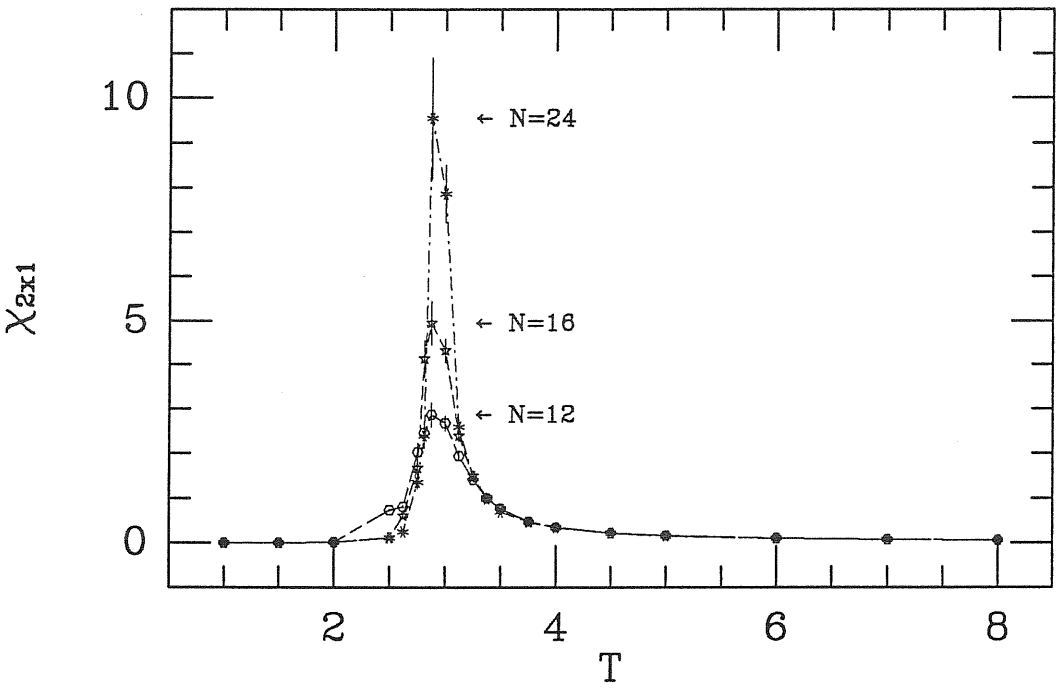

Fig. 5.4: Susceptibility relative to the order parameter $P_{(2\times1)}$ vs. temperature in the KJT model. The arrows indicate the position of the peaks for the three different sizes of the system.

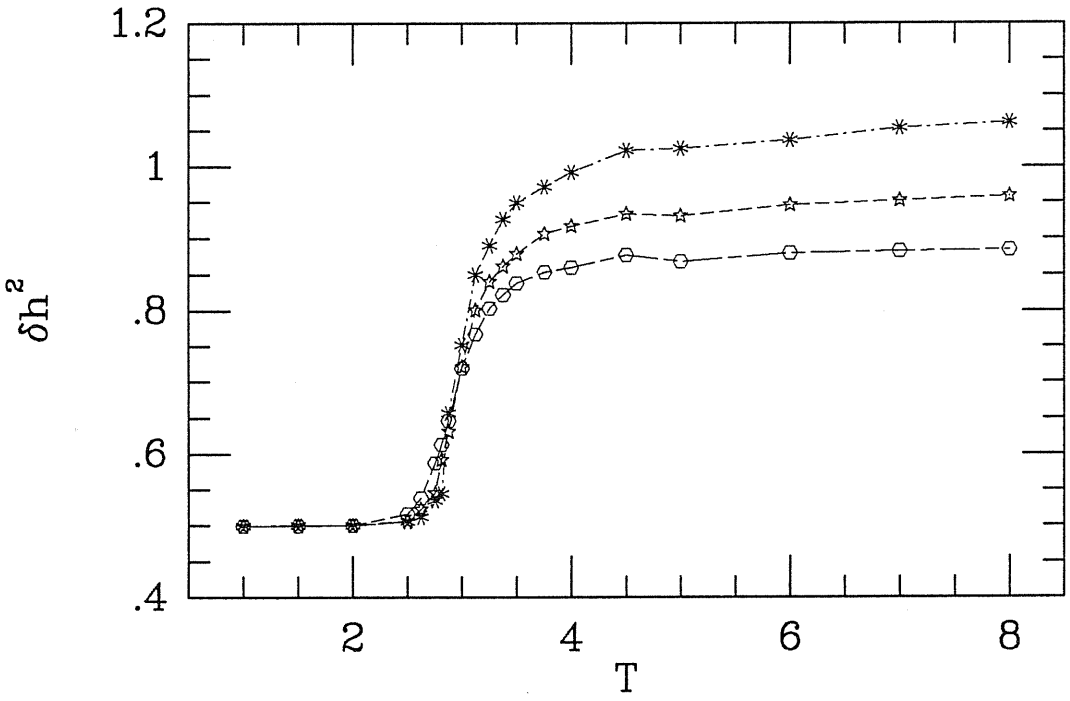

Fig. 5.5: Height fluctuations vs. temperature in the KJT model.

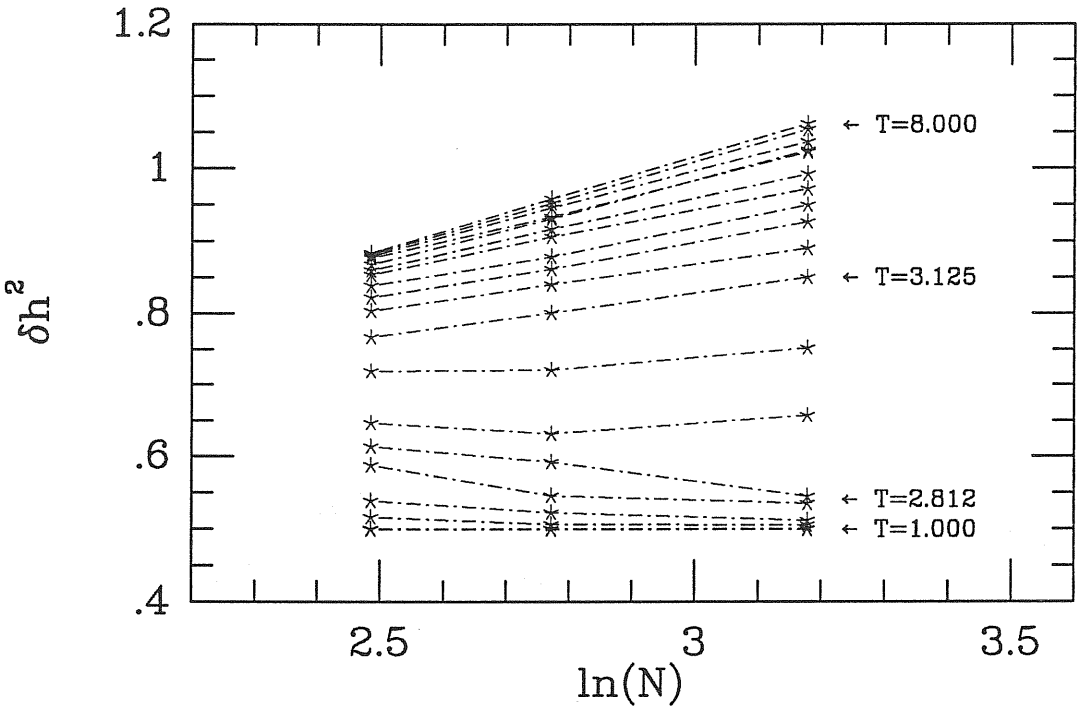

Fig. 5.6: Height fluctuations vs. logarithm of the size in the KJT model for the 20 temperature values investigated. The lines plotted should be straight only for $T \geq T_R$, which can be estimated around $T_R \simeq 3.1$.

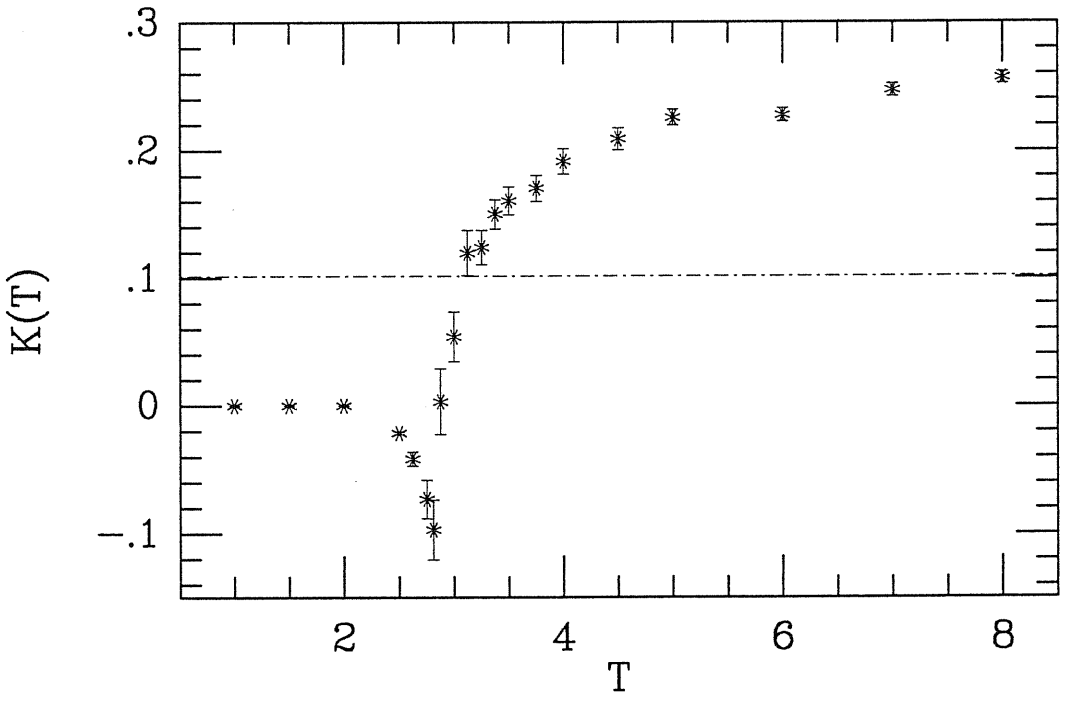

Fig. 5.7: $K(T)$ vs. temperature in the KJT model. The line indicates the position of the universal value $1/\pi^2$.

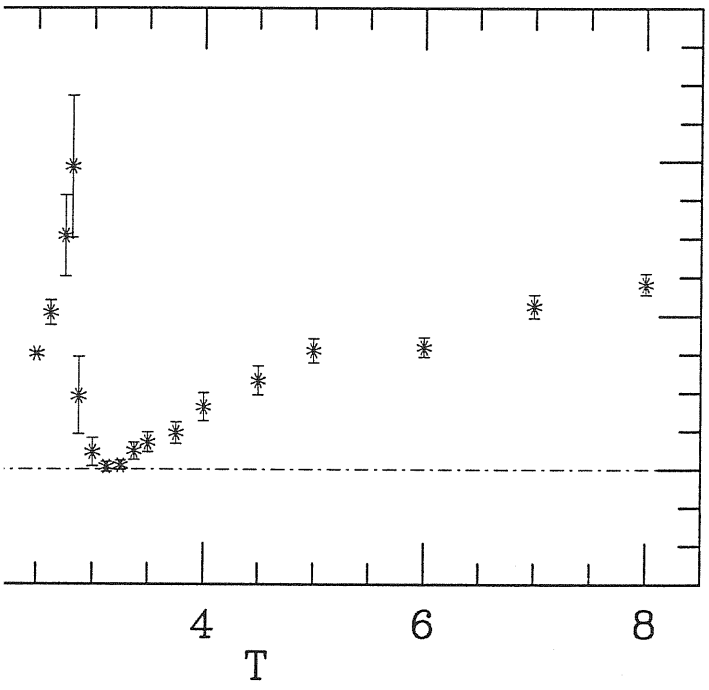

vs. temperature in the KJT model. The line indicates the

Conclusions and outlook

A recent approach to the problem of reconstruction and roughening of the (110) clean noble metal surfaces suggesting a possible (and in some cases very intimate) connection between these two surface phenomena, and ever more recent experimental data supporting this attitude, had lead to the formulation of the KJT Hamiltonian.

This SOS Hamiltonian is defined on the lattice of surface sites, and treats exactly in the same way (with the same coupling strengths) the atoms in the two equivalent anisotropic sublattices which make up the lattice. The structure of the Hamiltonian thus contains essential features for the description of both the above mentioned aspects. Indeed its energy parameters can be chosen so as to reproduce a (2×1) missing-row reconstructed ground state (as is the case for Au and Pt at low temperatures), while its six-vertex constraint on the height variables is particularly suited for the study of a roughening transition.

Second- and third-neighbour interactions must be considered, although the presence of the strong six-vertex constraint does not allow to identify the KJT Hamiltonian (in its spin version) with a kind of ANNNI model, and possibly even changes the universality class of the transitions.

The richness of the model is the primary reason for its complexity, which turns out compelling in the choice of a numerical approach for an investigation of its properties. For this reasons, a Monte Carlo simulation has been carried out.

Since one can adjust the energy parameters of the Hamiltonian so as to fit those of the exactly solved BCSOS model, a test study has been carried out on this system model and interesting information have been extracted. In particular, some features deserve particular consideration, such as the finite-size effects on the power law behaviour of the quasi-Bragg scattering peaks. The test demonstrates the correctness of the Monte Carlo algorithm, since many of the known results of the BCSOS model are reproduced, like the rounded anomaly in the specific heat preceeding the transition temperature and the absence of singularities. Furthermore we have proven the possibility of extracting an estimate of the roughening transition temperature by examining the behaviour of the height fluctuations as a function of both temperature and system size. In this way, the value $T_R = 5.68 \pm 0.42$ has been obtained, which agrees with the exact value $T_R = 5.77$.

In addition, coherent and total scattering intensities have been calculated, both confirming the BCSOS predictions. From the power-law behaviour of the total scattering intensity as a function of parallel momentum transfer, valid for $T \geq T_R$, the exponent τ has been extracted. The results show strong finite-size effects which should apply to experimental systems too, owing to the presence on a real surface of finite coherent scattering domains (mosaic structure). These effects seem also to depend on the perpendicular momentum transfer q_z in a non-trivial way.

Since universality arguments predict a specific value of τ exactly at the roughening transition temperature, and since it is an experimental practice to exploit this behavior in order to extract T_R from data, a more careful analysis of these effects is required. In the present study this can be achieved both through an enlargement of the maximum system size (which up to now has been made up of $2 \times 24 \times 24$ surface sites), and a study of anisotropic box shapes and their conse-

quences in the values of τ. Also, the subtraction of the coherent part from the total scattering intensity should be performed, for a more accurate comparison with experiments. In essence, however, the pronounced finite-size effects themselves are still to be understood and quantified.

The above procedure, applied to the KJT model, has provided rather interesting results. Two different phase transitions have been found in the system. A critical deconstruction transition at $T \simeq 2.87$, revealed by the presence of a pronounced peak in both the specific heat and the "2×1 susceptibility" clearly diverging with size, followed by a roughening transition at $T \simeq 3.1$. The latter transition appears to be in the Kosterlitz-Thouless universality class like all the other roughening transition observed in SOS models, hence of infinite order.

These findings are in good overall agreement with the previous study of Kohanoff *et al.* [87,19,18] who started with a slightly different model and, using the strip transfer-matrix method, found deconstruction and roughening at two different temperatures.

There is also a fairly good agreement with the complex model of den Nijs (section 3.3) which, among others, contemplates the possibility of an Ising deconstruction transition followed by an infinite order roughening transition for Au and Pt. The concept of disordered flat phase has been created precisely to describe the nature of the surface between the two transitions, where no more missing row order is present but the surface remains flat on the whole. The difference is found mainly within the unification attempted by den Nijs, who tries to describe all noble and near-noble metal surfaces in one model, but identifies as "preroughening" what for systems like Au or Pt is actually a deconstruction transition.

A comparison between the KJT model and the model of Villain an Vilfan (section 3.2) can be attempted, and the conclusion is that in both the two tran-

sitions are separate and deconstruction comes first, although in the latter model the roughening transition may not necessarily belong the the Kosterlitz-Thouless universality class. This is possibly because the Villain-Vilfan model is not strictly of the SOS type, but rather an empirical model based on symmetry considerations, the results of which are subject (as the same authors have successively recognized) to the choice of different energy parameters for the formation of steps.

We now come to a discussion of the relevance of our model and calculations to the missing-row reconstructed (110) surfaces of Au, Pt and Ir.

For Au(110) , deconstruction has been shown to occur near $700K$[105,31], while roughening has not yet been investigated. The parameters chosen in our calculation of chapter 5 were aimed at describing precisely Au (110) . However, that choice of parameters implies a reduced temperature unit of $\sim 1000K$, which means a deconstruction temperature of $\sim 2900K$ and a roughening temperature of $\sim 3100K$. This is clearly wrong, since Au melts at $1336K$. In our view, this does not invalidate the results obtained. The physics contained in the KJT Hamiltonian is still valid in the sense that the model embodies all the main symmetry aspects (both for the in-plane and the off-plane degrees of freedom) connected with the reconstruction and roughening of real (110) metal surfaces. Only a more careful reconsideration of its parametrization from microscopic quantities is therefore needed.

For Pt(110) , deconstruction has been studied by X-ray scattering by Robinson *et al.*, who found it to be near $1080K$[21]. In spite of the suggestion made in that work that roughening probably occurs at the same temperature, the evidence is not compelling, and T_R is uncertain there too. For example, Villain and Vilfan[83] show that the disordered Au(110) surface would exhibit a shifted diffuse scattering peak (which is the main evidence Robinson *et al.* provide to support the occurrence

of a roughening transition) even if it were flat, provided certain conditions are satisfied. Similarly, Jug and Tosatti[17] discussed a phase diagram which exhibits an incommensurate region between deconstruction and roughening. In such region the Bragg peak would of course shift, without any implications of roughening.

For Ir(110) , where a (2×1) recostruction has also been reported[106,107,108,109], the situation appears less clear, and recent studies failed even to detect the (2×1) state[110].

It should be rather interesting if calculations of scattering intensities through our Monte Carlo approach for the KJT model would reveal features in the peak position above the deconstruction transition similar to those found by Robinson *et al.* This is a direction to be pursued in future developments of this work. An optimization of the algorithm will also lead to the possibility of investigating larger system sizes and of performing more accurate finite-size scaling analyses, in order to extract the critical exponents of the lower transition and to clearly identify its universality class.

Moreover, it is worth noting that the energy parameters chosen in the present study correspond to a point located exactly in the middle of the (2×1) region of the ground state phase diagram. As a possible test of the model, a different parametrization shifting this point nearer to the (2×1) - (1×1) coexistence may show an increase in the separation between the two transition temperatures as the disordered flat phase enlarges its stability range.

Bibliography

[1] B. E. Hayden, K. C. Prince, P. J. Davie, G. Paolucci and G. M. Bradshaw, *Solid State Commun.* **48**, 325 (1983)

[2] S. M. Francis and N. V. Richardson, *Surface Sci.* **152/152**, 63 (1985)

[3] M. Copel, W. R. Graham, T. Gustafsson and S. M. Yalisove, *Solid State Commun.* **53**, 695 (1985)

[4] J. W. M. Frenken, R. L. Krans, J. F. van der Veen, E. Holub-Krappe and K. Horn, *Phys. Rev. Lett.* **59**, 2307 (1987)

[5] G. A. Held, J. L. Jordan-Sweet, P. M. Horn, A. Mak and R. J. Birgeneau, *Phys. Rev. Lett.* **59**, 2075 (1987)

[6] G. Binnig, H. Rohrer, Ch. Gerber and E. Weibel, *Surface Sci.* **131**, 1379 (1983)

[7] J. Möller, J. Niehus and W. Heiland, *Surface Sci.* **166**, L111 (1986)

[8] W. Moritz and D. Wolf, *Surface Sci.* **163**, L655 (1985)

[9] K. H. Rieder, T. Engel and N. Garcia, in: *Proc. 4th Intern. Conf. on Solid Surfaces*, Cannes, 1986, p.861

[10] I. K. Robinson, *Phys. Rev. Lett.* **50**, 1145 (1983)

[11] I. K. Robinson, Y. Kuk and L. C. Feldman, *Phys. Rev.* **B29**, 4762 (1984)

[12] L. D. Marks, *Phys. Rev. Lett.* **51**, 1000 (1983)

[13] M. Copel and T. Gustafsson, *Phys. Rev. Lett.* **57**, 723 (1986)

[14] J. Villain and I. Vilfan, *Surface Sci.* **199**, 165 (1988)

[15] A. Trayanov, A. C Levi and E. Tosatti, *Europhys. Lett.* **8**, 657 (1989)

[16] A. Trayanov, A. C. Levi and E. Tosatti, *Surface Sci.* **233**, 184 (1990)

[17] G. Jug and E. Tosatti, *Phys. Rev.* **B42**, 969 (1990)

[18] J. Kohanoff, G. Jug and E. Tosatti, *J. Phys.* **A23**, L209, (1990)

[19] J. Kohanoff, G. Jug and E. Tosatti, *J. Phys.* **A** (in press)

[20] A. C. Levi and M. Touzani, *Surface Sci.* **218**, 223 (1989)

[21] I. K. Robinson, E. Vlieg and K. Kern, *Phys. Rev. Lett.* **63**, 2578 (1989)

[22] G. Binnig and H. Rohrer, *Surface Sci.* **126**, 236 (1983)

[23] H. P. Bonzel and S. Ferrer, *Surface Sci.* **118**, L111 (1982)

[24] H. P. Bonzel and S. Ferrer, *Surface Sci.* **119**, 234 (1982)

[25] K. M. Ho and K. P. Bohnen, *Europhys. Lett.* **4**, 345 (1987)

[26] K. M. Ho and K. P. Bohnen, *Phys. Rev. Lett.* **59**, 1833 (1987)

[27] F. Ercolessi, A. Bartolini, M. Garofalo, M. Parrinello and E. Tosatti,*Physica Scripta* 19, 399 (1987)

[28] F. Ercolessi, M. Parrinello and E. Tosatti, *Philos. Mag.* **A58**, 213 (1988)

[29] E. Bauer, in *Structure and Dynamics of Surfaces II*, Eds. W. Schommers and P. von Blanckenhagen, Springer, Heidelberg, 1987, p. 115

[30] R. F. Willis, in *Dynamical Phenomena at Surfaces*, Eds. F. Nizzoli, K. H. Rieder and R. F. Willis, Spinger, Berlin, 1985, p. 126

[31] J. C. Campuzano, M. S. Foster, G. Jennings, R. F. Willis and W. Unertl, *Phys. Rev. Lett.* **54**, 2684 (1985)

[32] S. J. G. Mochrie, *Phys. Rev. Lett.* **59**, 304 (1987)

[33] P. Zeppenfeld, K. Kern, R. David and G. Comsa, *Phys. Rev. Lett.* **62**, 63 (1989)

[34] P. Bak, *Solid State Commun.* **32**, 581 (1979)

[35] M. Schick, *Progr. Surf. Sci.* **11**, 245 (1981)

[36] M. Guillope' and B. Legrand, *Surface Sci.* **215**, 577 (1989)

[37] R. M. Nieminen,*Physica Scripta* **T19**, 320 (1987)

[38] M. S. Daw and M. I. Baskes, *Phys. Rev.* **B29**, 6443 (1984)

[39] S. M. Foiles, M. I. Baskes and M. S. Daw, *Phys. Rev.* **B33**, 7983 (1986) and Erratum: *Phys. Rev.* **B37**, 10378 (1988)

[40] L. D. Roelofs and E. I. Martir, preprint

[41] L. D. Roelofs, S. M. Foiles, M. S. Daw and M. I. Baskes, preprint submitted to *Surface Sci.*

[42] W. K. Burton and N. Cabrera, *Disc. Faraday Soc.* **5**, 33 (1949)

[43] W. K. Burton, N. Cabrera and F. C. Frank, *Philos. Trans. R. Soc. Lond.* **243A**, 299 (1951)

[44] L. Onsager, *Phys. Rev.* **65**, 117 (1944)

[45] J. D. Weeks, in *Ordering in Stongly Fluctuating Condensed Matter Systems*, Ed. T. Riste, Plenum Press, New York, 1980, p. 292

[46] H. van Beijeren and I. Nolden, in *Structure and Dynamics of Surfaces II*, Eds. W. Schommers and P. von Blanckenhagen, Springer, Heidelberg, 1987, p. 259

[47] S. T. Chui and J. D. Weeks, *Phys. Rev.* **B14**, 4978 (1976)

[48] J. M. Kosterlitz and D. Thouless,*J. Phys.* **C6**, 1181 (1973)

[49] J. M. Kosterlitz,*J. Phys.* **C7**, 1046 (1974)

[50] H. van Beijeren, *Phys. Rev. Lett.* **38**, 993 (1977)

[51] H. E. Lieb, *Phys. Rev. Lett.* **18**, 1046 (1967)

[52] H. E. Lieb and F. Y. Wu, *Two dimensional ferroelectric models*, in *Phase Transition and Critical Phenomena*, Eds. C. Domb and M. S. Green, Academic, New York, 1972, p. 331

[53] R. J. Baxter, *Exactly Solved Models in Statistical Mechanics*, Academic, Lon-

don, 1982

[54] L. Pauling, *J. Am. Chem. Soc.* **57**, 2680 (1935)

[55] J. C. Slater, *J. Chem. Phys.* **9**, 16 (1941)

[56] F. Rys, *Helv. Phys. Acta* **36**, 536 (1963)

[57] C. Jayaprakash, W. F. Saam and S. Teitel, *Phys. Rev. Lett.* **50**, 2017 (1983)

[58] W. F. Saam, C. Jayaprakash and S. Teitel, in *Quantum Fluids and Solids - 1983*, Eds. E. D. Adams and G. G. Ihas, A.I.P., New York, 1983, p. 371

[59] C. Jayaprakash and W. F. Saam, *Phys. Rev.* **B30**, 3916, (1984)

[60] G. Wulff, *Z. Krist. Mater.* **34**, 449 (1901)

[61] C. Herring, *Phys. Rev.* **82**, 87 (1951)

[62] J. C. Heyraud and J. J. Métois, *Surface Sci.* **128**, 334 (1983)

[63] S. G. Lipson, *Contemp. Phys.* **28**, 117 (1987)

[64] J. E. Avron, L. S. Balfour, C. G. Kuper, J. Landau, S. G. Lipson and L. S. Schulman, *Phys. Rev. Lett.* **45**, 814 (1980)

[65] S. Balibar and E. Castaing, *J. Phys. Lett. (Paris)* **41**, L329 (1980)

[66] K. O. Keshishev, A. Ya Parshin and A. V. Babkin, *Zh. Eksp. Theor. Fiz.* **80**, 716 (1981) [*Sov. Phys. JETP* **53**, 362 (1981)]

[67] S. G. Lipson and E. Polturak, in *Progress in Low Temperature Physics*, Vol XI, Ed. D. F. Brewer, Elsevier, 1987, p. 127

[68] S. Balibar and E. Castaing, *Surface Sci. Reports* **5**, 87 (1985)

[69] P. E. Wolf, F. Gallet, S. Balibar, E. Rolley and P. Nozières, *J. Phys. (Paris)* **46**, 1987 (1985)

[70] F. Gallet, P. Nozières, S. Balibar and E. Rolley, *Europhys. Lett.* **2**, 701 (1986)

[71] C. Rottman, M. Wortis, J. C. Heyraud and J. J. Métois, *Phys. Rev. Lett.* **52**, 1009 (1984)

[72] A.F. Andreev, *Zh. Eksp. Theor. Fiz.* **80**, 2042 (1981) [*Sov. Phys. JETP* **53**,

1063 (1981)]

[73] C. Rottman and M. Wortis, *Phys. Rev.* **29**, 328 (1984)

[74] Y. Carmi, S. G. Lipson and E. Polturak, *Phys. Rev.* **B36**, 1894 (1988)

[75] D. S. Fisher and J. D. Weeks, *Phys. Rev. Lett.* **50**, 1077 (1983)

[76] J. Lapojoulade, J. Perreau and A. Kara, *Surface Sci.* **129**, 59 (1983)

[77] J. Villain, D. R. Grempel and J. Lapujoulade, *J. Phys.* **F15**, 809 (1985)

[78] F. Fabre, D. Gorse, B. Salanon and J. Lapojoulade, *J. Phys. (Paris)* **48**, 1017 (1987)

[79] M. den Nijs, E. K. Riedel, E. H. Conrad and T. Engel, *Phys. Rev.* **55**, 1689 (1985)

[80] E. H. Conrad, R. M. Aten, D. S. Kaufman, L. R. Allen, T. Engel, M. den Nijs and E. K. Riedel, *J. Chem. Phys.* **84**, 1015 (1986)

[81] D. L. Blanchard, D. F. Thomas, H. Xu and T. Engel, *Surface Sci.* **222**, 477 (1989)

[82] J. Villain, J. L. Rouvière and I. Vilfan, preprint

[83] J. Villain, and I. Vilfan, preprint

[84] E. Lieb, *Phys. Rev. Lett.* **20**, 1445 (1968)

[85] M. den Nijs, *Phys. Rev. Lett.* **64**, 435 (1990)

[86] M. den Nijs, preprint

[87] J. Kohanoff, Magister Philosophiæ Thesis, S.I.S.S.A.-I.S.A.S. Trieste, 1989 – unpublished

[88] J. Villain and P. Bak, *J. Phys. (Paris)* **42**, 657 (1981)

[89] K. Binder and D. P. Landau, *Surface Sci.* **61**, 577 (1976)

[90] K. Binder and D. P. Landau, *Phys. Rev.* **B21**, 1941 (1980)

[91] K. Binder, W Kinzel and D. P. Landau, *Surface Sci.* **117**, 232 (1982)

[92] K. Binder and D. P. Landau, *Surface Sci.* **108**, 503 (1981)

[93] D. P. Landau, *Phys. Rev.* **B27**, 5604 (1983)

[94] U. Garibaldi, A. C. Levi, R. Spadacini and G. E. Tommei, *Surface Sci.* **48**, 649 (1975)

[95] G. E. Tommei, A. C. Levi and R. Spadacini, *Surface Sci.* **125**, 312 (1982)

[96] V. Bortolani and A. C. Levi, *Riv. Nuovo Cim.* **9(11)**, 1 (1986)

[97] A. C. Levi, R. Spadacini and G. E. Tommei, in *The Structure of Surfaces II*, Eds. J. F. van der Veen and M. A. Hove, Springer, vol 11, 1988

[98] R. W. Youngblood, J. D. Axe and B. M. McCoy, *Phys. Rev.* **B21**, 5212 (1980)

[99] R. W. Youngblood and J. D. Axe, *Phys. Rev.* **23**, 232 (1981)

[100] K. Binder, in *Monte Carlo methods in statistical physics*, Ed. K. Binder, Springer, 1979, p. 1

[101] N. Metropolis, A. W. Rosenbluth, M. N. Rosenbluth, A. H. Teller and E. Teller, *J. Chem. Phys.* **21**, 1087 (1953)

[102] G. Jacucci and A. Rahman, *Nuovo Cim.* **4D**, 341 (1984)

[103] R. H. Swendsen, *Phys. Rev.* **B15**, 5421 (1977)

[104] R. H. Swendsen, *Phys. Rev.* **B18**, 492 (1978)

[105] H. Jagodzinski, W. Moritz and D. Wolf, *Surface Sci.* **77**, 233 (1978)

[106] M. Copel, P. Fenter and T. Gustafsson, *J. Vac. Sci. Technol.* **A5**, 742 (1987)

[107] G. L. Kellog, *J. Vac. Sci. Technol.* **A5**, 747 (1987)

[108] K. Müller, J. Witt and O. Schütz, *J. Vac. Sci. Technol.* **A5**, 757 (1987)

[109] Q. J. Gao and T. T. Tsong, *J. Vac. Sci. Technol.* **A5**, 761 (1987)

[110] W. Hetterich and W. Heiland, *Surface Sci.* **210**, 129 (1989)

Ringraziamenti

La lista dei ringraziamenti è necessariamente lunga se vuole comprendere (come è destinata a fare) tutti gli amici della SISSA che mi hanno in un modo o nell'altro sostenuto in questo caldo periodo di tesi e, più in generale, in questi due anni passati a Trieste. L'ordine che seguirò nel ricordarli è assolutamente casuale, dettato soltanto da associazioni di idee e da ricordi di particolari momenti in loro compagnia.

Inizierò con coloro che hanno sopportato per quasi un anno tale noioso compagno di stanza (me stesso), e cioè Chen Xiaojie ed Enrico Smargiassi, cui va il mio apprezzamento per l'incoraggiamento che mi hanno costantemente fornito, anche e soprattutto nei momenti 'bui' della tesi. Un ringraziamento particolare va a Chen, il quale si è adoperato con pazienza per più di un mese nell'insegnarmi l'uso di un complesso programma di dinamica molecolare, anche se ad un certo punto la sua fatica è stata vanificata dalla mia decisione di lasciar perdere tutto e rivolgermi ad un nuovo argomento.

Non posso ora esimermi dal ricordare "l'insuperato ed insuperabile Maestro di tutti noi", Pasquale Pavone, per la totale disponibilità e l'eccezionale abilità grafica (non disgiunte, anzi sostenute da una filosofia di vita che non so se definire "siciliana" o come altro), qualità che hanno reso prezioso il suo "invaluable aesthetic advice", nelle parole di Jorge Kohanoff, cui va il mio saluto assieme a quello per la moglie Clarisa. L'Hamiltoniana oggetto di questa tesi è figlia sua, e mi

rincresce non aver avuto maggiori possibilità di discutere e lavorare con lui. A proposito di IBM, un apprezzamento va anche a Orio Tomagnini, che ha il merito di avere scoperta la formula per continuare a fare fisica guadagnando il triplo di noi.

Con Andrea Ferrante ho avuto diverse discussioni sul metodo Monte Carlo e sulla trattazione degli errori (suo è il programma che li ricava dai valori istantanei delle grandezze utilizzato in questa tesi), ma preferisco ricordarlo per una colta discussione linguistica, certamente più interessante e fruttuosa, sugli usi ed i significati di due termini dei nostri rispettivi dialetti ("mona" e "belin").

A Miklos Gulacsi riconosco la vitalità e l'ottimismo cha ha propagato a tutto il terzo piano del Bellavista, mai superato in questo però da Pierino Silvestrelli, le cui affermazioni piene di speranza e di gioia verso la vita e la fisica mi hanno costantemente incoraggiato e spronato(!).

Discorso a parte va fatto per Michele Fabrizio: nel confronto fra me e lui esce nettamente perdente, ma solo perchè ha una automobile peggiore della mia: la nostra amicizia si è sicuramente cementata dopo aver corso rischi mortali sul suddetto mezzo. Devo poi riconoscere gli scambi linguistici avuti con Jair Botina nelle lunghe sere passate alla SISSA; io non ne ho ricavato nulla, ma lui ha imparato due lingue (l'italiano e lo spagnolo).

A Guido Goldoni devo rimproverare di non avermi mai fatto assaggiare un solo piatto insaporito dal suo mitico "aceto balsamico di Vignola invecchiato 200 (o 300?) anni", ma lo perdono nelle speranza di rifarmi presto, ad Antonella Longo e a Marco Buongiorno Nardelli riconosco una carica di simpatia fuori dal comune, e non posso che vantarmi della loro amicizia. Prometto poi a Marco Reni di accompagnarlo in una delle sue prossime passeggiate in montagna, purchè la quota massima non superi i 500 metri ed il sentiero abbia una larghezza minima

di 2 metri e 30 centemetri, con al più lo 0.48 % di dislivello.

Auguro lunga strada ad Andrea Danani, ringraziandolo per l'inesauribile ottimismo che traspone in tutto ciò che fa, ed anche per le consistenti dosi di cioccolato svizzero e di fonduta con cui ha reso meno tristi le lunghe sere di inverno ai suoi coinquilini, ringrazio altresì Alberto Carlini che, per un motivo o per l'altro, non ha mai potuto usufruirne, facendo così in modo che la spartizione del suddetto bottino avvenisse fra due e non tre contendenti.

A proposito di mangiare, difficilmente dimenticherò i "pizzicotti" che Valeria Bonservizi ci ha proposto in occasione dell'ultimo capodanno nella sua casa di campagna a Sorci, così accogliente ed ospitale, un ricordo particolare va poi a Stefano Borgani che, fra le altre cose, mi ha insegnato una massima di cui farò tesoro (*"quando pozzo m'appallozzo: spesso pozzo!"*) ed uno ancora più particolare al patè della madre. Gran premio speciale della giuria infine al tiramisù di Laura Reina, assieme ad una menzione per la tenacia dimostrata assieme ad Ettore Aldrovandi nelle "prove di resistenza alla SISSA": il record di durata notturna davanti ad un terminale va decisamente a loro.

A Edgar Cifuentes mi legano, assieme all'amore per Mozart, due esperienze in particolare, il concerto dei Pink Floyd a Venezia e l'aver condiviso un letto in occasione del ricordato capodanno, e non posso che augurarmi che entrambe non abbiano più a ripetersi. A Paolo Soriani invece un semplice saluto, ed un augurio per un sereno futuro "a tre".

E come scrisse una volta Norma Reggiani

aos movimentos da vida